New Insights into Decomposition of Metathesis-Active Methylidenes

Stephanie Rufh

Thesis submitted to the
Faculty of Graduate and Postdoctoral Studies
University of Ottawa
in partial fulfillment of the requirements for the degree of

Master of Science

Center for Catalysis Research and Innovation
Department of Chemistry and Biomolecular Science
Ottawa-Carleton Chemistry Institute
Faculty of Science
University of Ottawa

Table of Contents

List of Figures

List of Schemes

Abstract

Olefin metathesis is one of the most powerful tools in current use for the assembly of carbon-carbon bonds. The advent of easily-handled ruthenium catalysts, along with new awareness of ring-closing metathesis (RCM), led to widespread adoption of metathesis methodologies in synthetic organic chemistry. Relative robustness to air and water, and tolerance for an impressive range of functional groups, is attested to by the recent appearance of RCM in pharmaceutical manufacturing processes. However, challenges remain, particularly with respect to the ease with which these catalysts undergo loss of the critical Ru=CHR functionality that enables metathesis. This limits not only metathesis productivity, but also selectivity, because the Ru products can promote unwanted C=C migration reactions. Many decomposition pathways have been found to culminate in activation of the *N*-heterocyclic carbene (NHC; most typically an H_2IMes) ligand. In consequence, NHC truncation is a widely accepted design solution. This thesis work was aimed at assessing the validity of this proposition from several perspectives.

Hundreds of metathesis catalysts are now known, but the second-generation Grubbs catalyst (**GII**) is still most widely used. This work began with examining the role of Lewis bases in promoting decomposition of the second-generation Grubbs catalyst, $RuCl_2(H_2IMes)(PCy_3)(=CHPh)$ **GII**, under conditions of metathesis. Small Lewis donors, ranging from pyridine and DMSO to THF and water, were shown to greatly accelerate loss of the methylidene ($[Ru]=CH_2$) ligand. Associative donor binding was shown to promote dissociation of PCy_3, a powerful nucleophile which then attacks at the methylidene carbon. Attempts to probe the reversibility of this step revealed no reformation of the $[Ru]=CH_2$ unit, suggesting that nucleophilic attack to form a $[Ru]–CH_2PCy_3^+$ moiety is the key decomposition event. Ensuing C-H activation of a ligand (e.g. the *o*-methyl of H_2Mes or IMes), with abstraction of a chloride ligand, results in elimination of $[MePCy_3]Cl$. Two potential preventative measures were examined. These involved, first, the use of phosphine scavengers to intercept the liberated PCy_3 ligand during metathesis, and second, truncation of an *N*-mesityl group to *N*-methyl to inhibit C-H activation. While phosphine scavenging proved somewhat successful in increasing metathesis yields, lower activity was observed for the catalyst with the modified NHC ligand.

The negative impact of a smaller NHC on catalyst activity is of particular interest, given that curtailed NHC bulk has been proposed as the key to improved catalyst robustness, as noted above.

To clarify this issue, truncation of the nitrogen substituents was taken to the extreme by replacing both *N*-mesityl groups with *N*-methyl. Accordingly, the reaction chemistry of the first-generation Grubbs catalyst, $RuCl_2(PCy_3)_2(=CHPh)$ **GI** with 1,3,4,5-tetramethylimidazol-2-ylidene (IMe_4) was explored. The small size of this NHC ligand precludes access to a stable mono-IMe_4 catalyst corresponding to **GII**: rather, an initial *cis*-$RuCl_2(IMe_4)_2(=CHPh)$ species is thought to rapidly convert to a highly stable face-bridged dimer, the observed product. The latter complex exhibits minimal catalytic activity, even in the trivial RCM of diethyl diallylmalonate (DDM). Synthesis of the corresponding edge-bridged dimer was accomplished, but activity remained poor. To simulate an active catalyst, IMe_4 was added to **GIm**. Complete loss of the methylidene ligand was observed within minutes at RT. Importantly, however, decomposition was traced to rapid bimolecular coupling, with loss of the methylidene ligand as ethylene, rather than nucleophilic abstraction. Coupling is inhibited for the benzylidene system by the increased steric bulk of [Ru]=CHPh relative to $[Ru]=CH_2$, a feature well established in more conventional catalyst systems. We conclude that moving from H_2IMes to a smaller NHC to inhibit C-H activation is not a practical solution for improving catalyst robustness. Rather, catalyst redesign should focus on protecting the $[Ru]=CH_2$ moiety to prevent loss of the methylidene ligand via either nucleophilic abstraction or bimolecular coupling.

List of Contributions

Publications (F = Full Paper, C = Communication)

3F. **S.A. Rufh** and D.E. Fogg. "NHC Truncation Accelerates Decomposition of Olefin Metathesis Catalysts." *ACS Catalysis*, submitted for publication.

Manuscript in preparation.

2C. C.S. Higman, **S.A. Rufh**, R McDonald, and D.E. Fogg. "Synthesis and Dynamic Behaviour of a Dimeric Ruthenium Benzylidene Complex Bearing a Truncated *N*-Heterocyclic Carbene Ligand." *J. Organomet. Chem.* **2017**, *847*, 162 – 166. Highlighted on All Things Metathesis blog.

1F. W.L. McClennan, **S.A. Rufh**, J.A.M. Lummiss, and D.E. Fogg. "A General Decomposition Pathway for Phosphine-Stabilized Metathesis Catalysts: Lewis Donors Accelerate Methylidene Abstraction." *J. Am. Chem. Soc.* **2016**, *138*, 14668 – 14677.

Presentations (O = Oral; presenting author in bold)

O5. **S.A. Rufh** and D.E. Fogg "Examining Ligand Truncation as a Design Strategy in Metathesis Catalysts." 100th Canadian Society for Chemistry Conference, Toronto, ON, May 28 – June 1, 2017

O4. **S.A. Rufh** and D.E. Fogg "Decomposition of Metathesis Catalysts: Impact of Ligand Truncation." 2017 Ottawa-Carleton Chemistry Institute Research Day, Ottawa, ON, May 25, 2017 (1st Prize: Oral Contributions)

O3. **S.A. Rufh** and D.E. Fogg "Intercepting Deactivation of Phosphine-Stabilized Metathesis Catalysts." 49th Inorganic Discussion Weekend, Hamilton, ON, November 11–13, 2016

O2. **S.A. Rufh**, C.S. Higman, and D.E. Fogg "Catalyst Deactivation in Olefin Metathesis: A Case for Redesign." 99th Canadian Society for Chemistry Conference, Halifax, NS, June 5–9, 2016

O1. **S.A. Rufh**, C.S. Higman, and D.E. Fogg "Catalyst Deactivation in Olefin Metathesis: A Case for Redesign." 24th Canadian Symposium on Catalysis, Ottawa, ON, May 8–11, 2015

Acknowledgements

First and foremost, I would like to thank my supervisor Prof. Deryn Fogg for all your support. Our lengthy discussions have trained me to think critically, and to always question the best way to approach a problem. Your enthusiasm and rigorous approach to science have shaped my perspective as a chemist, and will stick with me through all my future endeavors. I would also like to thank Prof. Lisa Rosenberg, my undergraduate supervisor at the University of Victoria, for first training me in the arts of research and air-sensitive chemistry. My experience in your lab was invaluable in preparing me for my graduate studies.

To the NMR experts at uOttawa, Dr. Glenn Facey and Dr. Gang Ye, thank you for your technical expertise. Your input and guidance have been an immense help in completing the experiments for my thesis.

To my past and present labmates, thank you for your friendship and indispensable advice. Emma, I can't imagine making it through the past two years without your encyclopedic knowledge and our regular walks to Loblaws. You always encouraged me to work harder, smarter, and with resilience. Goof Troop, thank you for indulging me in Lord of the Rings movie nights and weekly breakfast outings. Alex, our crib games and trips to Tim's were always a welcome relief. Daniel, your positive attitude (even in chemical adversity!) has always brightened my day. Carolyn and Gwen, your mentorship and training has been crucial to my development as a chemist. Billy, Craig, Adrian, Jesse, Andrew, and Stephan, thank you for your support and for acting as my sounding board – I will always be grateful that our time in the Fogg lab overlapped.

To my family: Mom, Dad, Larry, Genny, Lauren, Michael, my wonderful grandparents, and everyone else – your unending love, encouragement, and understanding have always motivated me when I've struggled. To Ashley and Bryce, thank you for always supporting me unconditionally and pushing me to be the best version of myself, academically or otherwise.

Nathan Fielder, thank you for the tips on how to stay motivated to complete a task, and for reminding me to think outside the box.

List of Compounds

Organic and main group compounds

H_2IMes	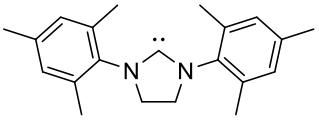	IMes	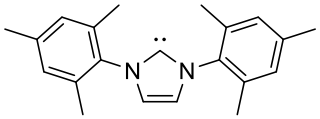
H_2IPr	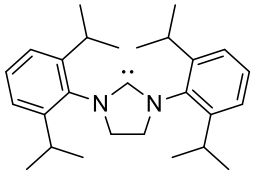	IMe_4	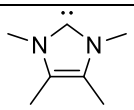
IMe_2	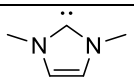	H_2IMeMes	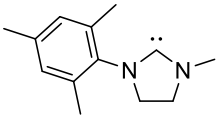
IMeMes	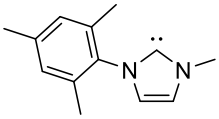	DDM	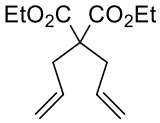
DMT	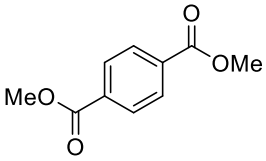	TMB	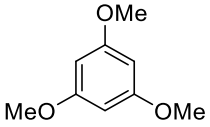
KTp	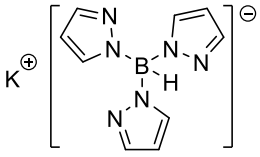	Amberlyst-15	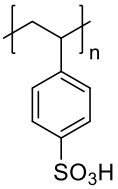
Merrifield-Cl	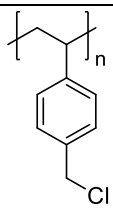	Merrifield-I	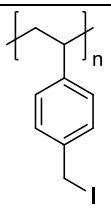

BnI	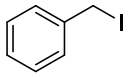	BAr_4^F	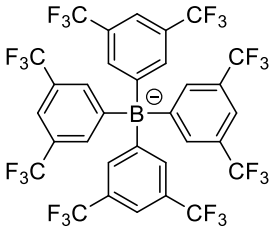
1	$[MePCy_3]Cl$	**2a**	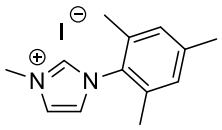
2b	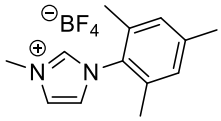	**3**	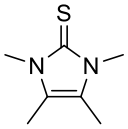
4	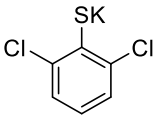	**5**	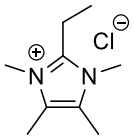

Transition metal complexes

Ta-1	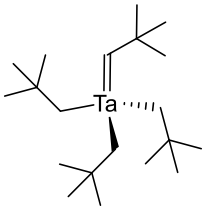	**Mo-1**	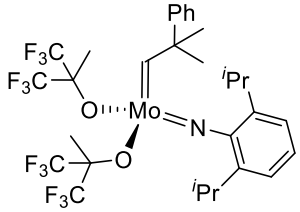
W-1	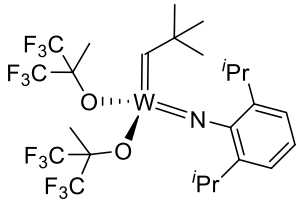	**GI**	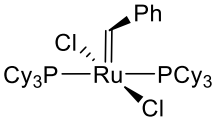
GII	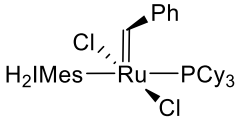	**GIm**	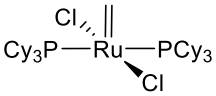

GIIm	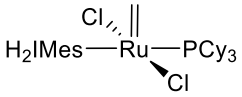	**GIIm'**	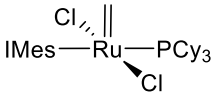
GIII	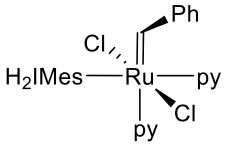	**GII-I**	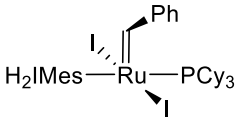
HI	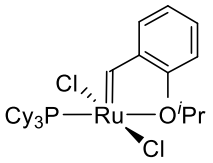	**HII**	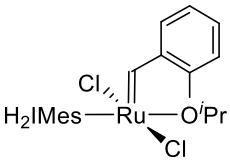
Ru-1	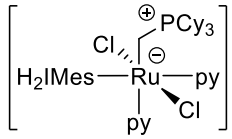	**Ru-2a**	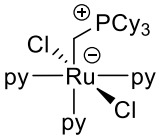
Ru-2b	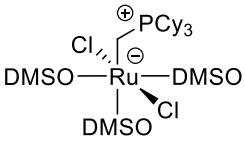	**Ru-3a**	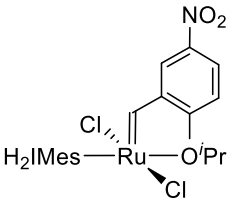
Ru-3b	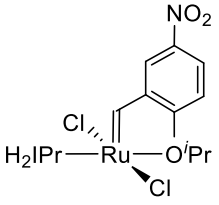	**Ru-4**	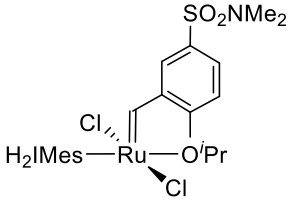
Ru-5a	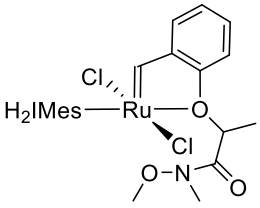	**Ru-5b**	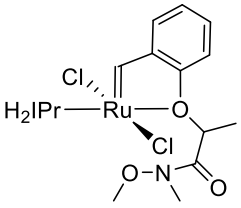
Ru-6	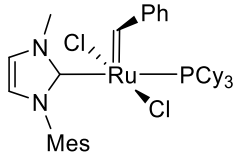	**Ru-7**	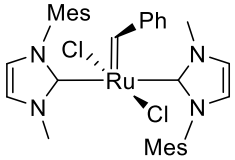

HC	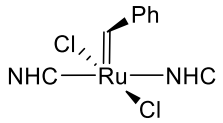	**Ru-8a**	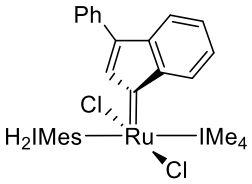
Ru-8b	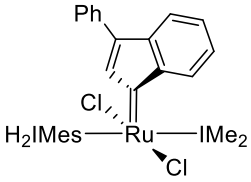	**Ru-9**	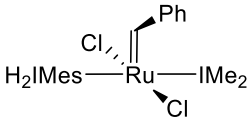
Ru-10	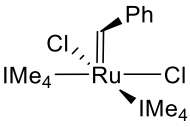	**Ru-11a**	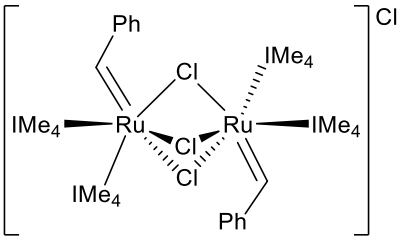
Ru-11b	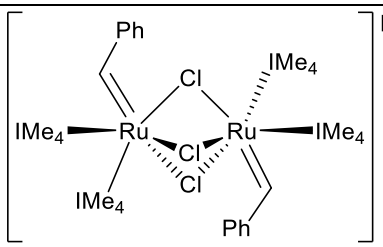	**Ru-12**	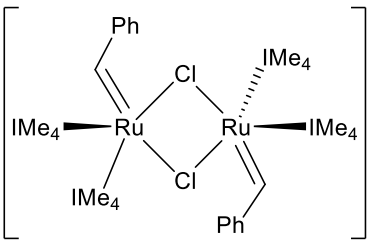
Ru-13	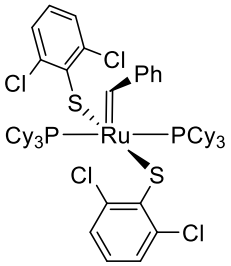	**Ru-14**	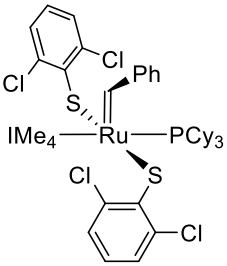
Ru-15	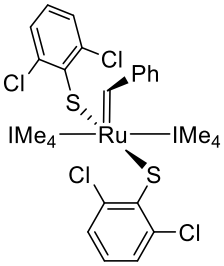	**GII’’**	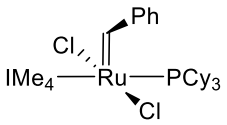

GIIm''	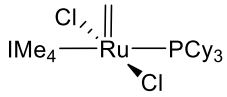	**Ru-16**	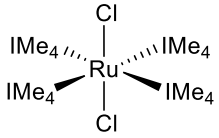
Ru-17	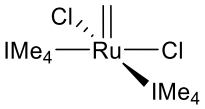	**Ru-18**	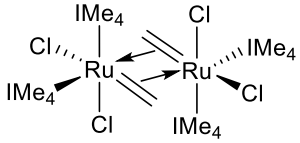
Ru-19	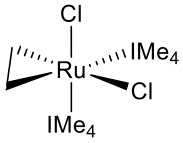		

List of Abbreviations

ADMET	Acyclic diene metathesis
Ar	Aryl
BI	Boehringer-Ingelheim
CAAC	Cyclic alkyl amino carbene
CM	Cross-metathesis
COSY	Correlation spectroscopy
DAD	Donor-accelerated decomposition
DCE	1,2-Dichloroethane
DDM	Diethyl diallylmalonate
DMT	Dimethyl terephthalate
DMSO	Dimethyl sulfoxide
EBD	Edge-bridged dimer
Equiv	Equivalent
EtOH	Ethanol
EXSY	Exchange spectroscopy
FBD	Face-bridged dimer
FID	Flame ionization detector
GC	Gas chromatography
HCV	Hepatitis C virus
H_2IMes	1,3-Bis-(2,4,6-trimethylphenyl)imidazolin-2-ylidene
HMBC	Heteronuclear multiple bond correlation
HMQC	Heteronuclear multiple quantum coherence
Hz	Hertz
IMes	1,3-Bis-(2,4,6-trimethylphenyl)imidazol-2-ylidene
IR	Infrared
IS	Internal standard
KTp	Potassium trispyrazolylborate
L	Neutral ligand donor

MALDI-TOF	Matrix-assisted laser desorption/ionization time-of-flight
MCB	Metallacyclobutane
MeCN	Acetonitrile
MeOH	Methanol
Mes	2,4,6-trimethylphenyl
MS	Mass spectrometry
NHC	*N*-heterocyclic carbene
NMR	Nuclear magnetic resonance
NOESY	Nuclear Overhauser spectroscopy
NP	Nanoparticle
ppm	Parts per million
py	Pyridine
RCM	Ring-closing metathesis
ROMP	Ring-opening metathesis polymerization
RT	Room temperature
Ru-H	Ruthenium hydride
SHOP	Shell Higher Olefin Process
THF	Tetrahydrofuran
TLC	Thin-layer chromatography
TMB	1,3,5-Trimethoxybenzene
TMS	Tetramethylsilane
TON	Turnover number

Chapter 1. Introduction

1.1 Catalysis

Catalysts play an invaluable role in sustainable chemical manufacturing. As compounds that increase the rate of chemical reactions without being consumed, catalysts are a staple of "green chemistry".[1] Catalysis routinely enables the construction of new bonds via routes that are energetically demanding to access by stoichiometric means, while eliminating the waste associated with stoichiometric reactions. It is therefore ideally aligned with current global priorities for sustainable processes: reducing the energy required for chemical transformations, and reducing the proportion of waste. High demand for pharmaceuticals and plastics, buttressed by the expanding understanding of organometallic chemistry, has greatly advanced the implementation of transition-metal catalysis in chemical manufacturing over the past several decades. The broad importance of catalytic methodologies to human wellbeing is highlighted by the fifteen Nobel Prizes in Chemistry awarded in the field since 1901.[2] Increasingly, these showcase advances with important potential to reduce the environmental footprint[3,4] of pharmaceutical and specialty chemicals (e.g. agrochemicals) manufacturing: asymmetric catalysis (2001),[5-7] palladium-catalyzed cross-coupling (2010),[8,9] and olefin metathesis (2005).[10-12] Of note in this context is the 2005 founding of the American Chemical Society's Green Chemistry Institute (ACS-GCI), ACS GCI Pharmaceutical Roundtable (ACS GCIPR), which brings together leading pharmaceutical corporations (including AstraZeneca, Eli Lilly, GlaxoSmithKline, Merck, Pfizer, and Schering-Plough).

One measure of catalyst productivity is the number of times it can complete a catalytic cycle before decomposing (Figure 1.1).[13] Understanding catalyst decomposition chemistry is imperative in

References begin on page 14

redesigning processes, or the catalysts themselves, for longer lifetimes. This thesis work focuses on improving our understanding of decomposition pathways in olefin metathesis, and identifying structural parameters that could contribute to the design of longer-lived catalysts.

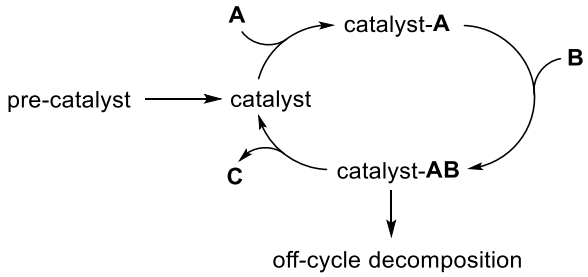

Figure 1.1 A model catalytic cycle.

1.2 Olefin Metathesis

1.2.1 History, Development, and Significance of Olefin Metathesis

Olefin metathesis is a metal-catalyzed process in which two olefins react to form a new carbon-carbon double bond. Its applications encompass multiple reaction types (Figure 1.2), of which key examples are cross-metathesis (CM), ring-closing metathesis (RCM), ring-opening metathesis polymerization (ROMP), and acyclic diene metathesis (ADMET). Olefin metathesis has transformed synthetic organic chemistry. For their work in the development of metathesis catalysts and elucidation of the mechanism involved, Robert Grubbs,[10] Richard Schrock,[11] and Yves Chauvin[12] were awarded the 2005 Nobel Prize in Chemistry.

References begin on page 14

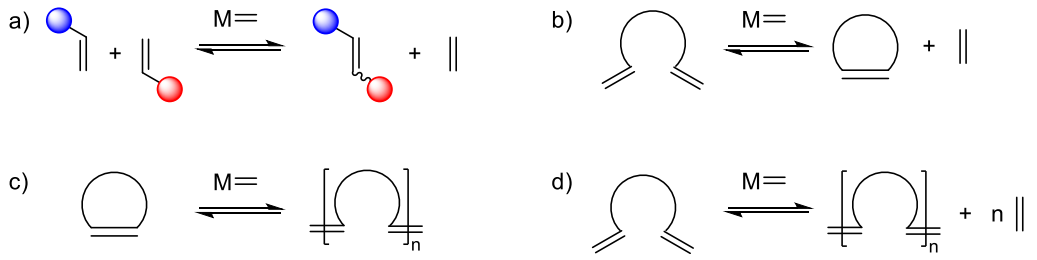

Figure 1.2 Major metathesis reactions. (a) Cross-metathesis, (b) ring-closing metathesis, (c) ring-opening metathesis polymerization, (d) acyclic diene metathesis.

One of the earliest documented findings of olefin metathesis is a 1955 patent by Anderson and Merckling of DuPont, which described the use of $TiCl_4$ as a catalyst in the ring-opening polymerization of norbornene.[14] Mo and W catalysts soon followed, for reactions such as the conversion of propylene to ethylene and butenes,[15] and the ring-opening polymerization of cyclopentene.[16] The term "olefin metathesis" was coined in 1967 by Calderon, who showed that bond cleavage and redistribution in fact occur at the C=C functionality.[17,18] While this established the basis for the olefin redistribution process, the mechanism was the subject of much debate. Several incorrect mechanisms were proposed, with various metal intermediates (Figure 1.3).[18-20] However, none of these correctly predicted the product distribution for all substrates examined.

References begin on page 14

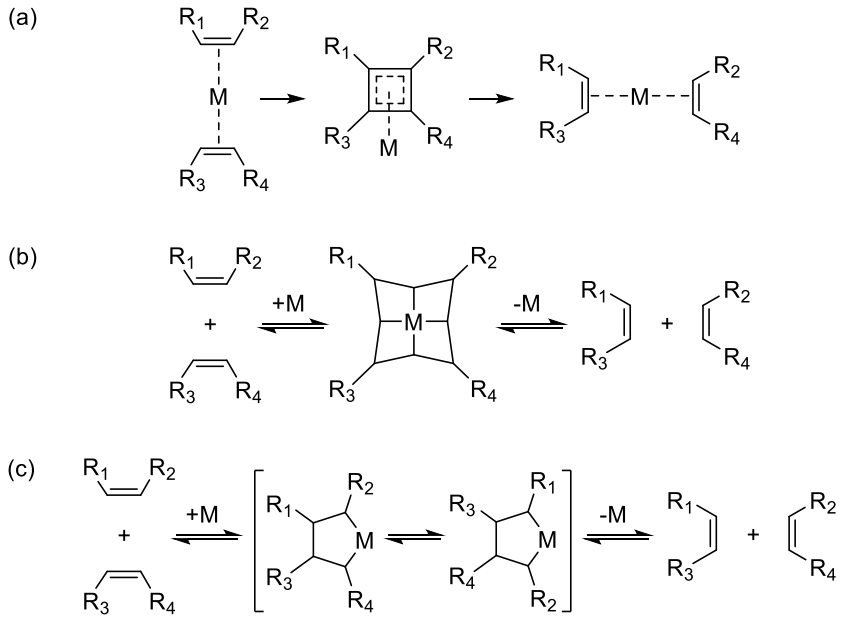

Figure 1.3 Proposed olefin metathesis mechanisms by (a) Calderon (1968), (b) Pettit (1971), (c) Grubbs (1972).

A breakthrough in mechanistic understanding resulted from the work of Chauvin and Hérisson highlighting the role of the metal carbene (later termed a metal alkylidene) intermediate.[21] The transformation was proposed to involve the [2+2] cycloaddition of an olefin with a metal alkylidene to form a metallacyclobutane (MCB) intermediate, and subsequent cycloreversion to release new metal alkylidene and olefin products (Scheme 1.1).[21] This proposal was based in part on the observation of a 1:2:1 distribution of C9:C10:C11 products in the cross-metathesis of cyclopentene with 2-pentene, which is not possible for the "conventional mechanism" of Figure 1.3a. The Chauvin mechanism was subsequently supported by isotopic labelling studies.[22-24]

References begin on page 14

Scheme 1.1 Key steps in the Chauvin mechanism: [2+2] cycloaddition to give an MCB intermediate, and cycloreversion to effect olefin exchange.

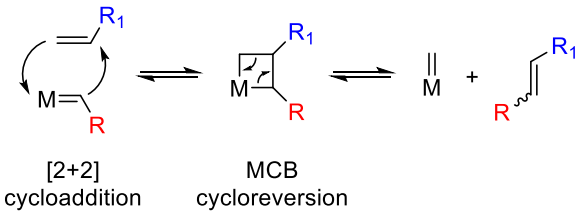

Industrial applications of metathesis began in the late 1960s. Petrochemicals benefitted from the implementation of metathesis for the conversion of low-cost propylene to butene and ethylene.[15] In the Phillips Triolefin Process, a WO_3 catalyst supported on silica was used to catalyze this transformation, with subsequent isomerization to convert 2-butene into high-purity 1-butene. The reverse reaction, known as Olefin Conversion Technology (OCT), gained popularity in the late 1970s as the price of propylene increased. OCT represents an increasingly important application of metathesis in the petrochemicals sector today, as one means of addressing the "propylene deficit" arising from the expanding use of shale gas as a source of petrochemicals. Another major application of industrial metathesis is seen in the Shell Higher Olefin Process (SHOP), in which ethylene is converted into C10-20 α-olefins by successive steps of oligomerization, isomerization, and finally metathesis.[25,26] Olefin products generated by this process have important applications in detergents and lubricants. Finally, ROMP of cyclooctene, dicyclopentadiene, and norbornene is used in the production of polymers for applications ranging from Kevlar to optically clear plastics.[26]

Expanding interest in olefin metathesis spurred the development of "well-defined" molecular catalysts bearing a metal-alkylidene bond (Figure 1.4a). In a breakthrough advance, Schrock reported in 1974 the first synthesis of a metal-alkylidene complex, **Ta-1**.[27] (Of note, the metathesis of cis-2-pentene by a related Ta complex was subsequently described,[28] although the claim of

References begin on page 14

metathesis activity by *any* Ta catalyst has since been called into question).[29] Significantly higher metathesis activity came with Schrock's development of group 6 metal complexes: that is, Mo and W alkylidene complexes such as **Mo-1** and **W-1**.[30-32] These catalysts offered high, tunable activity, owing to the ease with which ligand bulk and electronic properties could be modified, and they are now commercially available.

A major limitation of these catalysts, however, is their instability. Their susceptibility to thermal decomposition, and their high sensitivity to oxygen and water,[33] severely limited their uptake in organic synthesis. More robust catalysts were introduced in the 1990s, when Grubbs reported the first ruthenium metathesis catalysts (see, e.g., **GI**, Figure 1.4b).[34-36] Despite their lower activity relative to the Schrock catalysts, the ease of handling of the ruthenium catalysts was the breakthrough that put metathesis methodologies into the hands of practicing organic chemists. The subsequent development of more reactive "second-generation" catalysts, bearing a stabilizing *N*-heterocyclic carbene (NHC) ligand in place of a phosphine, further expanded their scope. Of the second-generation catalysts reported in 1999 (**GII**[37] and **GII'**;[38] Figure 1.4b), **GII** remains the most popular metathesis catalyst used today, despite the commercially availability of more than 60 alternatives.[39] Currently most important among these, in addition to **GII**, are phosphine-free catalysts such as **HII** (Figure 1.4b).

References begin on page 14

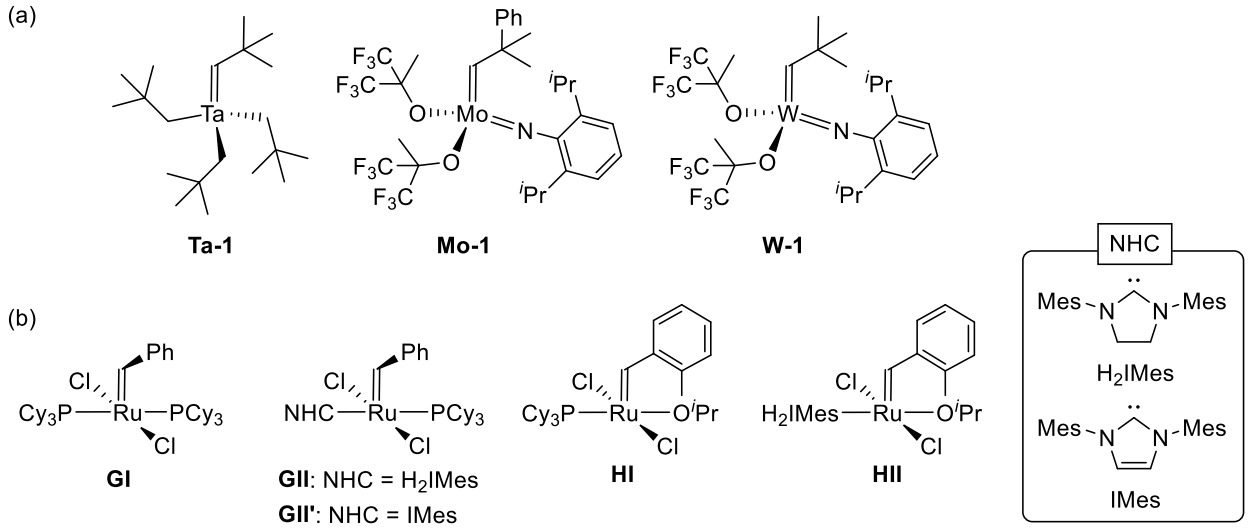

Figure 1.4 (a) Well-defined olefin metathesis catalysts based on group 5 and 6 metals, (b) the Grubbs and Hoveyda catalysts.

1.2.2 Recent Implementations of Metathesis in Industry

Despite the fact that olefin metathesis processes have been used for the production of petrochemicals and polymers since the 1960s, uptake in pharmaceutical and specialty chemicals manufacturing is very recent.[40] The delay in implementation was partially due to sensitivity of the catalysts to oxygen, water, and protic or oxygen-donor functional groups, which greatly hindered their utility (particularly in synthesis of biologically-relevant molecules, which are often rich in N, O, and S moieties). While some of these problems are alleviated by use of ruthenium metathesis catalysts, other challenges hamper use in large-scale metathesis processes. These include removal of the ethylene byproduct, which promotes catalyst decomposition, and the high dilutions required for RCM macrocyclization. Nevertheless, applications of olefin metathesis in pharma have advanced.[40]

One of the key areas of advance in pharma has been in the application of RCM to macrocyclization. In 2005, Boehringer-Ingelheim (BI) reported the first large-scale use of RCM, in a pilot production

References begin on page 14

of the Hepatitis C virus (HCV) inhibitor Ciluprevir for clinical trials (Scheme 1.2).[41,42] This was a remarkable advance, as the first example of RCM on industrial scale. While Ciluprevir ultimately failed in clinical trials and was never commercialized, this pioneering work was influential in expanding consideration of RCM in pharmaceutical process chemistry. The first commercial process involving RCM was Johnson & Johnson's route to HCV inhibitor Simeprevir,[43] rapidly followed by processes for two other HCV drugs, Paritaprevir[44,45] and Vaniprevir[46] (AbbVie and Merck, respectively; Figure 1.5).

Scheme 1.2 Synthesis of Ciluprevir via RCM macrocyclization.

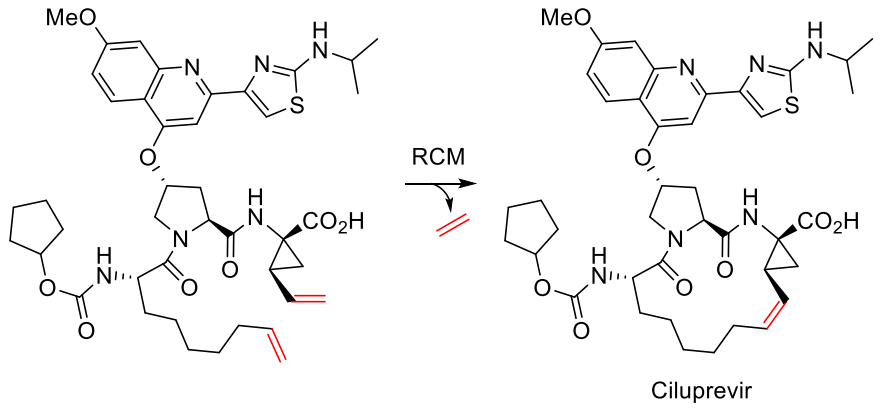

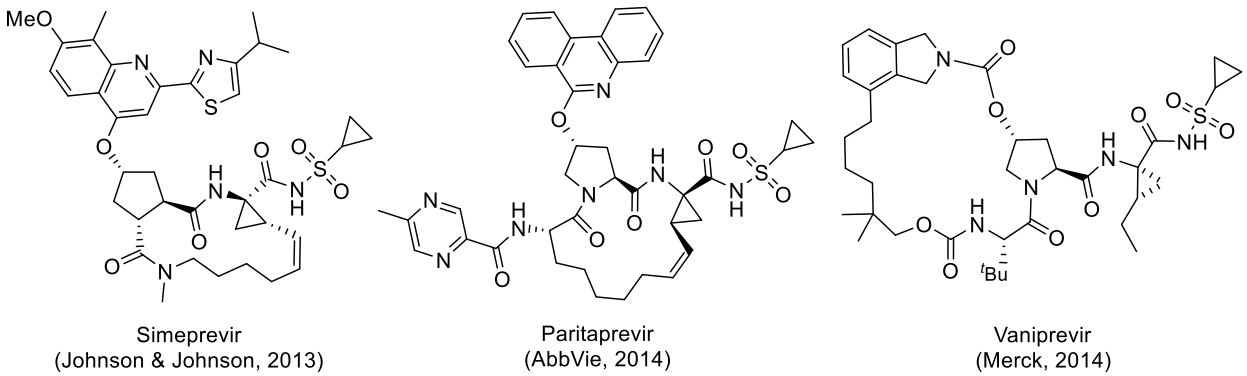

Figure 1.5 Structures of HCV drugs Simeprevir, Paritaprevir, and Vaniprevir

Parallel advances in cross-metathesis for specialty chemicals manufacturing have been claimed, although details are limited. These focus chiefly on high-performance rubbers[47] and metathesis of

References begin on page 14

renewable feedstocks. Metathesis of unsaturated plant oils derived from triglycerides, with successive transesterification, gives rise to many potential synthetic building blocks (Scheme 1.3).[48,49] Elevance Renewable Sciences reported the opening of a manufacturing facility for the metathesis of palm oil in 2013. Given the volumes of unsaturated palm, soy, and canola oil produced annually,[50] this gained much attention for the potential production of added-value specialty products from relatively low-cost renewable feedstocks. Key products include lubricants, fuels, waxes, synthetic oils, and precursors to other specialty chemicals.[40,48,51]

Scheme 1.3 Ethenolysis of plant oil triglycerides, and subsequent transesterification to yield high-value products.

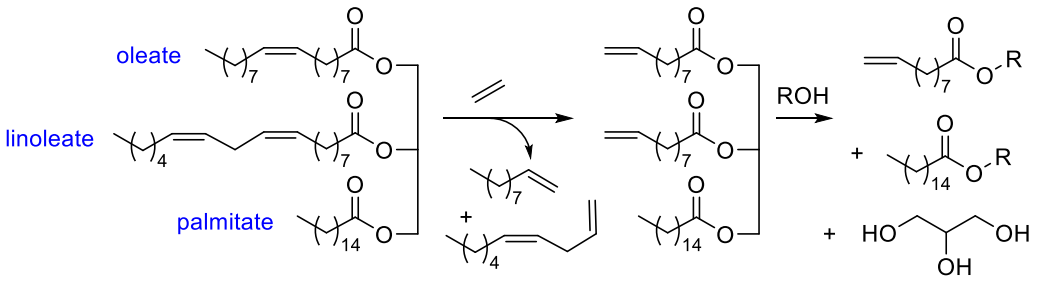

1.2.3 Significance of Catalyst Decomposition

The ruthenium metathesis catalysts are widely claimed to improve functional group tolerance relative to their group 6 predecessors. (This is often overstated: while true for aldehydes and alcohols, polar groups, for example, are often tolerated much better by the Mo and W catalysts).[52] More generally, reports from industry have shown decreased yields or unwanted side reactions in Ru-catalyzed metathesis when trace impurities are present. This is problematic for both product purity and batch reproducibility.[40] In BI's industrial-scale synthesis of Ciluprevir, ppm levels of morpholine (present in the technical-grade toluene solvent) were identified as a key factor limiting metathesis productivity.[41] Likewise, contaminating *N*-methyl morpholine and triphenylphosphine were found to be detrimental in the synthesis of Simeprevir.[53] In addition, residues from upstream

References begin on page 14

processes have been flagged as problematic, particularly N-donors such as 1,8-diazabicyclo[5.4.0]undec-7-ene (DBU) or secondary amines.[54] Catalyst decomposition has an adverse impact on process costs in large-scale syntheses,[53] owing both to decreased productivity (TONs) and the capacity of decomposed Ru products to promote unwanted side reactions.[55]

Olefin isomerization is one of the most significant side reactions triggered by catalyst decomposition,[52,56] generally resulting in the conversion of terminal olefins into internal olefins. Isomerization is widely believed to be promoted by hydridic ruthenium species (Ru-H) generated by catalyst decomposition. These Ru-H complexes may function via a hydride mechanism (Figure 1.6a), or a π-allyl mechanism (Figure 1.6b).[56] However, Carolyn Higman of the Fogg group has shown that RuHCl(CO)(H_2IMes)(PCy_3), one of the candidates most commonly regarded as responsible for isomerization, is not kinetically competent to account for all isomerization observed during metathesis.[57] In subsequent work, isomerization-active Ru nanoparticles (NPs) were shown to form under conditions of metathesis, although details of the pathways by which they are generated are not yet clear.[58]

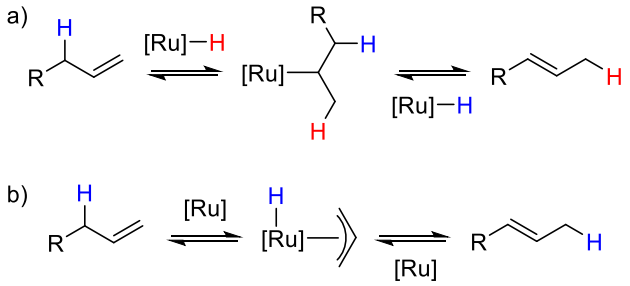

Figure 1.6 Possible mechanisms for olefin isomerization promoted by Ru-H species.

The decomposition products generated during metathesis can give important clues as to how catalyst decomposition occurs, and are therefore valuable in identifying weaknesses in catalyst or process design. To date, the majority of studies examining catalyst stability focus on the readily-

References begin on page 14

accessible precatalysts. However, these often fail to report on decomposition pathways *during* metathesis, as new vulnerabilities emerge in the active catalytic cycle (Scheme 1.4). Notably susceptible to decomposition are the metallacyclobutane (MCB) and the four-coordinate methylidene (which can react with free phosphine to generate the off-cycle resting state species **GIIm**). The MCB intermediate is relatively short-lived, and therefore challenging to study. However, resting state methylidene complexes are isolable, permitting examination of their decomposition in the absence of substrate. Synthesis of **GIIm** was first reported by Grubbs in 2001, albeit in low yields and purity.[59] This important species represents the resting state of the catalyst during metathesis by **GII**. A breakthrough in studying its behaviour was the 2012 report by Justin Lummiss of the Fogg group of a clean, high-yield route to **GIIm** and related species,[60] and his subsequent development of a route to isotopically-labelled ***GIIm**, bearing a ^{13}C-labelled methylidene ligand.[61]

Scheme 1.4 Catalytic cycle for metathesis of terminal olefins by GII, showing key Ru intermediates.

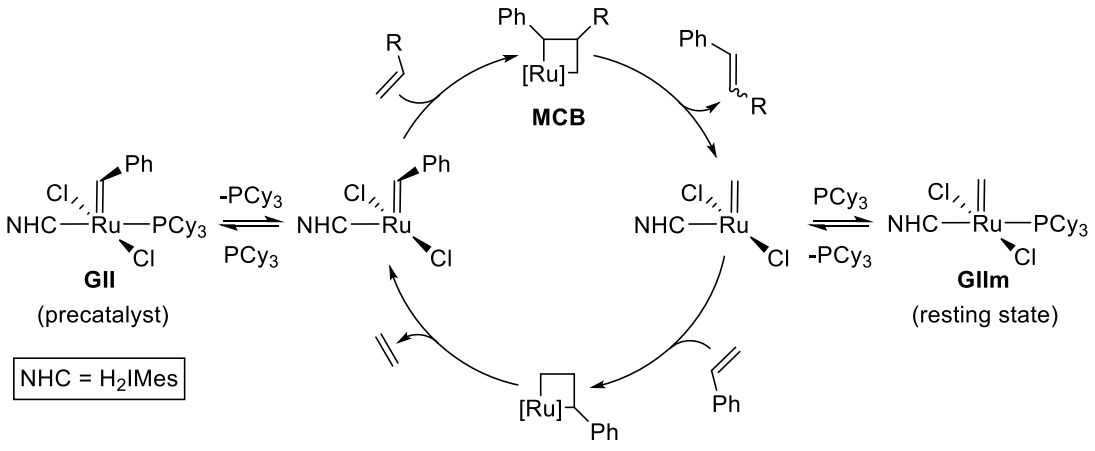

In an important early study using then-available material, Hong and Grubbs reported the thermolysis of **GIIm** in the absence of olefin.[62] The complex was heated for 3 days at 55 ºC, after which dinuclear Ru complex was isolated in 46% yield, and methyl phosphonium salt [MePCy$_3$]Cl

References begin on page 14

was observed (**1**; yield not reported) By analogy to chemistry established for other phosphine-bearing Ru alkylidenes,[63,64] decomposition was proposed to occur by nucleophilic attack of PCy_3 at the methylidene carbon, following which a complex multi-step pathway was suggested (Scheme 1.5). This decomposition process is slow, however, occurring over a span of days, and is therefore unlikely to be a significant contributor to decomposition on the timescale of catalysis (hours). It should be noted that, as with the Ru-H species mentioned above, the dinuclear decomposition product is not kinetically competent to account for the competing isomerization observed during metathesis.[57]

Scheme 1.5 Grubbs' proposed decomposition pathway for the thermolysis of GIIm.

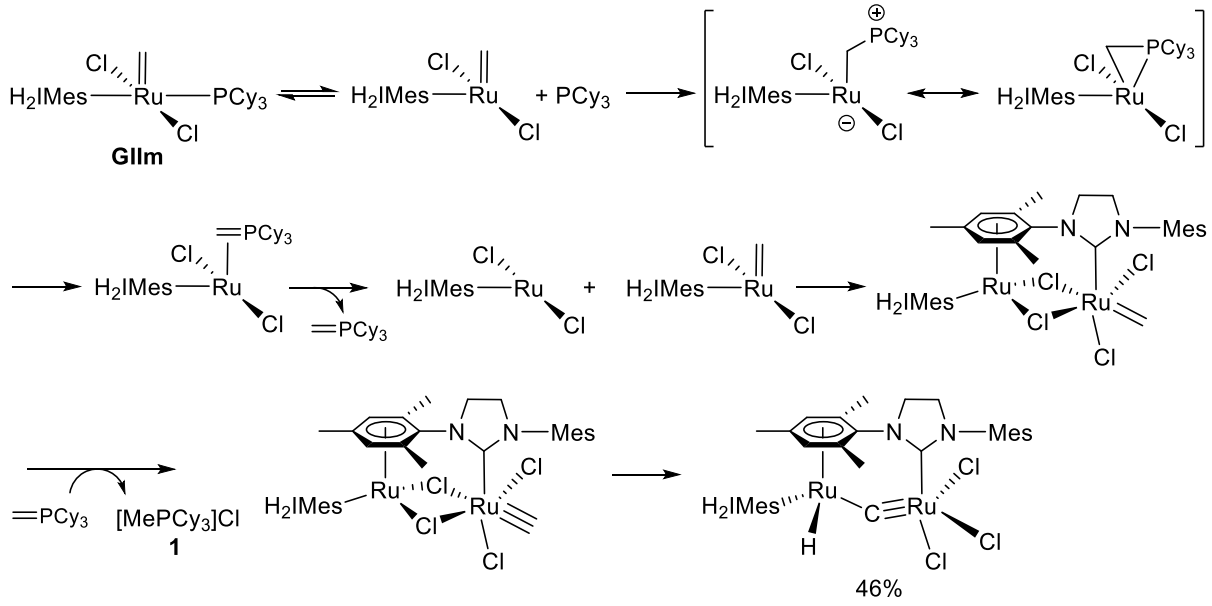

Although the Ru thermolysis product is probably ultimately irrelevant, a key suggestion in this paper was the nucleophilic attack by PCy_3 at the $[Ru]=CH_2$ carbon, with elimination of the methylidene functionality as methylphosphonium salt **1**. This is in fact a primary vector for the decomposition of the four-coordinate methylidene species derived from **GIIm**.[63-65] Justin Lummiss and William McClennan of the Fogg group demonstrated that attack at the methylidene

References begin on page 14

generates a transient σ-alkyl species,[66] which decomposes by facile C-H activation of the cis-NHC ligand.[61,67] This pathway is accelerated in the presence of pyridine, which promotes loss of PCy_3, from **GIIm**.[66]

While this thesis work focuses primarily on the role of phosphine in decomposition of the active methylidene species, MCB decomposition is also important. This too can involve the PCy_3 ligand present in **GII**, as demonstrated by Gwen Bailey of the Fogg group. Specifically, nucleophilic attack of PCy_3 on methyl acrylate was shown to generate a highly basic enolate, which abstracts a proton from the active catalyst[68] (likely from the MCB intermediate; Scheme 1.6). This has now been shown to be one specific example of a more general pathway, in which Brønsted bases with a wide range of base strengths (DBU, NEt_3, and pyrrolidine) deprotonate the MCB, and thus limit catalyst lifetimes.[69,70]

Scheme 1.6 Reaction of PCy_3 with electron deficient olefins, and proposed deprotonation of MCB by phosphonium product.

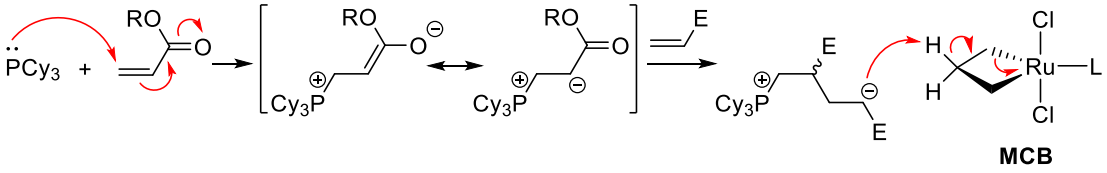

1.3 Scope of this Thesis

As discussed above, phosphine-stabilized metathesis catalysts decompose rapidly in the presence of sterically accessible nitrogen donors, which promote nucleophilic attack of PR_3 at the [Ru]=CH_2 moiety. This thesis work examines the generality of this decomposition pathway, and assesses widely-accepted ideas regarding design criteria for longer-lived catalysts. One simple solution is to replace the phosphine ligand with a low-nucleophilicity alternative. Many phosphine-free catalysts are now available, including **HII**. However, these are generally prepared from the

References begin on page 14

phosphine catalysts, and are therefore more costly. Chapter 2 presents experimental details. Chapter 3 examines "donor-accelerated deactivation" of **GIIm**, with particular respect to the capacity of weaker donors to promote decomposition, and probes the reversibility of PCy_3 attack at the methylidene carbon. Two potential means of increasing catalyst robustness are also considered: first, the feasibility of using phosphine scavengers to prevent methylidene abstraction, and second, the capacity to inhibit C-H activation of the NHC ligand by replacing one *N*-mesityl substituent with *N*-Me. In Chapter 4, the impact of truncating both nitrogen substituents to *N*-Me is examined. The reactions of the IMe_4 ligand with the first-generation Grubbs catalyst **GI** are explored, as well as the behaviour of a methylidene intermediate generated by reaction of **GIm** with this ligand. Ligand truncation is shown to accelerate decomposition of the $[Ru]=CH_2$ moiety by an unexpected pathway. In Chapter 5, the key findings of this thesis work are reviewed, and future work is suggested.

1.4 References

(1) Rothenberg, G., *Catalysis*. Wiley-VCH: Weinheim, 2008.
(2) Thayer, A. M. *Chem. Eng. News,* **2013**, *91*, 68.
(3) Sheldon, R. A., *Green Chemistry and Catalysis*. Wiley-VCH: Chichester, 2007.
(4) Sheldon, R. A. *Green Chem.* **2007**, *9*, 1273–1283.
(5) Knowles, W. S. *Angew. Chem., Int. Ed.* **2002**, *41*, 1999–2007.
(6) Noyori, R. *Angew. Chem., Int. Ed.* **2002**, *41*, 2008–2022.
(7) Sharpless, K. B. *Angew. Chem., Int. Ed.* **2002**, *41*, 2024–2032.
(8) Negishi, E.-i. *Angew. Chem., Int. Ed.* **2011**, *50*, 6738–6764.
(9) Suzuki, A. *Angew. Chem., Int. Ed.* **2011**, *50*, 6722–6737.
(10) Grubbs, R. H. *Angew. Chem., Int. Ed.* **2006**, *45*, 3760–3765.
(11) Schrock, R. R.; *Angew. Chem., Int. Ed.* **2006**, *45*, 3748–3759.
(12) Chauvin, Y. *Angew. Chem., Int. Ed.* **2006**, *45*, 3741–3747.
(13) Crabtree, R. H. *Chem. Rev.* **2015**, *115*, 127–150.
(14) Anderson, A. W.; Merckling, N. G. Polymeric bicyclo[2.2.1]hept-2-ene. U.S. Patent No. 2721189, 1955.
(15) Banks, R. L.; Bailey, G. C. *Ind. Eng. Chem. Prod. Res. Dev.* **1964**, *3*, 170–173.
(16) Natta, G.; Dall'Asta, G.; Mazzanti, G. *Angew. Chem., Int. Ed.* **1964**, *3*, 765–772.
(17) Calderon, N.; Chen, H. Y.; Scott, K. W. *Tetrahedron Lett.* **1967**, 3327–3329.
(18) Calderon, N.; Ofstead, E. A.; Ward, J. P.; Judy, W. A.; Scott, K. W. *J. Am. Chem. Soc.* **1968**, *90*, 4133–4140.

References begin on page 14

(19) Lewandos, G. S.; Pettit, R. *J. Am. Chem. Soc.* **1971**, *93*, 7087-7088.
(20) Grubbs, R. H.; Brunck, T. K. *J. Am. Chem. Soc.* **1972**, *94*, 2538-2540.
(21) Hérisson, J. L.; Chauvin, Y. *Makromol. Chem.* **1971**, *141*, 161–176.
(22) Katz, T. J.; McGinnis, J. *J. Am. Chem. Soc.* **1975**, *97*, 1592–1594.
(23) McGinnis, J.; Katz, T. J.; Hurwitz, S. *J. Am. Chem. Soc.* **1976**, *98*, 605-606.
(24) Grubbs, R. H.; Burk, P. L.; Carr, D. D. *J. Am. Chem. Soc.* **1975**, *97*, 3265-3267.
(25) Keim, W. *Angew. Chem., Int. Ed.* **2013**, *52*, 12492–12496.
(26) Mol, J. C. *J. Mol. Catal. A* **2004**, *213*, 39–45.
(27) Schrock, R. R. *J. Am. Chem. Soc.* **1974**, *96*, 6796–6797.
(28) Schrock, R.; Rocklage, S.; Wengrovius, J.; Rupprecht, G.; Fellmann, J. *J. Mol. Catal.* **1980**, *8*, 73–83.
(29) Katz, T. J. *New J. Chem.* **2006**, *30*, 1844–1847.
(30) Schrock, R. R.; DePue, R. T.; Feldman, J.; Schaverien, C. J.; Dewan, J. C.; Liu, A. H. *J. Am. Chem. Soc.* **1988**, *110*, 1423–1435.
(31) Schrock, R. R.; Murdzek, J. S.; Bazan, G. C.; Robbins, J.; DiMare, M.; O'Regan, M. *J. Am. Chem. Soc.* **1990**, *112*, 3875–3886.
(32) Fox, H. H.; Lee, J. K.; Park, L. Y.; Schrock, R. R. *Organometallics* **1993**, *12*, 759–768.
(33) Schrock, R. R. *Chem. Rev.* **2009**, *109*, 3211–3226.
(34) Nguyen, S. T.; Johnson, L. K.; Grubbs, R. H.; Ziller, J. W. *J. Am. Chem. Soc.* **1992**, *114*, 3974–3975.
(35) Nguyen, S. T.; Grubbs, R. H.; Ziller, J. W. *J. Am. Chem. Soc.* **1993**, *115*, 9858–9859.
(36) Schwab, P.; Grubbs, R. H.; Ziller, J. W. *J. Am. Chem. Soc.* **1996**, *118*, 100–110.
(37) Scholl, M.; Ding, S.; Lee, C. W.; Grubbs, R. H. *Org. Lett.* **1999**, *1*, 953–956.
(38) Huang, J.; Stevens, E. D.; Nolan, S. P.; Petersen, J. L. *J. Am. Chem. Soc.* **1999**, *121*, 2674–2678.
(39) Grela, K., *Olefin Metathesis-Theory and Practice*. Wiley: Hoboken, NJ, 2014.
(40) Higman, C. S.; Lummiss, J. A. M.; Fogg, D. E. *Angew. Chem., Int. Ed.* **2016**, *55*, 3552–3565.
(41) Nicola, T.; Brenner, M.; Donsbach, K.; Kreye, P. *Org. Process Res. Dev.* **2005**, *9*, 513–515.
(42) Tsantrizos, Y. S.; Ferland, J.-M.; McClory, A.; Poirier, M.; Farina, V.; Yee, N. K.; Wang, X.-j.; Haddad, N.; Wei, X.; Xu, J.; Zhang, L. *J. Organomet. Chem.* **2006**, *691*, 5163–5171.
(43) Rosenquist, Å.; Samuelsson, B.; Johansson, P.-O.; Cummings, M. D.; Lenz, O.; Raboisson, P.; Simmen, K.; Vendeville, S.; de Kock, H.; Nilsson, M.; Horvath, A.; Kalmeijer, R.; de la Rosa, G.; Beumont-Mauviel, M. *J. Med. Chem.* **2014**, *57*, 1673−1693.
(44) Niu, D.; Liu, D.; Moore, J. D.; Xu, G.; Sun, Y.; Gai, Y.; Tang, D.; Or, Y. S.; Wang, Z. Preparation of quinoxalinyl macrocycles, especially quinoxalinyloxyproline-containing cyclic peptides, as hepatitis C virus (HCV) NS3-NS4A protease inhibitors for use in pharmaceutical compositions containing a cytochrome P450 monooxygenase inhibitor. US20090005387A1, 2009.
(45) Enanta Pharmaceutical. Annual Report. Filed with the United States Security and Exchange Commission, **2014**.
(46) Kong, J.; Chen, C.-Y.; Balsells-Padros, J.; Cao, Y.; Dunn, R. F.; Dolman, S. J.; Janey, J.; Li, H.; Zacuto, M. J. *J. Org. Chem.* **2012**, *77*, 3820–3828.
(47) Ong, C.; Mueller, J. M. Ruthenium based catalysts for the metathesis of nitrile rubbers. WO2011023674A1, 2011.

References begin on page 14

(48) Chikkali, S.; Mecking, S. *Angew. Chem., Int. Ed.* **2012**, *51*, 5802−5808.
(49) Biermann, U.; Bornscheuer, U.; Meier, M. A. R.; Metzger, J. O.; Schafer, H. J. *Angew. Chem., Int. Ed.* **2011**, *50*, 3854–3871.
(50) US Department of Agriculture, Oil Crops Yearbook (Online), Table 47, accessed July 21, **2015**. http://www.ers.usda.gov/data-products/oil-crops-yearbook.aspx.
(51) Dubois, J.-L., Refinery of the future: Feedstock, process, products. In *Biorefinery: from Biomass to Chemicals and Fuels*, Aresta, M.; Dibenedetto, A.; Dumeignil, D., Eds. Walter de Gruyter: Berlin, 2013; Vol. 2.
(52) van Lierop, B. J.; Lummiss, J. A. M.; Fogg, D. E., Ring-Closing Metathesis. In *Olefin Metathesis-Theory and Practice*, Grela, K., Ed. Wiley: Hoboken, NJ, 2014; pp 85–152.
(53) Farina, V.; Horváth, A., Ring-Closing Metathesis in the Large-Scale Synthesis of Pharmaceuticals. In *Handbook of Metathesis*, Grubbs, R. H.; Wenzel, A. G., Eds. Wiley-VCH: Weinheim, 2015; Vol. 2, pp 633–658.
(54) Wang, H.; Goodman, S. N.; Dai, Q.; Stockdale, G. W.; Clark, W. M. *Org. Process Res. Dev.* **2008**, *12*, 226–234.
(55) Schrodi, Y., Mechanisms of Olefin Metathesis Catalyst Decomposition and Methods of Catalyst Reactivation. In *Handbook of Metathesis*, Grubbs, R. H.; Wenzel, A. G., Eds. Wiley-VCH: Weinheim, 2015; pp 323–342.
(56) Larionov, E.; Li, H.; Mazet, C. *Chem. Commun.* **2014**, *50*, 9816–9826.
(57) Higman, C. S.; Plais, L.; Fogg, D. E. *ChemCatChem* **2013**, *5*, 3548-3551.
(58) Higman, C. S.; Lanterna, A. E.; Marin, M. L.; Scaiano, J. C.; Fogg, D. E. *ChemCatChem* **2016**, *8*, 2446–2449.
(59) Sanford, M. S.; Love, J. A.; Grubbs, R. H. *J. Am. Chem. Soc.* **2001**, *123*, 6543–6554.
(60) Lummiss, J. A. M.; Beach, N. J.; Smith, J. C.; Fogg, D. E. *Catal. Sci. Technol.* **2012**, *2*, 1630–1632.
(61) Lummiss, J. A. M.; Botti, A. G. G.; Fogg, D. E. *Catal. Sci. Technol.* **2014**, *4*, 4210–4218.
(62) Hong, S. H.; Day, M. W.; Grubbs, R. H. *J. Am. Chem. Soc.* **2004**, *126*, 7414–7415.
(63) Werner, H.; Stuer, W.; Weberndorfer, B.; Wolf, J. *Eur. J. Inorg. Chem.* **1999**, 1707–1713.
(64) Hansen, S. M.; Rominger, F.; Metz, M.; Hofmann, P. *Chem. – Eur. J.* **1999**, *5*, 557–566.
(65) Galan, B. R.; Pitak, M.; Keister, J. B.; Diver, S. T. *Organometallics* **2008**, *27*, 3630–3632.
(66) Lummiss, J. A. M.; McClennan, W. L.; McDonald, R.; Fogg, D. E. *Organometallics* **2014**, *33*, 6738–6741.
(67) Trnka, T. M.; Morgan, J. P.; Sanford, M. S.; Wilhelm, T. E.; Scholl, M.; Choi, T.-L.; Ding, S.; Day, M. W.; Grubbs, R. H. *J. Am. Chem. Soc.* **2003**, *125*, 2546–2558.
(68) Bailey, G. A.; Fogg, D. E. *J. Am. Chem. Soc.* **2015**, *137*, 7318–7321.
(69) Lummiss, J. A. M.; Ireland, B. J.; Sommers, J. M.; Fogg, D. E. *ChemCatChem* **2014**, *6*, 459–463.
(70) Ireland, B. J.; Dobigny, B. T.; Fogg, D. E. *ACS Catal.* **2015**, *5*, 4690−4698.

References begin on page 14

Chapter 2. Experimental Methods

2.1 General Procedures

2.1.1 Reaction Conditions

Reactions were carried out under N_2 using standard glovebox and Schlenk techniques,[1] unless otherwise noted. Clean glassware was oven-dried at 110 °C for at least 1 h, then allowed to cool under vacuum prior to use. Room temperature is ca. 25 °C for glovebox work, or 23 °C for Schlenk work. Reactions above RT were carried out using a thermostatted oil bath.

2.1.2 Reagents

Reagents PCy_3 (97%, Strem), CuCl (97%, Sigma-Aldrich), CuI (98%, Sigma-Aldrich), 2,6-dichlorobenzenethiol (97%, Alfa Aesar), HBF_4 (48 wt% in H_2O, Sigma-Aldrich), $NaBF_4$ (>98%, Sigma-Aldrich), $NaBAr_4^F$ (98%, Strem), NaH (95%, Sigma-Aldrich), KH (99%, Fisher Scientific), potassium (98% in mineral oil, Sigma-Aldrich), ethylene (BOC Ultra-High Purity Grade 3.0, 99.9%, Linde), Amberlyst-15 ion exchange resin (Sigma-Aldrich), and standards 1,3,5-trimethoxybenzene (TMB, Sigma-Aldrich), dimethyl terephthalate (DMT, >99%) dodecane (>99%, Sigma-Aldrich), potassium hydrotris(1-pyrazolyl)borate (KTp, >99%, Sigma-Aldrich), pyrene (98%, Sigma-Aldrich), and anthracene (97%, Sigma-Aldrich) were used as received. Pyridine (>99%, Fisher), NEt_3 (99%, Alfa Aesar), DMSO (>99%, BDH), and MeCN (>99%, Fisher) were distilled from CaH_2 under N_2. Hexamethylphosphoramide, tetramethyl urea (both 99%, Sigma-Aldrich), diethyl diallylmalonate (DDM; 98%, Sigma-Aldrich), and deionized water were degassed by five consecutive freeze-pump-thaw cycles and stored under N_2 in the glovebox.

The following materials were prepared according to literature procedures: the first-generation Grubbs catalyst $RuCl_2(PCy_3)_2(=CHPh)$ **GI**,[2] its methylidene resting state $RuCl_2(PCy_3)_2(=CH_2)$

References begin on page 30

GIm,[3] the second-generation catalysts $RuCl_2(NHC)(PCy_3)(=CHPh)$ (**GII**,[4] NHC = H_2IMes; **GII'**,[5] NHC = IMes) and their corresponding methylidene species $RuCl_2(NHC)(PCy_3)(=CH_2)$ (**GIIm**,[3] NHC = H_2IMes; **GIIm'**,[3] NHC = IMes), alkylphosphonium species $RuCl_2(CH_2PCy_3)(py)_3$ **Ru-2a**[6] and $RuCl_2(CH_2PCy_3)(DMSO)_3$ **Ru-2b**,[7] H_2IMes,[8] IMes,[9] Merrifield-I,[10] 1-methyl-3-(2,4,6-trimethylphenyl)imidazolium iodide **2a**,[11] and 1,3,4,5-tetramethylimidazole-2(3H)-thione **3**[12].

2.1.3 Solvents

Dry, oxygen-free hexanes, THF, C_6H_6, CH_2Cl_2, C_7H_8, and Et_2O were obtained using a Glass Contour or Anhydrous Engineering solvent purification system (SPS), and stored in the glovebox. Karl-Fisher titrations prior to sieve treatment were performed on hexanes, THF, C_6H_6, and CH_2Cl_2 by Alexandre Goudreault of this research group: hexanes (4.1 ppm), THF (3.6 ppm), C_6H_6 (4.1 ppm), CH_2Cl_2 (5 ppm). Standard distillation methods[13] were used to purify and degas other solvents: MeOH from I_2-activated Mg turnings, acetone from $CaSO_4$, and pentane (Fisher ACS grade, pre-dried for 24 h over $MgSO_4$) from P_2O_5. All organic solvents were stored in the glovebox over activated 4 Å sieves for at least 16 h prior to use, with the exception of MeOH (stored over 3 Å sieves) and acetone, which was not stored over sieves, as they cause self-condensation.

2.1.4 Deuterated Solvents

Deuterated solvents (Cambridge Isotopes or Sigma Aldrich) were used as received for the NMR analysis of air-stable species. For analysis of oxygen- and moisture-sensitive species, deuterated solvents were degassed by five consecutive freeze-pump-thaw cycles and stored in the glovebox over activated 4 Å sieves for at least 16 h prior to use, with the exception of DCE-d_4 which was obtained in ampoules packed under N_2 and used as received.

References begin on page 30

2.1.5 Instrumentation

2.1.5.1 NMR Spectroscopy

^{1}H, $^{13}C\{^{1}H\}$, $^{31}P\{^{1}H\}$, ^{19}F, and ^{1}H-^{1}H NOESY/EXSY NMR spectra were recorded on a Bruker Avance 300, Avance II 300, or Avance 400 spectrometer at RT unless otherwise noted. ^{1}H and $^{13}C\{^{1}H\}$ spectra were referenced to the residual proton or carbon signal of the deuterated solvent used; $^{31}P\{^{1}H\}$ spectra were referenced externally to 85% H_3PO_4 at 0 ppm. For oxygen- and moisture-sensitive samples, spectra were acquired in screw-top (J. Young or Rotoflo) NMR tubes.

2.1.5.2 Gas Chromatography

GC quantification was performed on an Agilent 7890A or 7683B Series autosampling GC, each equipped with a flame ionization detector (FID) and an Agilent HP-5 polysiloxane column (30 m length, 320 μm diameter). An inlet split ratio of 10:1 was used, with an inlet temperature of 250 ºC. Helium (UHP grade) was used as the carrier gas to maintain a column pressure of 11.5 psi, and the FID response was maintained between 5 – 2000 ρA. Samples were diluted with CH_2Cl_2 (ACS reagent grade) prior to injection, giving analyte concentrations of ca. 5 mM. Retention times for substrates, products, and internal standards were confirmed by GC-MS and NMR analysis. For GC quantification, calibration curves (peak area vs. concentration) were constructed for substrates and products relative to internal standard (decane or dodecane) in the relevant concentration regime, to account for the dependence of signal intensity on detector response. Conversions and yields for catalytic runs were measured by integration of peak areas for the analyte relative to internal standard, and compared to the initial ratios.

2.1.5.3 MALDI-TOF Mass Spectrometry

Mass spectra were recorded on a Bruker Daltonics UltraFleXtreme MALDI time-of-flight (MALDI-TOF) spectrometer interfaced to an N_2-filled glovebox. Matrix (pyrene or anthracene;

References begin on page 30

100 mM) and analyte (5 mM) stock solutions were prepared in the glovebox in either C_6H_6 or CH_2Cl_2, and mixed in a 25:1 ratio, giving a final matrix to analyte ratio of 500:1.[14] MALDI target plates were spotted by the dried-droplet method in ca. 2 μL aliquots, then inserted into the spectrometer loading chamber via a custom-designed anaerobic interface. Samples were analyzed immediately to minimize premature matrix evaporation.

2.2 Experimental Data for Chapter 3

2.2.1 Impact of Lewis Donors on RCM with $RuCl_2(H_2IMes)(PCy_3)(=CHPh)$ GII

In a representative procedure using H_2O as the donor, a Schlenk tube was loaded with diethyl diallylmalonate (48 mg, 0.2 mmol), dodecane (34 mg, 0.2 mmol; internal standard), H_2O (90 μL, 0.01 mmol) and toluene (1.8 mL). An aliquot was removed for GC-FID analysis to establish the starting ratio of DDM to dodecane. To the flask was added catalyst **GII** from a stock solution in toluene (33 μL of a 3.0 mM solution containing 12.8 mg **GII** in 5.0 mL toluene; 0.001 mmol, 0.05 mol%). The reaction was heated for 2 h at 50 ± 1 °C in an oil bath in the glovebox. A sample was then removed, quenched with KTp (10 mg/mL in THF; 10 equiv vs **GII**), and analyzed by GC-FID; see Appendix A1.3, Figure A7, and Table 3.1 in Chapter 3.

References begin on page 30

2.2.2 Reaction of $RuCl_2(IMes)(PCy_3)(=CH_2)$ GIIm' with Lewis Donors

In these experiments, the total methylidene integration (^{1}H NMR analysis) was measured vs. the internal standard TMB after 2 h and 4 h at 50 °C, and percent decomposition was calculated. $^{31}P\{^1H\}$ NMR analysis was used to identify deactivation products. A representative procedure using 10 equivalents of DMSO as the Lewis donor is shown below.

In the glovebox, a J. Young NMR tube was charged with **GIIm'** (231 μL of a 43.3 mM stock solution in C_6D_6; 0.01 mmol) and TMB (ca. 1 mg), followed by 369 μL of C_6D_6 to bring the sample to a total concentration of 17 mM **GIIm'**. The sample was removed from the glovebox and a ^{1}H NMR spectrum was measured to establish the **GIIm'** : TMB ratio at t_0. The NMR tube was returned to the glovebox and DMSO (7 μL, 0.1 mmol, 10 equiv) was added. The sample was shaken to mix and heated in an oil bath at 50 ºC. At 2 h and 4 h, ^{1}H and $^{31}P\{^1H\}$ NMR spectra were obtained. For DMSO (10 equiv) after 2 h: $^{31}P\{^1H\}$ NMR (121 MHz, C_6D_6): δ 40.7 (s, 88%, **GIIm'**), 33.9 (s, 7%, $[MePCy_3]Cl$), 10.4 (s, 5%, PCy_3). ^{1}H NMR (300 MHz, C_6D_6): δ 18.75 (s, 88%, [Ru]=CH_2 of **GIIm'**). For representative spectra for the DMSO experiment above, see Appendix A1.2, Figures A5 and A6.

2.2.3 Probing Reactivity of $RuCl_2(CH_2PCy_3)L_3$ (L = py, DMSO) σ-alkyl Complexes Ru-2

In a representative procedure, a solution of **Ru-2a** (11 mg, 0.016 mmol) and DMT (ca. 3 mg, internal standard) in C_6D_6 (660 μL) was added to a J. Young NMR tube in the glovebox. A ^{1}H NMR spectrum was measured to establish the starting ratio of **Ru-2a** to DMT. The sample was returned to the glovebox, and DDM (40 mL, 0.16 mmol, 10 equiv) was added. The tube was shaken vigorously to effect mixing. No colour change was observed. ^{1}H NMR spectra measured at 15 min and 2 h showed no alkylidene signals, and no RCM product. The tube was then heated to 80 °C. No change was evident after 24 h.

References begin on page 30

2.2.4 Representative Procedure for RCM in the Presence of Phosphine Scavengers

RCM of DDM was carried out in both THF (0.1 mol% **GII**) and toluene (0.005 mol% **GII**), with catalyst loading such that the control experiments did not afford complete conversion to the ring-closed product. Scavengers used: CuCl, CuI, Amberlyst-15 resin, benzyl iodide, and Merrifield-I resin. A representative procedure is given with CuI in THF.

A 4 mL vial in the glovebox was charged with DDM (48 mg, 0.2 mmol), dodecane (34 mg, 0.2 mmol; internal standard), and THF (1.9 mL). An aliquot was removed for GC-FID analysis to establish the starting ratio of DDM to dodecane. CuI (19 mg, 0.1 mmol, 50 mol%) and **GII** (16 μL of a 13 mM stock containing 10.9 mg **GII** in 1.0 mL THF; 0.0002 mmol, 0.1 mol%) were then added, and the suspension was stirred at room temperature for 24 h. A sample was then removed, quenched with KTp (10 mg/mL in THF), and analyzed by GC-FID (see Figure 3.4, Chapter 3).

2.2.5 Synthesis of 1-methyl-3-(2,4,6-trimethylphenyl)imidazolium tetrafluoroborate 2b

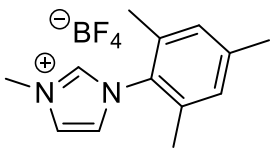

Synthesis of 1-methyl-3-(2,4,6-trimethylphenyl)imidazolium iodide **2a** was prepared by the method reported by Strassner et al.[11] Conversion to the tetrafluoroborate salt **2b** was effected by dissolving **2a** (1.00 g, 3.05 mmol) in H_2O (60 mL) and adding HBF_4 (0.5 mL, 4 mmol, 1.3 equiv) dropwise. The solution was left to stir for 16 h, after which a black precipitate (I_2) had formed. The latter was removed by filtration, and the filtrate was concentrated by rotary evaporation to give quantitative yield of **2b**. ^{1}H NMR ($CDCl_3$): δ 9.29 (s, 1H, N-C*H*-N), 7.76 (t, $^2J_{H\text{-}H}$ = 1.6 Hz, 1H, MeNC*H*=CH), 7.19 (t, $^2J_{H\text{-}H}$ = 1.7 Hz, 1H, Mes-N-C*H*=CH), 6.99 (s, 2H, Mes-*H*), 4.24 (s, 3H, N-CH_3), 2.33 (s, 3H, Mes *p*-CH_3), 2.06 (s, 3H, Mes *o*-CH_3). See Appendix A1.1, Figure A1.

References begin on page 30

2.2.6 Synthesis of 1-methyl-3-(2,4,6-trimethylphenyl)imidazole-2-ylidene (IMeMes)

Free IMeMes was prepared by analogy to the method for H_2IMes.[8] Accordingly, imidazolium tetrafluoroborate salt **2b** (870 mg, 3.0 mmol) was deprotonated with NaH (188 mg, 7.8 mmol, 2.6 equiv) in THF (15 mL) to afford the product as a brown oil. Yield: 540 mg (2.7 mmol, 90%). ^{1}H NMR (C_6D_6): δ 6.77 (s, 2H, Mes-*H*), 6.40 (d, $^3J_{H\text{-}H}$ = 3.6 Hz, 1H, Me-N-C*H*), 6.40 (d, $^3J_{H\text{-}H}$ = 3.6 Hz, 1H, Mes-N-C*H*), 3.47 (s, 3H, N-CH_3), 2.13 (s, 3H, Mes *p*-CH_3), 2.10 (d, 4JH-H, 6H, Mes *o*-CH_3). See Appendix A1.1, Figure A2.

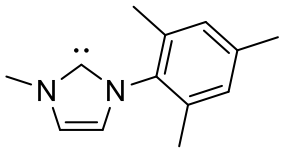

2.2.7 Synthesis of $RuCl_2(PCy_3)$(IMeMes)(=CHPh) Ru-6

$RuCl_2(PCy_3)$(IMeMes)(=CHPh) **Ru-6** was prepared by a glovebox method analogous to that for **GII**,[4] using IMeMes in place of H_2IMes. Accordingly, IMeMes (185 mg, 0.925 mmol, 2.7 equiv) was slowly added to a stirred solution of **GI** (280 mg, 0.340 mmol) in THF (7.5 mL) at room temperature. Stirring was continued until no **GI** remained (^{1}H NMR analysis; 48 h). Amberlyst-15 resin (434 mg, 2.04 mmol, 6 equiv) was then added to sequester the free PCy_3, and the suspension was stirred for 2.5 h at room temperature. The resin was filtered off, and the filtrate was concentrated to a black solid. Yield **Ru-6**/**7**: 206 mg (82%). Key ^{1}H NMR data (300 MHz, C_6D_6): δ 19.88 ppm (s, 20%, **Ru-6** rotamer), 19.74 ppm (s, 32%, **Ru-7**), 19.37 ppm (s, 48%, **Ru-6** rotamer). $^{31}P\{^1H\}$ NMR (121 MHz, C_6D_6): 35.4 (s, 34%, **Ru-6**), 10.4 (s, 66%, PCy_3). See Appendix 1.1, Figure A3. For VT $^{31}P\{^1H\}$ NMR spectrum, see Appendix A1.1, Figure A4.

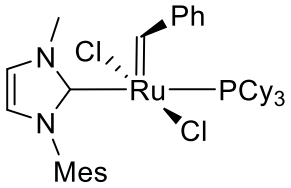

References begin on page 30

2.2.8 Activity of Ru-6 in the RCM of DDM

A 4 mL vial in the glovebox was loaded with diethyl diallylmalonate (48.1 mg, 0.2 mmol), dodecane (34.1 mg, 0.2 mmol; internal standard), and toluene (2 mL). An aliquot was removed for GC-FID analysis to establish the starting ratio of DDM to dodecane. To the vial, catalyst **Ru-6** was added (250 μL of a 11.9 mg/2 mL stock solution in toluene, 0.002 mmol, 1 mol%; note that catalyst is a mixture of ca. 68% **Ru-6** and 32% **Ru-7**). The reaction was heated at 40 ± 1 °C in an oil bath in the glovebox. Aliquots were removed at 15 min, 2 h, 5 h, and 25 h, quenched with KTp (10 mg/mL in THF; 10 equiv vs **GII**), and analyzed by GC-FID.

2.3 Experimental Data for Chapter 4

2.3.1 Synthesis of 1,3,4,5-tetramethylimidazol-2-ylidene (IMe_4)

In a modified version of a reported procedure,[12] thione **3** (1.51 g, 9.66 mmol) was dissolved in THF (60 mL) in a Schlenk flask in the glovebox, and the solution was chilled to -35 °C. Metallic potassium was removed from the mineral oil in which it was stored, cut into small pieces and rinsed with hexanes. Potassium chunks (4.5 g, 115 mmol, 12 equiv) were added to the chilled Schlenk flask, a condenser was attached, and the system was sealed and removed to the Schlenk line. The reaction was refluxed under N_2 for 4 h, over which time the potassium began to break into small fragments. A colour change from yellow to pale purple occurred within 1 h, and to pale green after an additional 2 h. The flask was returned to the glovebox, and the suspension filtered through Celite. The product was washed through with THF (3 x 5 mL), and the clear yellow filtrate was stripped to a tan solid, which was dissolved in C_6H_6 (10 mL) and filtered again. The filtrate was concentrated and the solid was washed with pentane (3 x 5 mL) to give clean IMe_4 as a pale yellow solid. Yield: 539 mg (45%). ^{1}H NMR (300 MHz, C_6D_6): δ 3.37 (s, 6H, N-CH_3), 1.58 (s, 6H, C-CH_3). See Appendix A2.1, Figure A8.

References begin on page 30

2.3.2 Synthesis of $[Ru_2(\mu\text{-}Cl)_3(IMe_4)_4(=CHPh)_2]Cl$ Ru-11a

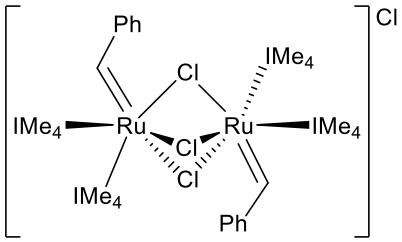

In the glovebox, a white powder of free IMe_4 (38 mg, 0.3 mmol, 2.1 equiv) was added to a purple solution of **GI** (120 mg, 0.15 mmol) in 15 mL C_6H_6. The solution immediately changed colour to brown. The solution was stirred for 18 h at 23 °C, over which time a green solid deposited. The solid was collected on a fine frit, and washed with benzene (3 x 2 mL) and pentane (3 x 2 mL) to obtain **Ru-11a** as an emerald-green powder. Yield: 50 mg (67%). ^{1}H NMR analysis of the combined brown filtrate and washings revealed multiple alkylidene-containing products. ^{1}H NMR of **Ru-11a** (DCE-d_4, 500 MHz, 298 K; for numbering system, see the Appendix A2.1, Figure A9: δ 20.93 (br s, $\Delta\omega_{1/2}$ = 6.6 Hz, [Ru]=C*H*Ph, H^{15}), 20.71 (br s, $\Delta\omega_{1/2}$ = 12.3 Hz, [Ru]=C*H*Ph, H^{15}), 20.43 (br s, $\Delta\omega_{1/2}$ = 9.2 Hz, [Ru]=C*H*Ph, H^{15}), 7.48 (t, $^3J_{H\text{-}H}$ = 7.0 Hz, 1H, H^{19}), 7.41 (d, $^3J_{H\text{-}H}$ = 7.4 Hz, 2H, H^{17}), 7.29–7.04 (overlapping multiplet, 2H, H^{18}), 4.39 (s, 3H, H^1), 3.93 (s, 3H, H^4), 2.83 (s, 3H, H^8), 2.14 (s, 3H, H^2), 2.05 (s, 3H, H^3), 1.96 (s, 3H, H^7), 1.68 (s, 3H, H^6), 1.51 (s, 3H, H^5). ^{13}C{^{1}H} NMR (DCE-d_4, 125.7 MHz, 298 K) δ 322.7 (C^{16}, located via the ^{1}H-^{13}C HMQC correlation with H^{15}), 172.6 (C^9 or C^{10}), 171.6 (C^{10} or C^9), 154.8 (C^{16}), 130.3–128.3 (overlap; C^{17}, C^{18}, C^{19}), 126.7 (C^{11}), 126.3 (two overlapping s, C^{12}, C^{14}), 125.1 (C^{13}), 36.4 (C^4), 35.4 (C^1), 34.6 (C^8), 32.5 (C^5), 9.9–8.9 (4 overlapping s, C^2, C^3, C^6, C^7). Satisfactory microanalysis could not be obtained, despite multiple attempts. For ^{1}H-^{1}H EXSY/NOESY spectrum, see Appendix 2.1A, Figure A10.

References begin on page 30

2.3.3 Assessment of $[Ru_2(\mu\text{-}Cl)_3(IMe_4)_4(=CHPh)_2]Cl$ Ru-11a Activity in RCM of DDM

A 4 mL vial was loaded with diethyl diallylmalonate (481 mg, 2 mmol), decane (285 mg, 2 mmol) and DCE (0.62 mL). A ca. 10 μL aliquot was removed for GC-FID analysis to establish the starting ratio of substrate to decane. **Ru-11a** (10.2 mg, 0.01 mmol, 1 mol% Ru) was then added, and the reaction was stirred open to a well-purged glovebox atmosphere for 24 h. Aliquots were taken from the stirred reaction at specific time intervals, quenched with KTp,[15] diluted with CH_2Cl_2 on the bench, and analyzed by GC-FID. See Figure 4.4 in Chapter 4.

2.3.4 Synthesis of $[Ru_2(\mu\text{-}Cl)_3(IMe_4)_4(=CHPh)_2]BF_4$ Ru-11b

In the glovebox, a 20 mL vial was loaded with **Ru-11a** (49.7 mg, 0.0487 mmol), $NaBF_4$ (10.7 mg, 0.0974 mmol, 2 equiv), and CH_2Cl_2 (5 mL). The reaction was stirred for one hour at room temperature, and reaction completion was determined by ^{19}F NMR (no change by ^1H NMR when counterion changed from Cl^- to BF_4^-). ^{19}F NMR (CH_2Cl_2, 282 MHz) δ -149.9 (s), -150.0 (s). See Appendix A2.1, Figure A11.

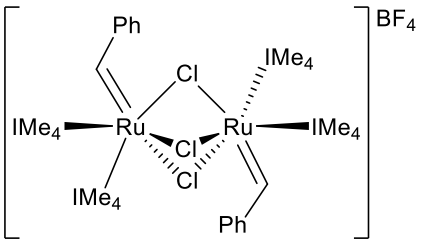

2.3.5 Synthesis of $[RuCl(IMe_4)_2(=CHPh)]_2[BAr_4F]_2$ Ru-12

In the glovebox, a 2-necked round bottom flask was charged with **Ru-11a** (48.6 mg, 0.0476 mmol), $NaBAr_4^F$ (84.7 mg, 0.0956 mmol, 2.0 equiv), and 10 mL CH_2Cl_2. The green solution was taken to the Schlenk line and refluxed for 1 h. The reaction was returned to the glovebox and filtered through Celite to remove NaCl. The product was washed through with CH_2Cl_2 (3 x 2 mL), and the filtrate was concentrated to a dark green solid. Yield **Ru-12**: 57 mg (45%). ^1H NMR (300 MHz, $CDCl_3$): δ 19.66 (s, 1H, [Ru]=C*H*Ph), 7.71

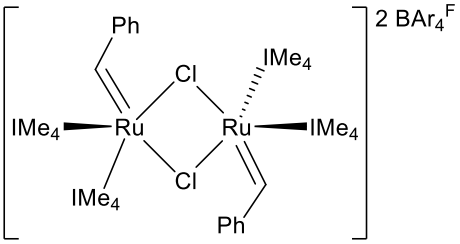

References begin on page 30

(s, 8H, BAr_4^F o-*H*), 7.53 (s, 4H, BAr_4^F p-*H*), 7.94–6.79 (overlapping m, 9H, [Ru]=CH*Ph*), 4.57 (s, 3H, IMe_4 N-*Me*), 4.39 (s, 3H, IMe_4 N-*Me*), 2.13 (s, 3H, IMe_4-*Me*), 2.09 (s, 3H, IMe_4-*Me*), 1.60 (s, 3H, IMe_4-*Me*), 1.30 (s, 3H, IMe_4-*Me*), 1.07 (s, 3H, IMe_4-*Me*). See Appendix A2.1, Figure A12. Complete removal of grease from the Ru dimer was not possible, as the complex oils out of aromatic and aliphatic solvents.

2.3.6 Synthesis of potassium 2,6-dichlorobenzenethiolate (4)

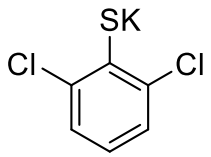

The synthesis was adapted from the method reported by Jensen.[16] Modifications included the use of pyridine in workup, and of KH suspended in mineral oil, rather than solid KH. In the glovebox, a Schlenk flask was charged with potassium hydride (30 wt% in mineral oil, 1.09 g, 8.16 mmol, 1.5 equiv) and THF (10 mL). Dropwise addition of a solution of 2,6-dichlorobenzenethiol (1.005 g, 5.615 mmol) in THF (30 mL) to the stirred mixture caused a milky white suspension to form, accompanied by H_2 gas. After 30 min, the flask was removed to the Schlenk line and heated to 50 °C for 25 min under N_2. THF was removed by vacuum, leaving a white residue which was returned to the glovebox. The solid was dissolved in a minimum volume of pyridine, and the solution was filtered through a plug of Celite, which was washed with pyridine until washings were colourless. The combined filtrate was concentrated until a white precipitate began to deposit. Hexanes (10 mL) were then added to precipitate a white solid, which was collected on a fine frit and washed with hexanes (4 x 5 mL). The solid was dried under vacuum. Yield: 0.513 g (42%). The product was insoluble in benzene, but ^{1}H NMR analysis in C_6D_6 was nevertheless useful in confirming complete consumption of the thiol precursor (SH singlet 4.35 ppm).

References begin on page 30

2.3.7 Synthesis of Ru(S(2,6-dichlorobenzene))$_2$(PCy$_3$)$_2$(=CHPh) Ru-13

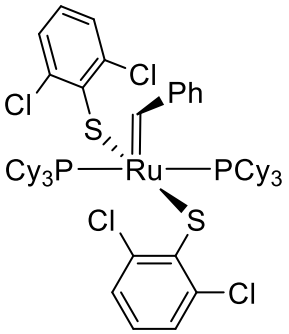

The synthesis was adapted from the method reported by Jensen,[16] but modified to use C_6H_6 in the workup rather than THF. In the glovebox, purple **GI** (0.100 g, 0.122 mmol) was suspended in C_7H_7 (4 mL) and THF (1 mL), and potassium 2,6-dichlorobenzenethiolate **4** (57.0 mg, 0.26 mmol, 2.2 equiv) was added to the stirred reaction. A dark brown solution was present after 2 h at RT. The solvent was stripped off, and the brown residue was redissolved in C_6H_6 (8 mL). The solution was filtered through Celite and concentrated to the point of saturation. Slow, dropwise addition of pentane afforded a purple-brown precipitate. The suspension was cooled to -35 °C, and the precipitate was filtered off while cold, washed with -35 °C pentane (4 x 2 mL), and dried under vacuum. **Ru-13** was isolated as a purple-brown solid (83.0 mg, 61% yield). ^{1}H NMR (300 MHz, C_6D_6) δ 15.85 (d, $^4J_{H\text{-}H}$ = 11.5 Hz, 1H, [Ru]=C*H*Ph), 7.62 (d, $^3J_{H\text{-}H}$ = 6.9 Hz, 2H, *o*-Ph), 7.03 (m, 3H, *m*-Ph, *p*-Ph), 6.85 (d, $^3J_{H\text{-}H}$ = 7.9 Hz, 4H, *m*-SAr), 6.25 (t, $^3J_{H\text{-}H}$ = 8.0 Hz, 2H, *p*-SAr), 2.76 – 0.32 (m, 66H, PCy$_3$). ^{31}P{^{1}H} NMR (121 MHz, C_6D_6) δ 54.9 (s). See Appendix A2.1, Figure A13.

2.3.8 Addition of IMe$_4$ to Ru(S(2,6-dichlorobenzene))$_2$(PCy$_3$)$_2$(=CHPh) Ru-13

Using 1 equiv IMe$_4$: In the glovebox, a solution of **Ru-13** (335 μL of a 10.0 mg/670 μL stock solution in C_6D_6; 0.0045 mmol) in C_6D_6 (500 μL) was prepared in a 4 mL vial. To the stirred brown solution, IMe$_4$ (26 μL of a 10.0 mg/460 μL stock solution in C_6D_6; 0.0045 mmol, 1.0 equiv) was added dropwise. The solution was stirred for 4 d at RT, until no further changes were observed for the ^{1}H NMR alkylidene integrations. Over this time, no colour change was observed. Key NMR signals: ^{1}H NMR (300 MHz, C_6D_6): δ 20.00 (s, 5%, [Ru]=C*H*Ph of bis-IMe$_4$ complex **Ru-15**),

References begin on page 30

16.73 (s, 18%, [Ru]=C*H*Ph of mono-IMe$_4$ complex **Ru-14**), 15.85 (d, $^3J_{H\text{-}P}$ = 11.3 Hz, 77%, [Ru]=C*H*Ph of **Ru-13**). See Appendix A2.2, Figure A14a.

Using 2 equiv IMe$_4$: In the glovebox, a solution of **Ru-13** (335 μL of a 10.0 mg/670 μL stock solution in C_6D_6; 0.0045 mmol) in C_6D_6 (300 μL) was prepared in J. Young NMR tube. To this brown solution, IMe$_4$ (11 μL of a 10.0 mg/100 μL stock solution in C_6D_6; 0.0090 mmol, 2.0 equiv) was added. After 24 h at RT, no colour change was observed. Key NMR signals: ^{1}H NMR (300 MHz, C_6D_6): δ 20.00 (s, 34%, [Ru]=C*H*Ph of bis-IMe$_4$ complex **Ru-15**), 16.73 (s, 9%, [Ru]=C*H*Ph of mono-IMe$_4$ complex **Ru-14**), 15.85 (d, $^3J_{H\text{-}P}$ = 11.1 Hz, 57%, [Ru]=C*H*Ph of **Ru-13**). ^{1}H NMR (300 MHz) of alkylidene region after addition of $CDCl_3$ (0.3 mL): δ 21.11, 20.83, 20.34 (three singlets, 35%, **Ru-11a**); 19.95 (d, $^3J_{H\text{-}P}$ = 15.3 Hz, 8%, **Ru-14**); 15.71 (d, $^3J_{H\text{-}P}$ = 11.8 Hz, 57%, **Ru-13**). See Appendix A2.2, Figure A14b.

2.3.9 Reaction of GIm with IMe$_4$

In the glovebox, pink **GIm** (6.6 mg, 0.0088 mmol) and DMT (ca. 1 mg; internal standard) were dissolved in C_6D_6 (1 mL) in a J. Young NMR tube, and the initial ratio of methylidene signal to DMT were established by ^{1}H NMR. IMe$_4$ (4.5 mg, 0.036 mmol, 4.1 equiv) was added to this solution, affording an immediate colour change from pink to pale orange, with deposition of a grey precipitate. ^{1}H NMR (300 MHz, C_6D_6) of supernatant: δ 3.71 (s, 12H, **Ru-16** N-C*H*$_3$), 1.96–1.07 (overlapping m, 66H, PCy$_3$), 1.79 (s, 12H, **Ru-16** C-C*H*$_3$). See Appendix A2.2, Figure A15. ^{31}P{^{1}H} NMR (121 MHz, C_6D_6): δ 10.4 (100%, PCy$_3$). See Appendix A2.2, Figure A16. ^{1}H NMR (300 MHz, $CDCl_3$) of precipitate (key identified signals): δ 3.82 (s, 6H, **5** N-C*H*$_3$), 3.34 (q, 2H, $^3J_{H\text{-}H}$ = 7.5 Hz, **5** C-C*H*$_2$-CH$_3$), 2.25 (s, 6H, **5** C-C*H*$_3$), 1.28 (t, 3H, $^2J_{H\text{-}H}$ = 7.4 Hz, **5** C*H*$_2$-C*H*$_3$). See Appendix A2.2, Figure A17. Key MALDI-TOF MS signals from supernatant are summarized in Appendix A2.3, Table A1. For mass spectrum, see Appendix A2.3, Figure A18. Key MALDI-

References begin on page 30

TOF MS signal from precipitate: (anthracene matrix; m/z) 153.089 ($C_7H_{17}N_2$, imidazolium salt **5**; calcd 153.139). See Appendix A2.3, Figure A19.

2.4 References

(1) Shriver, D. F.; Drezdzon, M. A., *The Manipulation of Air-Sensitive Compounds*. 2nd Ed. ed.; John Wiley & Sons: New York, 1986.
(2) Schwab, P.; Grubbs, R. H.; Ziller, J. W. *J. Am. Chem. Soc.* **1996**, *118*, 100–110.
(3) Lummiss, J. A. M.; Beach, N. J.; Smith, J. C.; Fogg, D. E. *Catal. Sci. Technol.* **2012**, *2*, 1630–1632.
(4) van Lierop, B. J.; Reckling, A. M.; Lummiss, J. A. M.; Fogg, D. E. *ChemCatChem* **2012**, *4*, 2020–2025.
(5) Scholl, M.; Trnka, T. M.; Morgan, J. P.; Grubbs, R. H. *Tetrahedron Lett.* **1999**, *40*, 2247–2250.
(6) Lummiss, J. A. M.; McClennan, W. L.; McDonald, R.; Fogg, D. E. *Organometallics* **2014**, *33*, 6738–6741.
(7) McClennan, W. L.; Rufh, S. A.; Lummiss, J. A. M.; Fogg, D. E. *J. Am. Chem. Soc.* **2016**, *138*, 14668−14677.
(8) Bates, J. M. Ruthenium Catalysts for Olefin Metathesis: Understanding the Boomerang Mechanism and Challenges Associated with Stereoselectivity. M.Sc. Dissertation, University of Ottawa, Ottawa, ON, 2014.
(9) Arduengo, A. J.; Dias, H. V. R.; Harlow, R. L.; Kline, M. *J. Am. Chem. Soc.* **1992**, *114*, 5530–5534.
(10) Zhao, X.; Ivanova, N.; Hadzovic, A.; Zimmer-De Iuliis, M.; Lough, A. J.; Morris, R. H. *Organometallics* **2008**, *27*, 503–508.
(11) Ahrens, S.; Peritz, A.; Strassner, T. *Angew. Chem., Int. Ed.* **2009**, *48*, 7908–7910.
(12) Kuhn, N.; Kratz, T. *Synthesis* **1993**, 561–562.
(13) Armarego, W. L. F.; Perrin, D. D., *Purification of Common Laboratory Chemicals*. 4th Ed. ed.; Butterworth-Heinemann: Oxford, 1997.
(14) Bailey, G. A.; Fogg, D. E. *ACS Catal.* **2016**, *6*, 4962–4971.
(15) Blacquiere, J. M.; Jurca, T.; Weiss, J.; Fogg, D. E. *Adv. Synth. Catal.* **2008**, *350*, 2849–2855.
(16) Jensen, V. R.; Occhipinti, G.; Hansen, F. R. Novel Olefin Metathesis Catalyts. WO 2012/032131 A1, 2012.

References begin on page 30

Chapter 3. Phosphine-Mediated Catalyst Decomposition: Assessment of Problems and Potential Solutions

Parts of this Chapter have been published. Sections 3.2.1 and 3.2.2 are reprinted with permission from: Donor-Induced Decomposition of the Grubbs Catalysts: Lewis Donors Accelerate Methylidene Abstraction. William L. McClennan, Stephanie A. Rufh, Justin A. M. Lummiss, and Deryn E. Fogg.* *J. Am. Chem. Soc.* **2016**, 138, 14668-14677. (http://pubs.acs.org/doi/abs/10.1021%2Fjacs.6b08372)

Author contributions: McClennan, Rufh, Lummiss, and Fogg wrote the manuscript. Decomposition studies of **GIIm** were carried out by McClennan, decomposition studies of **GIIm'** by Rufh. Catalysis with **GII** in the presence of donors carried out by Rufh.

3.1 Introduction

Primary and secondary amines,[1-4] as well as pyridine[5,6] and other nitrogen donors,[2,4,6-8] are known to be detrimental to metathesis productivity. This is particularly problematic in pharmaceutical manufacturing, where even trace amounts of such impurities have been shown to negatively impact RCM yields and batch reproducibility.[9-14] A common decomposition product for the second-generation Grubbs catalyst (**GII**) is the methylphosphonium salt [$MePCy_3$]Cl **1**.[15] Hong and Grubbs observed this byproduct, albeit in unknown amounts, following thermolysis of the resting-state methylidene species $RuCl_2(H_2IMes)(PCy_3)(=CH_2)$ **GIIm** (Scheme 3.1).[15] At the time, it was unclear whether formation of **1** occurred by intramolecular migration of PCy_3 (as reported by the Diver group for decomposition of **GI** by isocyanides),[16] or by PCy_3 loss and intermolecular attack.

Scheme 3.1 Thermolytic decomposition of GIIm in the absence of olefin

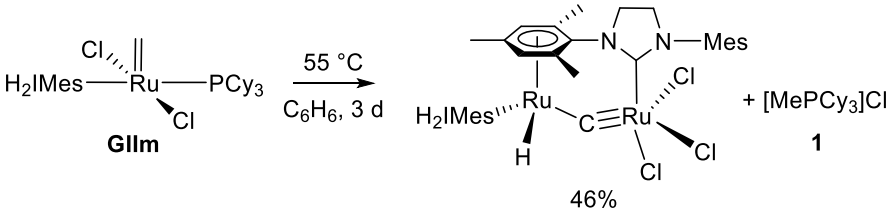

References begin on page 49

The second possibility would account for the slow rate of this process (which requires days at 55 °C in benzene), given the very low lability of the PCy_3 ligand in **GIIm**.[17,18] Importantly, however, Justin Lummiss of the Fogg group demonstrated that this decomposition pathway is dramatically faster (<5 min) in the presence of pyridine.[5] This was proposed to be due to accelerated loss of PCy_3 from **GIIm** following pyridine binding, which enables formation of σ-alkyl species **Ru-1a** (Scheme 3.2a) by nucleophilic attack of free PCy_3 on the [Ru]=CH_2 moiety. Elimination of the alkylphosphonium ligand as phosphonium salt **1** was attributed to C-H activation of a mesityl *o*-CH_3 group on the H_2IMes ligand and chloride abstraction. While **Ru-1a** is a transient intermediate, it was successfully trapped for the first-generation Grubbs methylidene (**GIm**), for which σ-alkyl species **Ru-2a** was isolated in 95% yield (Scheme 3.2b).

Scheme 3.2 Accelerated decomposition of methylidene complexes on exposure to pyridine. (a) Pathway proposed for GIIm. (b) Pathway observed for GIm.[a]

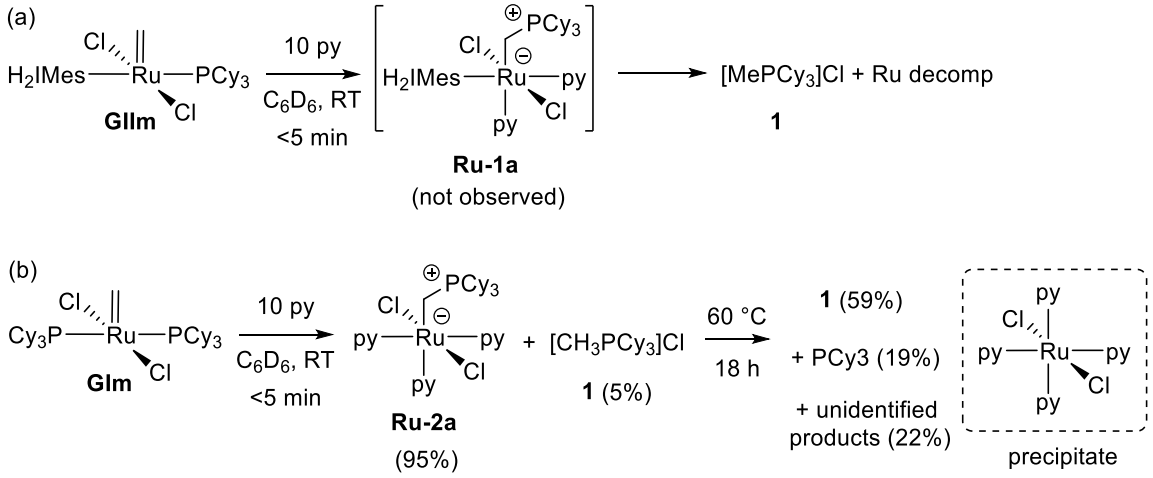

[a]Percentage shown is the proportion of total $^{31}P\{^1H\}$ NMR integration.

On longer thermolysis (18 h at 60 °C), tris-pyridine intermediate **Ru-2a** decomposed to yield several products, among which [$MePCy_3$]Cl **1** predominated (59% of total $^{31}P\{^1H\}$ NMR integration). The longer lifetime of the σ-alkyl intermediate **Ru-2a** relative to **Ru-1a** was attributed

References begin on page 49

to the presence of the H_2IMes ligand in the latter. Through C-H activation, the mesityl groups offer a proton source in proximity to the [Ru]-CH_2PCy_3 functionality. Elimination of **1** and cyclometallation (Scheme 3.3) is rapid.

Scheme 3.3 C-H activation of H_2IMes, and its subsequent cyclometallation.

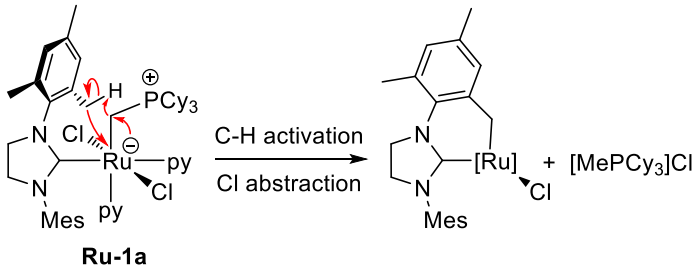

Ru-1a

This Chapter examines the scope of this decomposition pathway with respect to donor. Of particular interest is the effect of oxygen donors such as water and THF, given that metathesis in aqueous and ethereal media has been promoted as a potentially "greener" approach to process chemistry.[19-23] As well, several potential means of limiting such PR_3-promoted decomposition pathways are examined. While avoiding phosphine ligands in the catalyst is the most obvious solution (and many phosphine-free catalysts are now commercially available; Figure 3.1), their higher cost is unfavourable. An alternative solution involves use of a phosphine scavenger to remove free PCy_3 from the system following initiation, but before methylidene abstraction can occur (Scheme 3.4). This could offer improved catalyst productivity for existing catalysts; that is, without the need for new catalysts designed for tolerance toward nucleophiles.

References begin on page 49

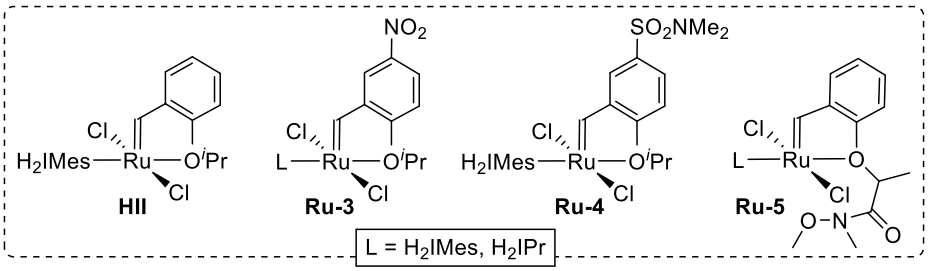

Figure 3.1 A selection of phosphine-free metathesis catalysts

Scheme 3.4 Transforming PCy_3-stabilized GII into a phosphine-free catalyst with a phosphine scavenger.

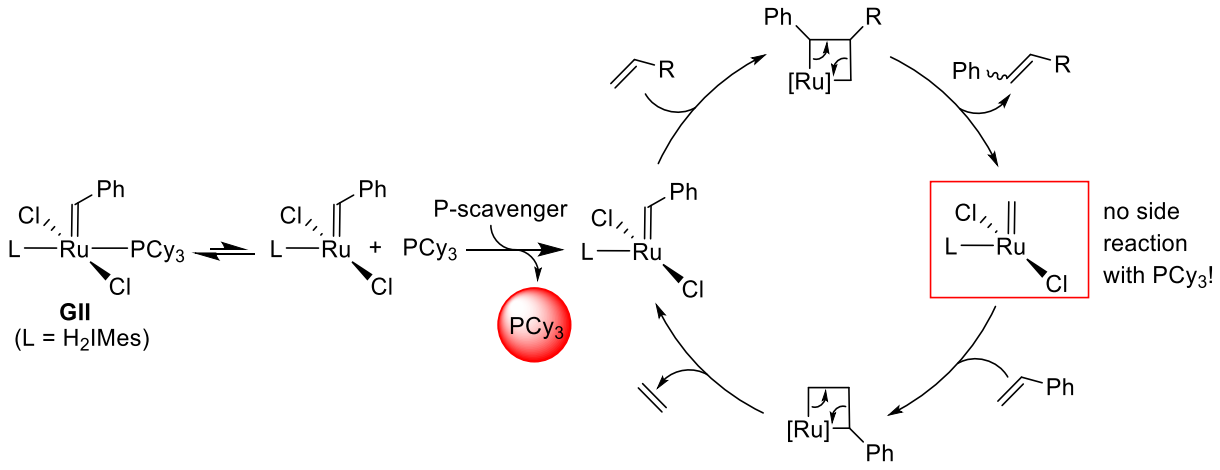

Phosphine scavenging during metathesis has used chiefly copper(I) halides. The Grubbs group showed that the ill-defined salt CuCl improves turnover numbers (TONs) in simple RCM reactions promoted by **GI**, although catalyst lifetimes suffered, with catalyst death sometimes observed before 95% conversion.[24] Results of phosphine-scavenging in metathesis with CuCl were not as impressive in second-generation systems, however. In a later study, Grubbs examined the impact of CuCl in cross-metathesis reactions of methyl vinyl ketone, with 5 mol% **GII** + 1.0 PCy_3 as the catalyst.[25] In this report, yields dropped by 50% relative to the control reaction with no added CuCl. Conversely, Lipshutz and co-workers reported that CuI in fact increased yields in **GII**-

References begin on page 49

promoted cross-metathesis of acrylates.[26] This proved most effective when metathesis was performed in ethereal solvents rather than the usual chlorinated or aromatic solvents.

Phosphine sequestration has also been pursued in *synthesis* of metathesis catalysts. Of particular interest are resin additives (Figure 3.2), which are attractive for the simplicity of workup. Thus, in synthesis of complexes such as **GII**, the byproduct PCy_3 can be removed by simple filtration, rather than extraction with pentane, which results in product losses. Building on a patent by Verpoort and co-workers,[27] Bianca van Lierop of the Fogg group described the efficacy of sulfonic acid resin Amberlyst-15 in the synthesis of a range of second-generation metathesis catalysts from their first-generation analogues.[28] This resin is highly effective in the removal of free PCy_3 (as well as excess NHC). However, extended exposure of the Ru products in solution causes competing decomposition. The Lipshutz and Morris groups independently reported that neutral Merrifield resins (specifically, the iodide resin Merrifield-I) could be successfully used as a phosphine scavenger.[29,30] In the Morris work, Merrifield-I was used to remove PPh_3 and $O{=}PPh_3$ byproducts formed in the synthesis of Ru hydride complexes, albeit with the caveat of halide exchange.[29] In the present chapter, CuCl, CuI, Amberlyst-15, and Merrifield-I were explored as candidates for phosphine sequestration during metathesis. Benzyl iodide was also examined, as a molecular analogue to the Merrifield-I resin.

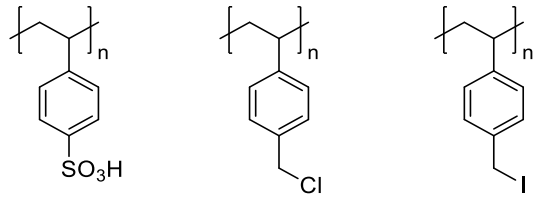

Figure 3.2 Amberlyst and Merrifield resins explored

References begin on page 49

A more fundamental approach to improving catalyst lifetime is ligand redesign, as noted above. In a recent review, Crabtree commented that "slimming" of the NHC ligand is expected to be the key to preventing C-H activation.[31] The Blechert group reported that truncating an H_2IMes mesityl group to methyl (Figure 3.3) resulted in metathesis activity comparable to **GII**.[32] However, decomposition was not examined. A final aspect of this Chapter therefore sought to examine whether C-H activation is indeed inhibited for the smaller NHC. To that end, the previously unreported unsaturated analogue, IMeMes (the structure of which provides a bridge to the fully truncated IMe_4 ligand discussed in the next Chapter) was synthesized and incorporated into a Grubbs-type catalyst.

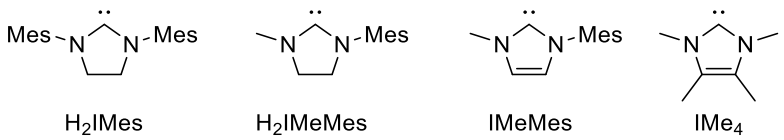

Figure 3.3 Structures of NHC ligands: H_2IMes and variants with truncated *N*-groups.

3.2 Results and Discussion

3.2.1 Impact of Lewis Donors on Metathesis with GII

The deleterious impact of amines in metathesis reactions catalyzed by **GII**[2] was noted above. The rapidity of decomposition, and the co-formation of [$MePCy_3$]Cl **1**, testify to the capacity of such *N*-donors to decompose the catalyst by methylidene abstraction. To assess the impact of weaker donors, we examined the metathesis productivities attainable for diethyl diallylmalonate (DDM) in the presence of added water or methanol, or in neat THF, MeCN, or DMSO. DDM was chosen as a test substrate in this chemistry because it is very readily cyclized, and any inhibiting effect is therefore an indication of serious problems.

References begin on page 49

The results are collected in Table 3.1. In the control experiment in anhydrous toluene, RCM was quantitative after 2 h at 50 °C at a catalyst loading of 0.05 mol%. This corresponds to a turnover number of 2,000. In neat THF, RCM activity dropped by more than 30%, to a TON of 1,440. The presence of 5% degassed H_2O in toluene caused a 65% drop in TON. With 5% MeOH, MeCN, and DMSO, the impact was even more detrimental: for the DMSO reaction, metathesis was essentially quenched. As noted above, the ease with which DDM normally undergoes RCM underlines the severity of this degradation in performance. It is worth pointing out that use of lower temperatures (i.e. reaction at 30 °C) does not inhibit methylidene abstraction. Indeed, the impact of donors on total metathesis productivity was in general even more deleterious at 30 °C, in keeping with prior findings that rates of metathesis increase faster at higher temperature than rates of decomposition.[7,33]

Table 3.1 Donor-Accelerated Decomposition: Impact of Weak Donors on Metathesis Productivity[a]

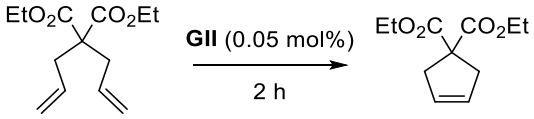

		%conv. (TON)[a]	
Entry	Solvent medium	50 °C	30 °C
1	toluene	100 (2000)[b]	100 (2000)[c]
2	THF	72 (1440)	13 (260)
3	20:1 toluene–H_2O	35 (700)	24 (480)
4	20:1 toluene–MeOH	18 (360)	5 (100)
5	20:1 toluene–MeCN	13 (260)	17 (340)
6	20:1 toluene–DMSO	1 (20)	1 (20)

[a]Calibrated GC-FID analysis; ± 2% in replicate runs. [b]Quantitative within 10 min. [c]Quantitative within 60 min.

References begin on page 49

3.2.2 Accelerated Decomposition of GIIm' in the Presence of Lewis Donors

To confirm that the damaging impact of these additives is indeed due to accelerated methylidene abstraction, their reactions with the resting-state methylidene complexes (both **GIIm** and its less labile IMes analogue **GIIm'**) were explored. Experiments with **GIIm** were carried out by Billy McClennan of the Fogg group. Shown in Table 3.2 is the proportion of [$MePCy_3$]Cl **1** formed, and the proportion of **GIIm** or **GIIm'** lost, after 2 h. In all cases, these amounts tally closely, indicating that methylidene abstraction is indeed the major pathway. The extent of decomposition should be compared to a baseline value of 10% or 3% for **GIIm** or **GIIm'**, respectively, in base-free control experiments (entry 1). Values for pyridine are shown as the final table entry, for comparison. In all cases, the trend seen with the IMes complex **GIIm'** parallels that with **GIIm**. While stronger Ru−PCy_3 binding for **GIIm'** relative to **GIIm** (in which the NHC backbone is saturated) lessens the impact on decomposition rates, it is important to note that this also limits entry into the active cycle for metathesis.

The NEt_3, phosphoramide, and urea additives shown in entries 2−4 were chosen for the detrimental impact of these and related nitrogen bases reported in other contexts, including in metathesis promoted by phosphine-free catalysts.[4,7,9,13,34,35] None show any significant impact, indicating that the Lewis basicity of the donor is irrelevant, if steric congestion hampers access to the methylidene ligand.[36] This is consistent with a prior finding by Justin Lummiss of this research group, which indicated that added DBU did not trigger methylidene abstraction during metathesis by **GII**.[2] Recent work by Gwen Bailey of this research group confirms that the negative impact of such bulky Lewis bases is due to deprotonation of the metallacyclobutane intermediate.[37]

Of note, however, even relatively weak donors such as MeCN, THF, and H_2O accelerate decomposition (entries 5−7). Addition of MeCN had minimal impact in small amounts (10 equiv),

References begin on page 49

but decomposition was quantitative at 2 h in neat MeCN (entries 5a, 5b). Similarly, while 10 equiv THF and H_2O proved relatively innocuous, a 10-fold increase led to ca. 30% or 50% decomposition, respectively, notwithstanding the weak oxophilicity of these ruthenium complexes. The heightened effect of water and methanol, relative to THF (entries 7a and 9, vs 6a), may be due to attractive hydrogen-bonding interactions between these H-bond donors and the chloride ligands. Additional decomposition pathways could be envisaged for these protic entities. While many reports take for granted the idea that water is well tolerated by Ru catalysts,[19,20,38] the Cazin group recently showed otherwise.[39] Likewise, methanol could be profoundly destructive, particularly if methoxides can be generated.[40] However, the phosphonium salt **1** was the sole or dominant phosphorus product in all cases, indicating that methylidene abstraction is the principal vector for decomposition.

Table 3.2 Loss of GIIm and GIIm', and Yield of [$MePCy_3$]Cl (1) on Treatment with L-Donors (*n* Equiv.) for 2 h at 50 °C[a]

Entry	L-donor	*n*	% **GIIm** lost (% **1** formed)	% **GIIm'** lost (% **1** formed)
1	none	0	10 (10)	3 (N.D.)
2	NEt_3	10	11 (11)	3 (N.D.)
3	$O=P(NMe_2)_3$	10	13 (13)	3 (N.D.)
4	$O=C(NMe_2)_2$	10	16 (16)	100 (83)
5a	MeCN	10	11 (11)	3 (N.D.)
5b		neat	100 (100)	
6a	THF	10	20 (20)	8 (8)
6b		100	30 (30)	
7a	H_2O	10	25 (25)	10 (10)
7b		100	49 (49)	
8a	DMSO	10	35 (35)	18 (16)
8b		100	93 (93)	
9	MeOH	10	49 (49)	29 (29)
10	pyridine	10	100 (100)[b]	100 (90)[c]

References begin on page 49

[a]C_6D_6 solvent, [Ru] = 20 mM. % Loss of **GIIm'** determined by ^{1}H NMR analysis, by integration of the methylidene signal vs internal standard (TMB); % **1** by $^{31}P\{^1H\}$ NMR analysis, as a percentage of total integration. N.D. = not determined; peak intensity insufficient for reliable ^{31}P NMR integration. **GIIm'** completes the mass balance, except where noted. [b]Complete in <10 min at RT. [c]For L = py, free PCy_3 accounts for the discrepancy between % **GIIm'** lost and % **1** formed.

The capacity of MeCN, THF, DMSO, H_2O, and MeOH to accelerate methylidene abstraction is important in understanding the poor metathesis performance of phosphine-functionalized catalysts in these solvents.[19,20,41,42] More generally, it provides the first clear explanation for low metathesis productivities in polar media, despite the correlation between solvent polarity and faster initiation (phosphine loss)[18] established for **GII**. This behavior is of particular note given interest in metathesis in water and "green" solvents, often bearing ether donors.[19-23] The impact of water holds arguably even greater significance, given its ubiquity as a contaminant in synthetic and process chemistry.

3.2.3 Probing the Reversibility of Nucleophilic PCy_3 Attack

An important question in this chemistry is whether PCy_3 attack at the [Ru]=CH_2 carbon to form the [Ru]–CH_2PCy_3 species is truly irreversible. If it is reversible, re-entry into the catalytic cycle and further metathesis should be possible (Scheme 3.5a). A simple test would involve reaction of an isolated σ-alkyl complex with a substrate such as DDM, to see if metathesis is observed. Ideally, such a complex would bear a strong donor (e.g. an NHC or PCy_3 ligand), which confers metathesis activity. However, C-H activation of such complexes is too high to permit isolation. In the H_2IMes system, the σ-alkyl complex cannot be observed, let alone isolated, while the IMes derivative is only transiently observed.[43] The only isolable σ-alkyl complexes known to date are the tris-L complexes **Ru-2**,[5,43] in which L represents pyridine and DMSO. While these compounds may be

References begin on page 49

insufficiently electron-rich at Ru to support metathesis, treatment with simple substrate DDM was pursued, in hopes that even minimal metathesis activity might be observed.

In these experiments (Scheme 3.5), the σ-alkyl complexes **Ru-2** were treated with DDM, the high metathesis activity of which was noted above (Scheme 3.5b). No metathesis was observed for pyridine-stabilized **Ru-2a** on addition of 10 equiv DDM, even after 24 h at 80 ºC. DMSO-stabilized **Ru-2b** was treated with a larger excess of DDM (100 equiv) under the same conditions, but again, no metathesis activity was observed. As noted above, the absence of metathesis activity in this experiment is not explicit evidence that PCy_3 attack at $[Ru]=CH_2$ is irreversible. This could potentially be probed further by (a) testing with norbornene, which readily undergoes metathesis with less electron-rich Ru centers; (b) undertaking ligand exchange of **Ru-2b** with a truncated NHC, to ensure metathesis activity without undergoing C-H activation. The latter option was explored by indirect means in a later section of this Chapter.

Scheme 3.5 Probing the reversibility of PCy_3 attack at $[Ru]=CH_2$: Reaction of σ-alkyl complexes Ru-2 with DDM

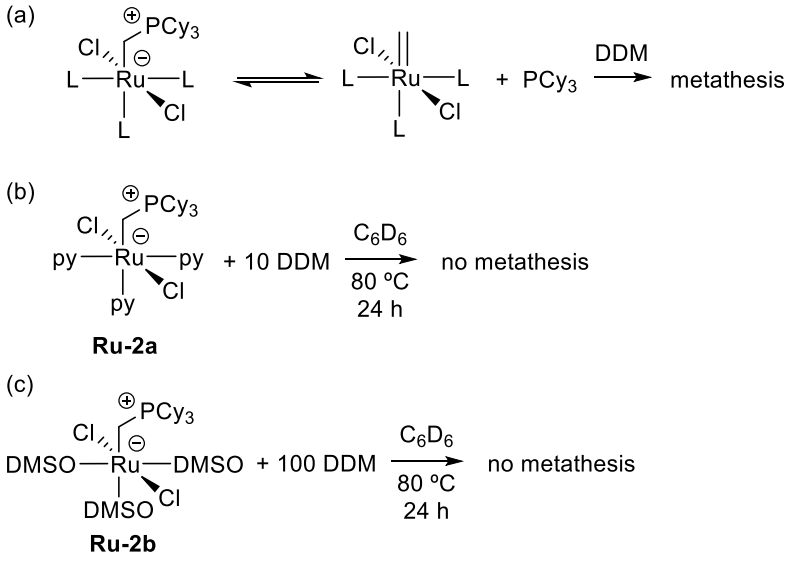

References begin on page 49

3.2.4 Impact of Phosphine Scavengers in Metathesis with GII

As exemplified above, the productivity of **GII** drops significantly when metathesis is performed in neat THF, owing to the susceptibility to donor-accelerated decomposition. The next phase of study therefore focused on examining whether phosphine scavengers could improve the metathesis activity of **GII** in this solvent. Reports have shown that copper(I) halides can increase metathesis yields with **GII** in ether[26] and in the presence of methanol.[44] However, a report by Grubbs showed that, in THF, several phosphine-scavenging additives (HCl/Et_2O, $CuCl_2$, CuCl, $B(C_6F_5)_3$, $Ni(COD)_2$, and $AlCl_3$) all lowered cross-metathesis yields with **GII** relative to the scavenger-free control.[25] The following candidates were screened in the RCM of the benchmark substrate DDM: copper (I) chloride and iodide (CuCl, CuI); Amberlyst-15 resin; benzyl iodide (BnI), and Merrifield-I resin (Figure 3.4). Conditions were chosen such that the control reactions did not reach completion, leaving room for improvement in the presence of phosphine scavengers. Thus, in the absence of additives, RCM was carried out using **GII** for 24 h at RT in toluene or THF. Catalyst loadings were increased by 20 times in THF to compensate for the lower activity in this solvent: that is, to 0.005 mol% **GII** in toluene, and 0.1 mol% in THF. RCM yields in these control experiments reached 61% and 81%, respectively.

CuCl proved to be highly detrimental to metathesis activity in both solvents (as indeed it did when used in the CM of the electron-deficient substrate methyl vinyl ketone).[25] In sharp contrast, CuI increased yields by 26% (to 87%) in C_7H_8, and by 19% (to 100%) in THF. Of note is its efficacy in toluene, despite Lipshutz' finding that ethereal solvents were more effective than aromatic and chlorinated solvents.[26] Amberlyst-15 resin severely reduced activity in toluene (to ca. 10% RCM yield), but had essentially no impact in THF. Yields in THF do not reach those observed for CuI and Merrifield-I, likely due to competing catalyst decomposition in the presence of Amberlyst-15:

References begin on page 49

Daniel Luis do Nascimento of the Fogg group has shown that **GII** exposed to 4 equiv Amberlyst-15 (THF, RT) undergoes a strikingly high 54% decomposition after just 2 h. [45] To account for the detrimental impact of the resin in toluene compared to THF, it is suggested that in THF the catalyst is relatively stabilized by solvent binding, forming a six-coordinate complex. In toluene, however, no such stabilization is possible, and the five- and four-coordinate catalyst species are more vulnerable to decomposition by resin reactivity.

Use of the Merrifield resin in toluene enabled metathesis yields comparable to CuI. Improvements were also seen in THF, though to a lesser extent (maximum 93% RCM). The improved performance relative to the control reaction is particularly striking given that formation of **GII-I** via halide exchange is a potential side reaction promoted by Merrifield-I (Scheme 3.6). Indeed, Morris exploited this capacity of the resin to synthesize RuHI((*R*)-binap)(PPh_3) from its chloride analogue,[29] and Daniel do Nascimento of the Fogg group noted partial halide exchange when using Merrifield-I as a scavenger in the metathetical synthesis of (e.g.) **HI** from **GI**.[45] Halide exchange is difficult to reconcile, however, with the reduced metathesis activity reported by Dias and Grubbs for **GII-I** relative to **GII**. While a 250-fold increase in initiation rate was reported for **GII-I** relative to the parent chloride catalyst[18] (probably due to the increased steric bulk of the iodide ligand (which aids in displacing PCy_3), net metathesis activity was reportedly comparable to or lower than that of **GII**.[18,24] Attempts to use BnI as a soluble resin mimic were unsuccessful, as its use had no impact on TONs. The higher efficacy of the resin may be due to the multivalent effect, where clustering of active sites increases binding affinity for the phosphine. It is worth noting that phosphine-free catalyst **HII** reaches 100% conversion in both solvents under analogous conditions.

References begin on page 49

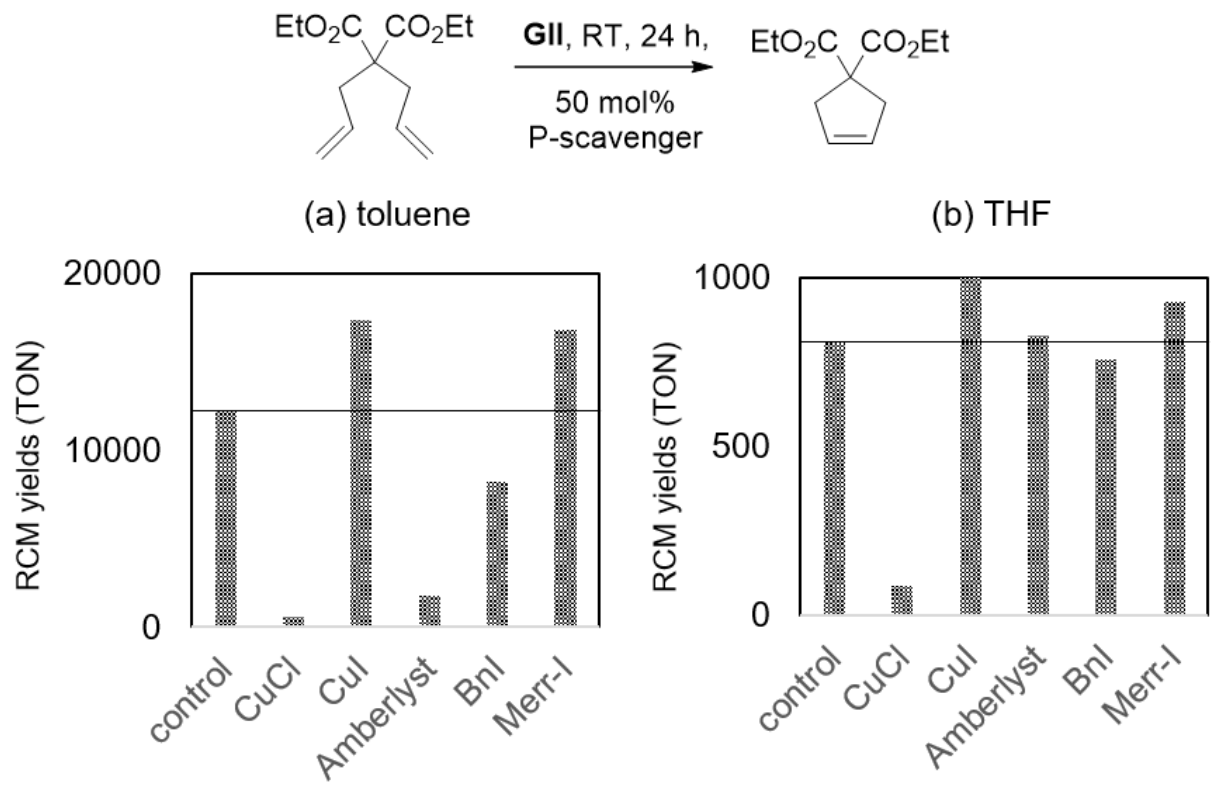

Figure 3.4 Impact of phosphine scavengers on RCM yields. (a) In toluene (0.005 mol% GII). (b) In THF (0.1 mol% GII). Line indicates yields in control experiments.

Scheme 3.6 Possible formation of GII-I by halogen exchange of GII by CuI or Merrifield-I

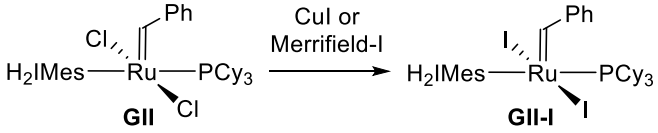

The foregoing demonstrates that the performance of phosphine-stabilized **GII** can be improved without resorting to a more costly phosphine-free catalyst, although the performance of the leading phosphine-free catalyst **HII** is not surpassed. While Amberlyst-15 resin and BnI were ineffective, CuI and Merrifield-I showed increased TONs relative to the control experiment. While CuI has previously been used as a phosphine scavenger in metathesis, use of Merrifield-I was not previously reported. Preliminary results show that Merrifield-I came a close second to CuI, with

References begin on page 49

the significant advantage of being readily removed by filtration after reaction, and not introducing an additional load of heavy metals (with potentially broader, unwanted activity, including redox activity). This study was limited, however, to RCM of DDM with **GII**. An expanded survey of substrate and catalyst scope is needed to assess its use more rigorously. Overall, these results also have major implications regarding the ability to achieve higher metathesis yields in greener solvents (many of which contain ether donors,[21-23] which are detrimental to catalyst lifetime).[43]

3.2.5 Synthesis and Use of a Metathesis Catalyst Bearing an IMeMes Ligand

To examine whether curtailed NHC bulk prevents C-H activation, the unsaturated carbene ligand IMeMes was explored, in which one *N*-mesityl group of IMes is truncated to *N*-Me (Figure 3.3, page 36). IMeMes was selected in preference to its saturated analogue H_2IMeMes, because faster rotation of the unsaturated carbenes about the Ru–NHC bond is expected to further retard C-H activation. For saturated NHCs, in contrast, the higher multiple-bond character in the Ru-C_{NHC} bond means that this ligand is held rigidly in position, favouring C-H activation.[17]

Free IMeMes was generated from imidazolium salt **2a** (itself synthesized by a literature method)[46] according to the methodology established for IMes.[47] The iodide salt was converted to its tetrafluoroborate salt **2b** by treatment with HBF_4, and free carbene IMeMes was generated by deprotonation of **2b** with NaH (Scheme 3.7).

References begin on page 49

Scheme 3.7 Synthesis of free IMeMes.

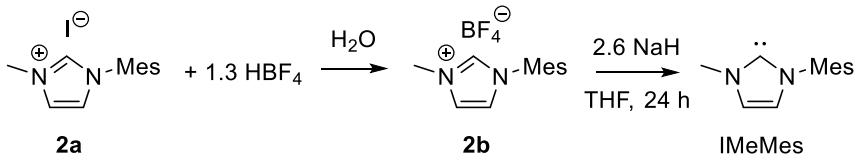

Catalyst **Ru-6** was then prepared by treatment of **GI** with IMeMes. Bis-NHC complex **Ru-7** was also formed as a minor product (ca. 32%, Scheme 3.8), even when the NHC was added slowly. Disubstitution with the IMeMes ligand is due to its reduced size relative to H_2IMes, as the latter is too bulky to form a bis-NHC complex. The impact of small NHC size on catalyst synthesis will be further discussed in Chapter 4.

Scheme 3.8 Synthesis of Ru-6, with formation of minor product Ru-7.

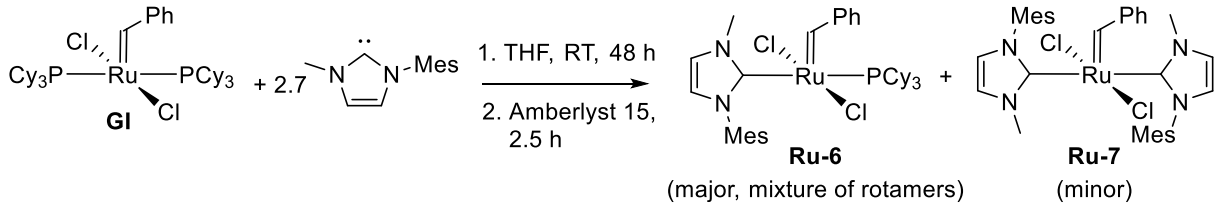

Also of note, two **Ru-6** alkylidene singlets are detected by ^{1}H NMR analysis (19.88 ppm, 20%; 19.37 ppm, 48%). These are assigned to NHC rotamers (Figure 3.5). Consistent with this, variable temperature ^{31}P{^{1}H} NMR (121 MHz, protio-THF; see Appendix A1.1, Figure A4) showed separation of the phosphine singlet (δ_P 35.4 ppm at RT) into two singlets (δ_P 35.5, 35.4 ppm) of **Ru-6** at –60 °C.

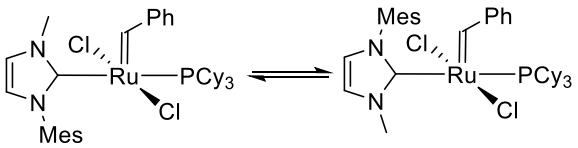

Figure 3.5 Rotamers of Ru-6

References begin on page 49

Despite the presence of ca. 32% **Ru-7** contaminant, **Ru-6** was tested in the RCM of DDM. Complete cyclization required over 5 h at 40 ºC (Figure 3.6), even at a catalyst loading of 1 mol%. In comparison, **GII** achieves complete cyclization within 2 h at a loading of 0.05 mol% at 30 °C. While **Ru-6** can indeed catalyze metathesis, its reduced activity relative to **GII** points toward limitations that will be explored in Chapter 4.

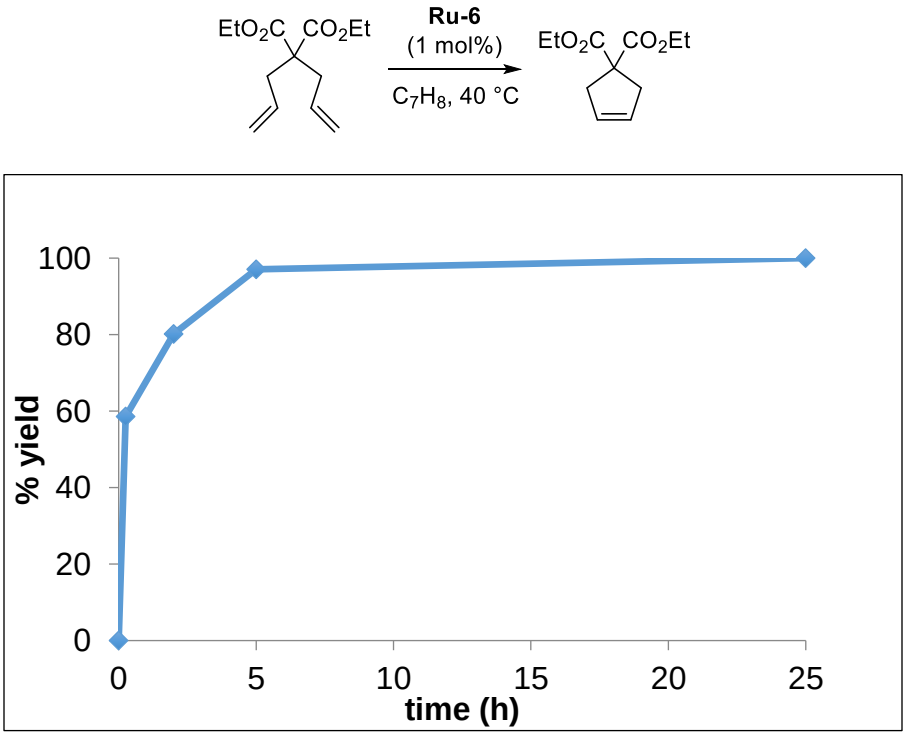

Figure 3.6 Rate curve for the RCM of DDM with Ru-6 (1 mol%).

3.3 Conclusions and Future Work

Despite the widespread use of **GII** in metathesis, its shortcomings are apparent: phosphine-mediated side-reactions are tied directly to catalyst decomposition. The data in this Chapter show that its decomposition is accelerated in the presence of sterically accessible Lewis donors, even weak oxygen donors. The negative impact of such donors on metathesis activity demonstrated in

References begin on page 49

benchmark RCM reactions highlights limitations on the potential utility of phosphine-stabilized catalysts in "green" ethereal or aqueous solvent media.

We then sought to probe the reversibility of nucleophilic attack by PCy_3 at the [Ru]=CH_2 moiety, to examine whether nucleophilic attack, or ensuing C-H activation of the NHC ligand, is the key deactivating event. This was complicated by the inability to isolate a σ-alkyl complex with a strong donor ligand, such as PCy_3 or H_2IMes. Despite this, it was shown that tris-L σ-alkyl complexes **Ru-2** did not form metathesis-active species even under forcing conditions. To probe this further, a reaction with a stronger driving force, such as ROMP of a norbornene derivative, could be tested instead.

If PCy_3 attack at [Ru]=CH_2 is accepted as irreversible, inhibiting attack may plausibly be considered key to improving catalyst lifetime. This is particularly important in donor solvents, which can accelerate decomposition. We therefore explored the use of phosphine scavengers in metathesis. It was shown that phosphine sequestration by Merrifield-I was effective in increasing TONs in the RCM of DDM, although it does not surpass CuI in this capability. However, the rich chemistry associated with Cu(I) may introduce problematic behaviour depending on substrate choice, which may be circumvented by the use of Merrifield-I. To assess this, a broader substrate scope should be examined, with particular consideration to the compatibility of scavengers with functionalized olefins.

Finally, we considered the possibility that C-H activation of the NHC ligand is the key deactivating event, meaning catalyst redesign should focus on curtailing the size of the NHC *N*-substituents. To examine this, a new catalyst bearing an NHC ligand with one *N*-mesityl truncated to an *N*-methyl was synthesized. Metathesis was relatively slow even with the benchmark substrate DDM,

References begin on page 49

however full cyclization was achieved nonetheless. Given its activity, this catalyst is not an improvement on the standard H_2IMes, although it may still be a more stable analogue. To probe this, future experiments should focus on testing its robustness toward nucleophilic phosphine attack by synthesizing the analogous methylidene complex of **Ru-6**. If a stable σ-alkyl intermediate is intercepted, this would show that C-H activation is in fact stalled by the reduced NHC size. However, the rate of the initial phosphine attack may be accelerated by the lack of steric protection at the methylidene, and should also be considered.

3.4 References

(1) Compain, P. *Adv. Synth. Catal.* **2007**, *349*, 1829–1846.
(2) Lummiss, J. A. M.; Ireland, B. J.; Sommers, J. M.; Fogg, D. E. *ChemCatChem* **2014**, *6*, 459–463.
(3) Lummiss, J. A. M.; Botti, A. G. G.; Fogg, D. E. *Catal. Sci. Technol.* **2014**, *4*, 4210–4218.
(4) Ireland, B. J.; Dobigny, B. T.; Fogg, D. E. *ACS Catal.* **2015**, *5*, 4690−4698.
(5) Lummiss, J. A. M.; McClennan, W. L.; McDonald, R.; Fogg, D. E. *Organometallics* **2014**, *33*, 6738–6741.
(6) P'Pool, S. J.; Schanz, H.-J. *J. Am. Chem. Soc.* **2007**, *129*, 14200–14212.
(7) van Lierop, B. J.; Lummiss, J. A. M.; Fogg, D. E., Ring-Closing Metathesis. In *Olefin Metathesis-Theory and Practice*, Grela, K., Ed. Wiley: Hoboken, NJ, 2014; pp 85–152.
(8) Lafaye, K.; Nicolas, L.; Guérinot, A.; Reymond, S. b.; Cossy, J. *Org. Lett.* **2014**, *16*, 4972−4975.
(9) Higman, C. S.; Lummiss, J. A. M.; Fogg, D. E. *Angew. Chem., Int. Ed.* **2016**, *55*, 3552–3565.
(10) Cohen, S. A.; Anderson, D. R.; Wang, Z.; Champagne, T. M.; Ung, T. A. Methods for treating a metathesis feedstock with metal alkoxides / peroxide poisons. US20140275681A1, 2014.
(11) Nicola, T.; Brenner, M.; Donsbach, K.; Kreye, P. *Org. Process Res. Dev.* **2005**, *9*, 513–515.
(12) Lübbe, C.; Dumrath, A.; Neumann, H.; Schäffer, M.; Zimmermann, R.; Beller, M.; Kadyrov, R. *ChemCatChem* **2014**, *6*, 684–688.
(13) Wang, H.; Goodman, S. N.; Dai, Q.; Stockdale, G. W.; Clark, W. M. *Org. Process Res. Dev.* **2008**, *12*, 226–234.
(14) Farina, V.; Horváth, A., Ring-Closing Metathesis in the Large-Scale Synthesis of Pharmaceuticals. In *Handbook of Metathesis*, Grubbs, R. H.; Wenzel, A. G., Eds. Wiley-VCH: Weinheim, 2015; Vol. 2, pp 633–658.
(15) Hong, S. H.; Wenzel, A. G.; Salguero, T. T.; Day, M. W.; Grubbs, R. H. *J. Am. Chem. Soc.* **2007**, *129*, 7961–7968.
(16) Galan, B. R.; Pitak, M.; Keister, J. B.; Diver, S. T. *Organometallics* **2008**, *27*, 3630–3632.

References begin on page 49

(17) Lummiss, J. A. M.; Higman, C. S.; Fyson, D. L.; McDonald, R.; Fogg, D. E. *Chem. Sci.* **2015**, *6*, 6739–6746.
(18) Sanford, M. S.; Love, J. A.; Grubbs, R. H. *J. Am. Chem. Soc.* **2001**, *123*, 6543–6554.
(19) Grela, K.; Gulajski, L.; Skowerski, K., Alkene Metathesis in Water. In *Metal-Catalyzed Reactions in Water*, Dixneuf, P. H.; Cadierno, V., Eds. Wiley-VCH: Weinheim, 2013; pp 291–336.
(20) Tomasek, J.; Schatz, J. *Green Chem.* **2013**, *15*, 2317–2338.
(21) Bantreil, X.; Sidi-Ykhlef, M.; Aringhieri, L.; Colacino, E.; Martinez, J.; Lamaty, F. *J. Catal.* **2012**, *294*, 113–118.
(22) Bilel, H.; Hamdi, N.; Zagrouba, F.; Fischmeister, C.; Bruneau, C. *Green Chem.* **2011**, *13*, 1448–1452.
(23) Miao, X.; Fischmeister, C.; Bruneau, C.; Dixneuf, P. H. *ChemSusChem* **2008**, *1*, 813–816.
(24) Dias, E. L.; Nguyen, S. T.; Grubbs, R. H. *J. Am. Chem. Soc.* **1997**, *119*, 3887–3897.
(25) Morgan, J. P.; Grubbs, R. H. *Org. Lett.* **2000**, *2*, 3153–3155.
(26) Voigtritter, K.; Ghorai, S.; Lipshutz, B. H. *J. Org. Chem.* **2011**, *76*, 4697–4702.
(27) Monsaert, S. F.; Verpoort, F. W. C. Process for preparation of ruthenium-based carbene catalysts with chelating alkylidene ligands. WO Patent App. WO 2011/091980 Al; CA+ 383210.
(28) van Lierop, B. J.; Reckling, A. M.; Lummiss, J. A. M.; Fogg, D. E. *ChemCatChem* **2012**, *4*, 2020–2025.
(29) Zhao, X.; Ivanova, N.; Hadzovic, A.; Zimmer-De Iuliis, M.; Lough, A. J.; Morris, R. H. *Organometallics* **2008**, *27*, 503–508.
(30) Lipshutz, B. H.; Blomgren, P. A. *Org. Lett.* **2001**, *3*, 1869–1871.
(31) Crabtree, R. H. *Chem. Rev.* **2015**, *115*, 127–150.
(32) Vehlow, K.; Maechling, S.; Blechert, S. *Organometallics* **2006**, *25*, 25–28.
(33) Monfette, S.; Eyholzer, M.; Roberge, D. M.; Fogg, D. E. *Chem. – Eur. J.* **2010**, *16*, 11720–11725.
(34) Wang, H.; Matsuhashi, H.; Doan, B. D.; Goodman, S. N.; Ouyang, X.; Clark, W. M. *Tetrahedron* **2009**, *65*, 6291–6303.
(35) Nagarkar, A. A.; Crochet, A.; Fromm, K. M.; Kilbinger, A. F. M. *Macromolecules* **2012**, *45*, 4447–4453.
(36) While binding of tertiary amines such as NEt_3 to Ru centers has been established, the complexes involved are typically less sterically congested arylphosphine derivatives. For a discussion of such complexes and their degradation products, see: (a) Fogg, D. E.; James, B. R. *Inorg. Chem.* **1995**, *34*, 2557–61. For examples of Ru complexes containing macrocyclic, tetradentate tertiary amines, see: (b) Wong, C.-Y.; Lee, F.-W.; Che, C.-M.; Cheng, Y. F.; Phillips, D. L.; Zhu, N. *Inorg. Chem.* **2008**, *47*, 10308–10316, and references therein.
(37) Bailey, G. A.; Lummiss, J. A. M.; Foscato, M.; Occhipinti, G.; McDonald, R.; Jensen, V. R.; Fogg, D.E., *J. Am .Chem. Soc.* **2017**, submitted.
(38) Burtscher, D.; Grela, K. *Angew. Chem., Int. Ed.* **2009**, *48*, 442–454.
(39) Guidone, S.; Songis, O.; Nahra, F.; Cazin, C. S. J. *ACS Catal.* **2015**, *5*, 2697–2701.
(40) Beach, N. J.; Lummiss, J. A. M.; Bates, J. M.; Fogg, D. E. *Organometallics* **2012**, *31*, 2349–2356.
(41) Zhao, Z.-X.; Wang, H.-Y.; Guo, Y.-L. *Rapid Commun. Mass Spectrom.* **2011**, *25*, 3401–3410.

References begin on page 49

(42) Stark, A.; Ajam, M.; Green, M.; Raubenheimer, H. G.; Ranwell, A.; Ondruschka, B. *Adv. Synth. Catal.* **2006**, *348*, 1934–1941.
(43) McClennan, W. L.; Rufh, S. A.; Lummiss, J. A. M.; Fogg, D. E. *J. Am. Chem. Soc.* **2016**, *138*, 14668−14677.
(44) Schulz, M. D.; Atkinson, M. B. J.; Elsey, R. J.; Thuo, M. M. *Transition Met. Chem.* **2014**, *39*, 763–767.
(45) do Nascimento, D. L.; Davy, E.; Fogg, D. E. *Catal. Sci. Technol.* **2017**, submitted.
(46) Ahrens, S.; Peritz, A.; Strassner, T. *Angew. Chem., Int. Ed.* **2009**, *48*, 7908–7910.
(47) Arduengo, A. J.; Dias, H. V. R.; Harlow, R. L.; Kline, M. *J. Am. Chem. Soc.* **1992**, *114*, 5530–5534.

References begin on page 49

Chapter 4. The Deleterious Effect of NHC Truncation on Catalyst Design

Sections 4.1, 4.2.1, 4.2.2, and 4.2.3 of this Chapter have been published in: Synthesis and Dynamic Behaviour of a Dimeric Ruthenium Benzylidene Complex Bearing a Truncated *N*-Heterocyclic Carbene Ligand. Carolyn S. Higman, Stephanie A. Rufh, Robert McDonald, and Deryn E. Fogg. *J. Organomet. Chem*. **2017**, 847, 162-166 (special issue in honour of John Gladysz). (https://doi.org/10.1016/j.jorganchem.2017.03.033)

Author contributions: Higman, Rufh, and Fogg wrote the manuscript. The synthesis of **Ru-11a** was developed by Higman, and repeated multiple times by Rufh. NMR characterization of **Ru-11a** was carried out by Higman and Rufh; catalysis with **Ru-11a** by Rufh.

4.1 Introduction

As noted in Chapter 3, NHC activation is a common structural feature in decomposition products formed by second-generation metathesis catalysts (Figure 4.1).[1-3] More generally, intramolecular C-H activation is known to plague *N*-mesityl and other *N*-aryl NHCs,[4-14] as well as their *N*-ethyl[15] or *N*-isopropyl[15,16] counterparts, and could potentially account for the poor metathesis activity of *N*-^{i}Pr NHC complexes.[17,18] Modification of the NHC ligand to curb such pathways (commonly via approaches involving, in Crabtree's phrase, "slimming" the NHC substituents)[2] has been highlighted as a key strategy for catalyst redesign in olefin metathesis.[1-3]

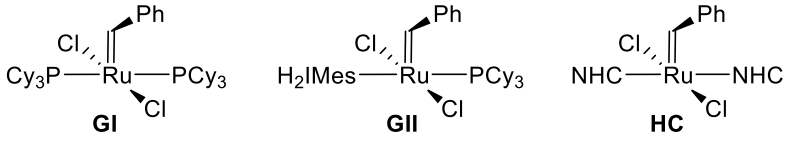

Figure 4.1 Ruthenium metathesis catalysts of the Grubbs and Herrmann classes (structures of GI and GII are reproduced here for convenience).

In studies designed to examine the validity of this proposition, we sought to access an analogue of **GII** bearing a truncated NHC ligand. In the IMe_4 ligand (IMe_4 = 1,3,4,5-tetramethylimidazol-2-ylidene; Figure 4.2), geometric constraints prohibit C-H activation. Relatively few ruthenium

References begin on page 68

complexes of IMe_4 have been reported, in comparison to the ubiquitous H_2IMes and IMes derivatives. The Whittlesey group has developed routes to hydride complexes bearing one,[7,19] two,[20,21] or four[22] such ligands. The sole example explored within the context of olefin metathesis is indenylidene complex **Ru-8a** (Figure 4.2), although related IMe_2 catalysts are known, including **Ru-8b**[23,24] and benzylidene complex **Ru-9**,[25] a mixed-NHC analogue of the Herrmann catalyst **HC** (see Figure 4.1).[26,27] These complexes exhibited low metathesis activity (requiring temperatures of ≥100 °C), but this is expected from the need to lose a strongly donating NHC ligand to open up a vacant site for olefin binding. Synthesis of a Grubbs-class IMe_n catalyst was therefore of interest.

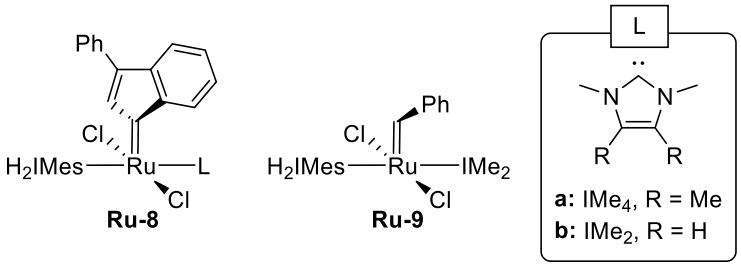

Figure 4.2 Ruthenium metathesis catalysts bearing the IMe_n ligand.

Attempts to prepare a mono-IMe_4 complex analogous to **GII**, however, yielded multiple products. While $RuCl_2(IMe_4)(PCy_3)(=CHPh)$ was ultimately isolated by Carolyn Higman of this research group, the synthetic chemistry was complicated by competing formation of poly-NHC byproducts. One aim of the present work was to clarify the nature of these species. The first part of this Chapter describes deliberate efforts to synthesize the bis-NHC complex $RuCl_2(IMe_4)_2(=CHPh)$ **Ru-10**. The facile dimerization of this species to afford $[Ru_2(\mu\text{-}Cl)_3(IMe_4)_4(=CHPh)_2]Cl$ **Ru-11a** accounts for the inability to access a mono-Ru product. Dimeric **Ru-11a** exhibits a rich dynamic behaviour at room temperature, which results in observation of three [Ru]=CHPh rotamers despite the putative equivalence of the two benzylidene sites. As such face-bridged dimers are notoriously unreactive

References begin on page 68

in metathesis,[28-31] a more reactive, edge-bridged dimer[32] was prepared by abstracting a bridging chloride ligand. Like its parent dimer, this complex showed minimal metathesis reactivity, despite the fact that re-opening of the dimer should give access to a basal site cis to the alkylidene ligand. This could indicate that NHC truncation has a *negative* impact on metathesis activity.

Many of the recent advances in understanding the decomposition of Grubbs-class catalysts[5,33,34] (Chapter 3) were enabled by Justin Lummiss' successful development of a high-yield synthetic route to the resting-state methylidene complexes **GIIm** and **GIIm'**. The corresponding IMe_n complexes, however, are unknown. Incorporation of IMe_4 into a methylidene complex was thus regarded as a priority in seeking to establish whether NHC truncation has a positive or negative impact. The last part of this Chapter describes efforts to access such a complex, and unexpected revelations about the deleterious impact of attenuating NHC bulk.

4.2 Results and Discussion

4.2.1 Synthesis of Face-Bridged Ru Benzylidene Dimer $[Ru(\mu\text{-}Cl)_3(IMe_4)_4(=CHPh)_2]Cl$ (Ru-11a)

Treating a solution of **GI** in benzene with a slight excess of IMe_4 (2.1 equiv) at ambient temperatures caused an immediate colour change from purple to brown, with slow deposition of a green solid. After 18 h, no further starting material was evident by ^1H NMR analysis, and the precipitate was filtered off and washed with benzene and hexanes. The product proved completely insoluble in hydrocarbon solvents (benzene, toluene, hexanes, pentane) or diethyl ether, and sparingly soluble in THF, but was soluble in chlorinated solvents. $^{31}P\{^1H\}$ NMR analysis in deuterated dichloroethane (DCE-d_4) indicated a phosphine-free complex, as anticipated, but three benzylidene singlets were evident in the ^1H NMR spectrum. NOESY-NMR studies revealed that these are due to a single, conformationally mobile ruthenium complex. Unexpectedly, however,

References begin on page 68

X-ray analysis of crystals grown by Carolyn Higman from CH_2Cl_2-pentane revealed that this species was not a mono-ruthenium product of type **Ru-10**, but rather dimeric **Ru-11a** (Scheme 4.1).[35] Formation of **Ru-11a** suggests either preferential formation of *cis*-**Ru-10**, or isomerization of initially-formed *trans*-**Ru-10** (plausibly driven by the unfavourable trans effect of two strongly σ-donating NHC ligands, in conjunction with the low steric demand of the IMe_4 ligand). Dimerization of *cis*-$RuCl_2L_2$(=CHR) precatalysts has been reported,[28,29,31,36] where not prohibited by ligand bulk or rigidity.[32,37-40] Indeed, in early studies by the Fogg group on Ru-phosphine derivatives, facile formation of such triply-bridged dimers was identified as a key decomposition pathway for *cis*-dichloro metathesis catalysts.[28,29]

Scheme 4.1 Synthesis of IMe_4 complex Ru-11a.[a]

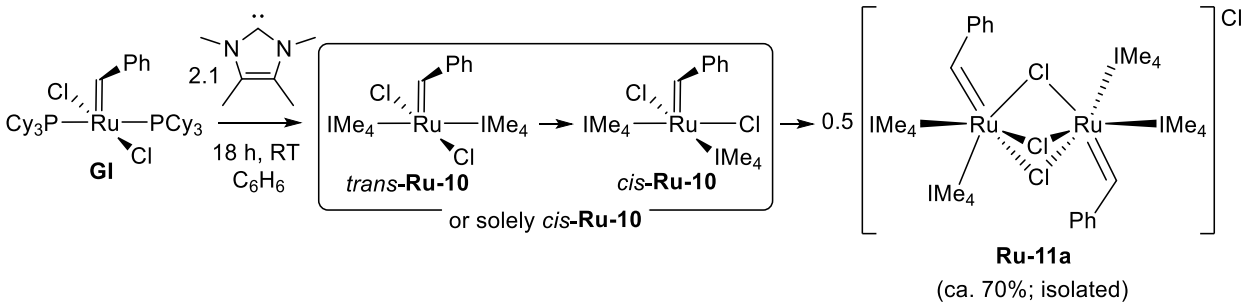

[a] A single rotamer is shown, for convenience.

4.2.2 Molecular Dynamics Study: [Ru]=CHPh and Ru-NHC Rotation

^{1}H NMR analysis of **Ru-11a** in DCE-d_4 at 500 MHz revealed three broad singlets in the alkylidene region, in a ratio of 10:4:1 (Figure 4.3a). These were assigned to the rotational isomers depicted, on the basis of the number and strength of [Ru]=CHPh–NMe correlations observed in ^{1}H-^{1}H NOE experiments. These data support the staggered [Ru]=CHPh conformation depicted, notwithstanding the mobility indicated by the breadth of the [Ru]=CHPh signals. Conformer **C**

References begin on page 68

indeed corresponds to the structure observed crystallographically. X-ray analysis of **GII**, in comparison, shows the benzylidene ligand eclipsed with the Cl–Ru–Cl axis.[41] The singlet multiplicity of the [Ru]=CHPh signal for **GII** likewise indicates a 90° dihedral angle between [Ru]=CH and Ru–P in solution.

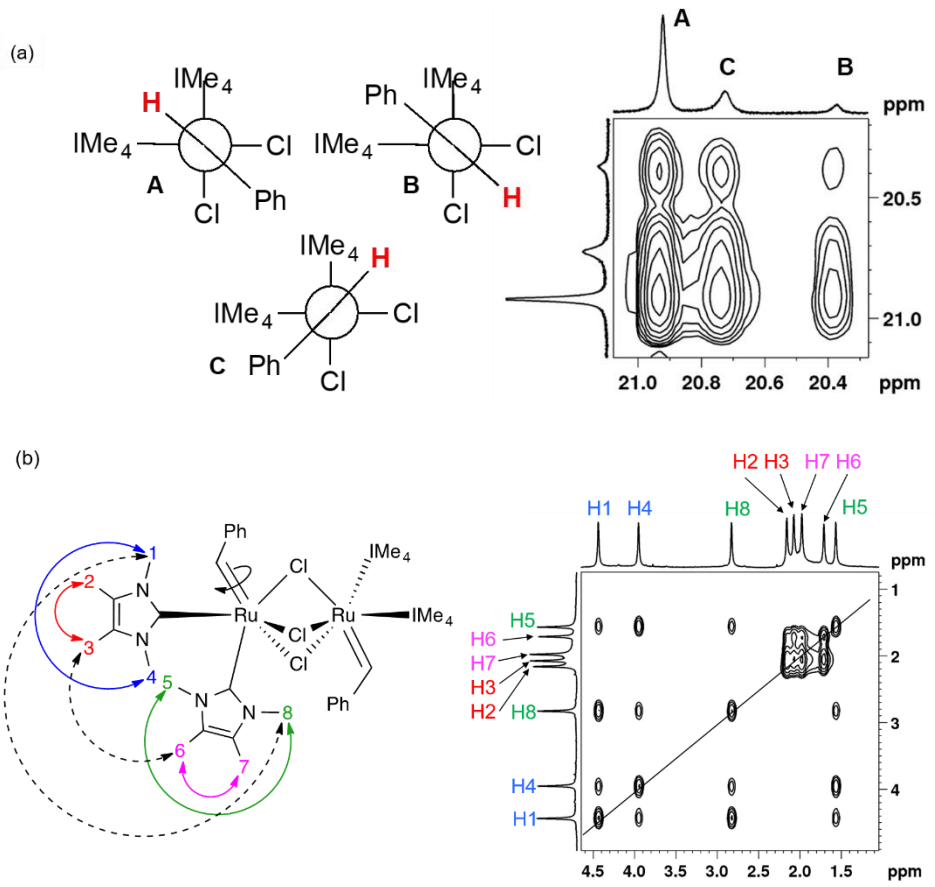

Figure 4.3 (a) Rotational isomers of Ru-11a, viewed down the Cl–Ru=CHPh bond, and ^{1}H-^{1}H EXSY NMR spectrum showing exchange coupling of all three benzylidene protons. (b) Rotational exchange of N*Me* and C*Me* groups, and ^{1}H-^{1}H EXSY NMR spectrum showing corresponding exchange coupling (500 MHz, 298 K, DCE-d$_4$).

The inequivalence of the adjacent IMe$_4$ ligands on a given Ru centre in **Ru-11a** implies that the NHC environments are distinguished by the orientation of these ligands relative to the [Ru]=CHPh vector. Efforts to probe this point by generating the corresponding methylidene analogue were

References begin on page 68

thwarted by the low metathesis activity described in Section 4.2.3, and rapid decomposition upon treatment of first-generation methylidene (**GIm**) with IMe_4 (details deferred to Section 4.2.5).

Key exchange correlations between the three rotamers of **Ru-11a** are summarized in Figure 4.3b. Solid arrows indicate exchange between methyl groups within the same NHC ligand, arising from rotation about the Ru-NHC bond. (Additional, through-space interactions of the benzylidene proton with four *N*-Me groups are evident in the ^{1}H-^{1}H NOESY spectrum: see Appendix A2.2, Figure A10). Facile rotation of unsaturated NHC ligands about the M–C_{NHC} bond is regarded[42,43] as a reflection of their poor π-acceptor capability, relative to the corresponding saturated NHCs,[43-45] in which stronger Ru→NHC backdonation results in a greater degree of double-bond character. Accordingly, the ease of rotation of the IMe_4 ligand is consistent with a high proportion of single-bond character in the Ru–C_{NHC} bond, amplified by the relative freedom from steric restrictions of this small NHC.

Also of note in Figure 4.3b is exchange of the methyl protons on adjacent NHC ligands (dashed arrows), signifying benzylidene rotation. Rotation about the [Ru]=CHPh bond offers experimental insight into the extent of double-bond character present in this moiety, when steric restrictions are eliminated. This has important potential implications for the stability of the [Ru]=CHR carbon. A more covalent, "Schrock-like" bond, for example,[46,47] should affect the vulnerability of the alkylidene carbon to nucleophilic attack. Further, benzylidene rotation has been related to initiation, in a DFT study of **GII** using the M06L functional.[48] PCy_3 loss was reported to occur only from the rotamer in which the benzylidene ligand is eclipsed with the NHC–Ru–PCy_3 axis, and inhibited benzylidene rotation in **GII** was proposed as a key contributor to the inverse trans effect established experimentally.

References begin on page 68

Efforts by Carolyn Higman to extract activation parameters for Ru–NHC and [Ru]=CHPh rotation were frustrated by the complexity of the system revealed by variable-temperature NMR experiments.[35] At 70 °C, the benzylidene signals for **B** and **C** coalesce, while the most downfield peak (**A**) remains a broad hump at its original location. At low temperature (-80 °C), yet more rotamers emerge. The participation of multiple species with different populations (i.e. different exchange parameters) precluded Eyring analysis.

Even on a qualitative basis, however, the rotational behaviour of the benzylidene ligand in sterically unencumbered **Ru-11a** is potentially informative. In **GII**, benzylidene rotation is restricted by steric conflict with the PCy_3 ligand[49] and π-π interactions between the phenyl and mesityl rings,[50] and hence does not report on the extent of double-bond character in the [Ru]=CHPh moiety. The facile rotation about the [Ru]=CHPh bond observed in **Ru-11a** is hence of interest, particularly for the potential inference of limited backdonation from the metal. In the extreme, this could point toward the validity of the Ru(II) descriptor.[47] An unanswered question, however, remains the ease with which the Ru=C d_π–p_π orbital can rotate via linear combination with two different atomic Ru d orbitals, without a reduction in bond order.

4.2.3 Assessing RCM Activity of Ru-11a

While the principal focus of this study was the identification and solution behaviour of face-bridged dimer **Ru-11a**, a brief assay of its metathesis activity was also undertaken. These experiments were conducted in dichloroethane, given the limited solubility of **Ru-11a** in non-chlorinated solvents. As expected from the behaviour previously established for such face-bridged, coordinatively saturated dimers,[28,29] RCM activity was very low. Thus, even the readily-cyclized diene diethyl diallylmalonate (DDM) underwent no reaction over 3 days at 40 °C in the presence of 1 mol% **Ru-11a** (Figure 4.4). Addition of HCl (1 equiv per Ru)[51] resulted in marginal

References begin on page 68

improvement, with 14% RCM after 72 h. In the presence of Amberlyst-15, an acidic ion exchange resin (8 equiv, 4 equiv per Ru), the RCM yield reached >50% after 72 h, possibly owing to abstraction of an IMe_4 ligand. These results reinforce the point that formation and dimerization of *cis*-dichloro ruthenium structures can provide an efficient decomposition pathway for metathesis catalysts.

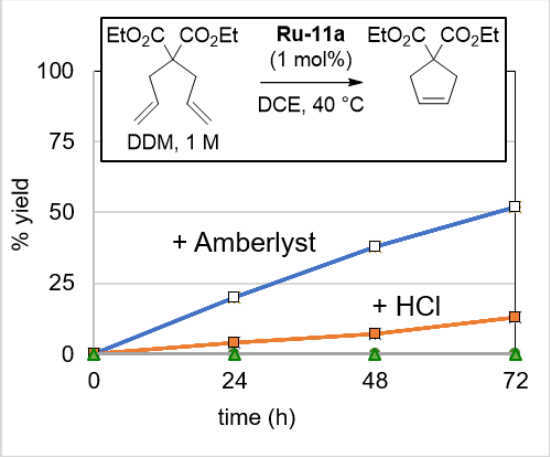

Figure 4.4 Attempted RCM of DDM by Ru-11a alone (green triangles), or with added HCl (filled orange squares), or Amberlyst-15 resin (blue squares).

The low metathesis activity of the dimers above is expected from the high stability of the $Ru_2(\mu\text{-}Cl)_3$ configuration, which impedes binding of olefin at a site cis to the benzylidene ligand. In contrast, related edge-bridged dimers exist in equilibrium with their mononuclear counterparts, and can exhibit high metathesis activity.[52] Chloride abstraction from **Ru-11a** was therefore undertaken, to see if an edge-bridged derivative would exhibit improved performance.

4.2.4 Synthesis and Catalytic Activity of Edge-Bridged Dimer Ru-12

While addition of $NaBF_4$ to **Ru-11a** at RT effected only counterion exchange, edge-bridged **Ru-12** was obtained by reaction with $NaBAr_4^F$ under more forcing conditions (Scheme 4.2). We anticipated significantly improved metathesis activity for **Ru-12**, given the precedents noted

References begin on page 68

above. Reaction with the readily-cyclized substrate DDM, however, resulted in only 5% RCM after 5 h at RT in CH_2Cl_2, at a catalyst loading of 1 mol%. The low activity may be due to facile regeneration of face-bridged **Ru-11** in solution, as NMR analysis post-metathesis revealed the three alkylidene singlets characteristic of this species, with no evidence of either **Ru-12** (δ_H 19.66 ppm in $CDCl_3$) or a methylidene resting-state species. The insolubility of **Ru-12** in aromatic and aliphatic solvents, and its minimal solubility in THF, limited examination of its behaviour in non-chlorinated solvent.

Scheme 4.2 Synthesis of edge-bridged dimer Ru-12.

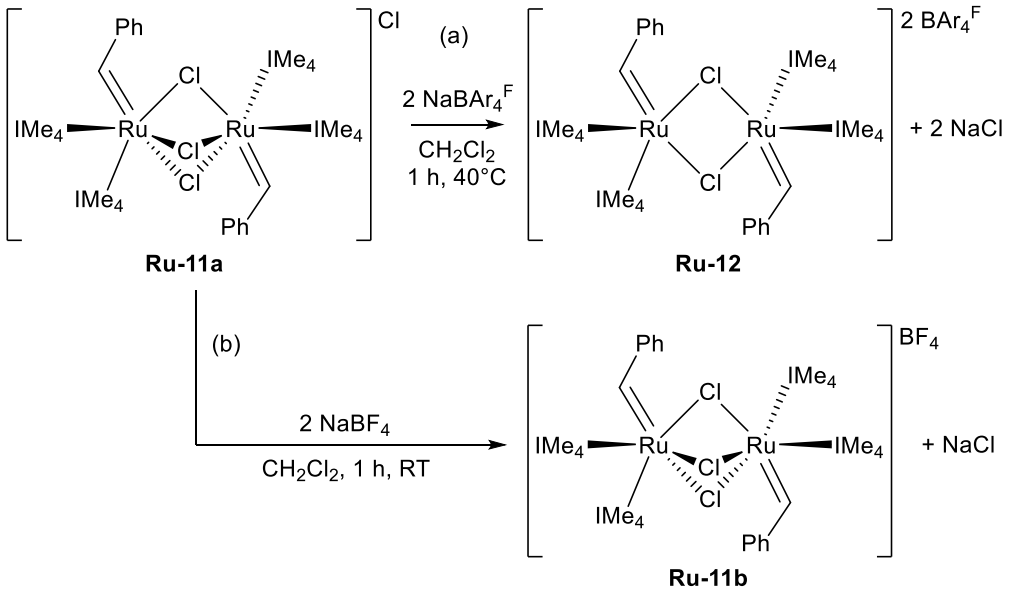

4.2.5 Reaction of IMe_4 with a bis-thioaryloxide analogue of GI

The chemistry above demonstrates that reaction of **GI** with IMe_4 does not afford access to a Grubbs-class, mono-IMe_4 catalyst. Instead, the small size of the NHC ligands results in installation of multiple IMe_4 ligands. Similar results were reported outside the context of metathesis by the Whittlesey[20-22] and Hepp[53] groups. To circumvent this problem, reaction of IMe_4 with the thioaryloxide **GI** analogue **Ru-13** was examined. The precursor was synthesized by Jensen's

References begin on page 68

procedure,[54] itself adapted from the original Fogg aryloxide methods[55,56] (Scheme 4.3). A notable feature of the bis-SAr analogue of **HII**, synthesized by Nikita Panov of the Fogg group, is the ease with which it reverts to its chloride parent in chlorinated solvents (unpublished work). While this is a limitation in the context of catalysis, it was viewed as a potential asset in the present work, as the thioaryloxide ligands can serve as bulky protecting groups to aid in installation of a single NHC ligand, subsequent replacement of which could generated the target complexes.

Accordingly, bis-thioaryloxide complex **Ru-13** was treated with one equivalent of IMe_4 at RT in C_6D_6. Even after 4 d, at which point conversion had reached only ca. 25%, the bis-IMe_4 product was observable (18% **Ru-14**; 5% **Ru-15**; Scheme 4.3). The initially-formed mono-IMe_4 complex **Ru-14** evidently reacts with IMe_4 at a rate comparable to that at which starting **Ru-13** undergoes ligand exchange.

Scheme 4.3 Synthesis of thioaryloxide complex Ru-13, and reaction with IMe_4.

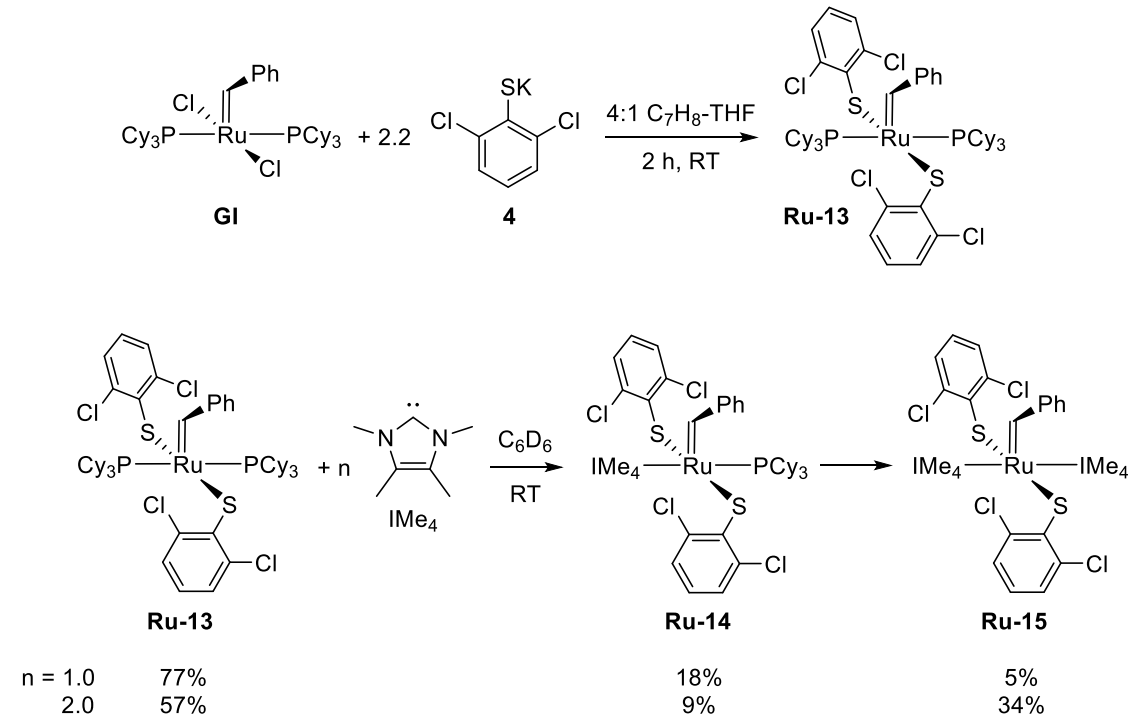

References begin on page 68

The mono- and bis-IMe_4 complexes are easily separated, however. Thus, on dissolving the mixture in CH_2Cl_2, the bis-IMe_4 complex **Ru-15** is converted to dimer **Ru-11a**, while the mono-IMe_4 complex **Ru-14** chlorinates to form the desired product, **GII''** (Scheme 4.4). Somewhat unexpectedly, **Ru-13** is not converted to chlorinated analogue **GI**, perhaps due to protection of the Ru centre by the two bulky PCy_3 ligands.

Separation of **Ru-11a** from the mixture was achieved by dissolving in C_6H_6 and filtering off the dimer. However, **Ru-13** and the desired product **GII''** could not be separated, as their solubilities were too closely similar.

Scheme 4.4 Deprotection of Ru-thioaryloxide complexes by treatment with $CDCl_3$

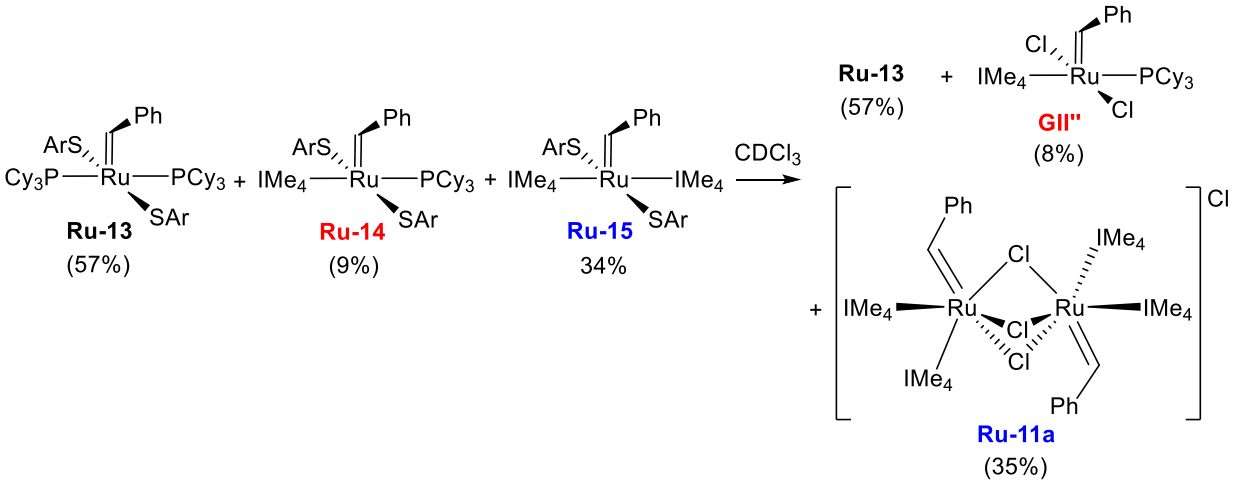

4.2.6 Treatment of GIm with IMe_4

The difficulty in terminating reaction at a mono-IMe_4 analogue of **GII** points toward the ease with which this sterically unprotected Ru centre can undergo unwanted reactions. We speculated that the reaction of the active species with nucleophiles might be a further instance of such problematic behaviour. To explore this point, we sought to examine the behaviour of the methylidene complex formed by reacting the first-generation methylidene complex **GIm** with IMe_4. While we

References begin on page 68

anticipated that the even greater steric accessibility of $RuCl_2(IMe_4)(PCy_3)(=CH_2)$ **GIIm''**, relative to benzylidene **GII''**, could cause rapid decomposition, we hoped that the rapidity of decomposition and the nature of the decomposition products (e.g. $[MePCy_3]Cl$) might confirm much more facile methylidene abstraction in this system. Unexpectedly, while decomposition was indeed fast, PCy_3 attack at the methylidene moiety was not a factor.

Addition of IMe_4 in any proportion from 1–4 to **GIm** in C_6D_6 (Scheme 4.5) resulted in immediate colour change from pink to orange, and deposition of a pale grey precipitate. ^1H NMR analysis indicated formation of identical products in all cases, differing only in yield relative to starting **GIm**. For the reaction with a fourfold excess of IMe_4, the supernatant showed complete loss of the methylidene singlet for **GIm** (19.41 ppm) within 10 min at RT, and no new methylidene signals were observed. Integration against an internal standard revealed 50% known $RuCl_2(IMe_4)_4$ (**Ru-16**; identified by NMR[53] and MALDI-TOF analysis), which accounts for half the consumed NHC. $^{31}P\{^1H\}$ NMR analysis showed solely free PCy_3. This is a key piece of evidence, indicating not merely loss of both phosphine ligands from **GIm**, but also that loss of the methylidene ligand is *not* due to abstraction by PCy_3, which would generate $[MePCy_3]Cl$ **1** (δ_P 34.5 ppm). To account for the insolubility of alkylphosphonium salt **1** in C_6D_6, the precipitate was redissolved in $CDCl_3$ for analysis, revealing no other ^{31}P-containing products. An important question, however, is the mass balance with respect to methylidene – that is, the fate of the methylidene ligand.

Scheme 4.5 NMR-tube reaction of GIm with excess IMe_4.

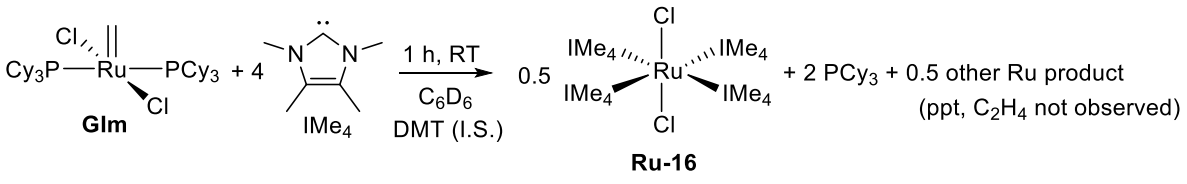

References begin on page 68

A potential vector for methylidene loss is bimolecular elimination of ethylene. Bimolecular coupling (BMC) of methylidene complexes is well precedented in the chemistry of early metal complexes, notably Mo and Re,[57-60] and has recently been demonstrated within the second-generation Ru catalysts by Gwen Bailey of this research group.[61] To examine whether C_2H_4 is liberated in the present reaction, the experiment was repeated in a completely filled J. Young NMR tube, to preclude partitioning of gaseous ethylene into the headspace. Again, no free ethylene was observed at the expected chemical shift (δ_H 5.25 ppm).

An alternative possibility is scavenging of liberated ethylene by binding to Ru, as observed by Gladysz and coworkers in Re systems.[59,60] While the details are obscured by the instability of this species, as outlined below, a proposed pathway is depicted in Scheme 4.6. In the initial reaction of **GIm** with IMe_4, the PCy_3 ligands are displaced and *cis*-**Ru-17** is formed, as in the benzylidene system (Section 4.2.1 above). Rapid bimolecular coupling gives methylidene-bridged dimer **Ru-18**, which eliminates ethylene to afford ethylene-bound **Ru-19**, and a coordinatively unsaturated Ru center, which reacts with the remaining IMe_4 to form **Ru-16**. Ethylene complex **Ru-19** appears to be unstable, and exhaustive efforts have not enabled its spectroscopic observation. The ultimate fate of ethylene, however, appears to be insertion into the Ru–IMe_4 ligand to liberate imidazolium salt **5**. Thus, MALDI-TOF analysis of the grey precipitate that deposits shows **5** as a primary product (Appendix A2.3, Figure A19), and a well-defined ethyl pattern is observed by ^{1}H NMR analysis (3.34 ppm, q, $^3J_{H\text{-}H}$ = 7.5 Hz, 2H, CH_2; 1.28 ppm, t, $^3J_{H\text{-}H}$ = 7.5 Hz, 3H, CH_3).

References begin on page 68

Scheme 4.6 Proposed decomposition of GIm upon treatment with 4 IMe$_4$.

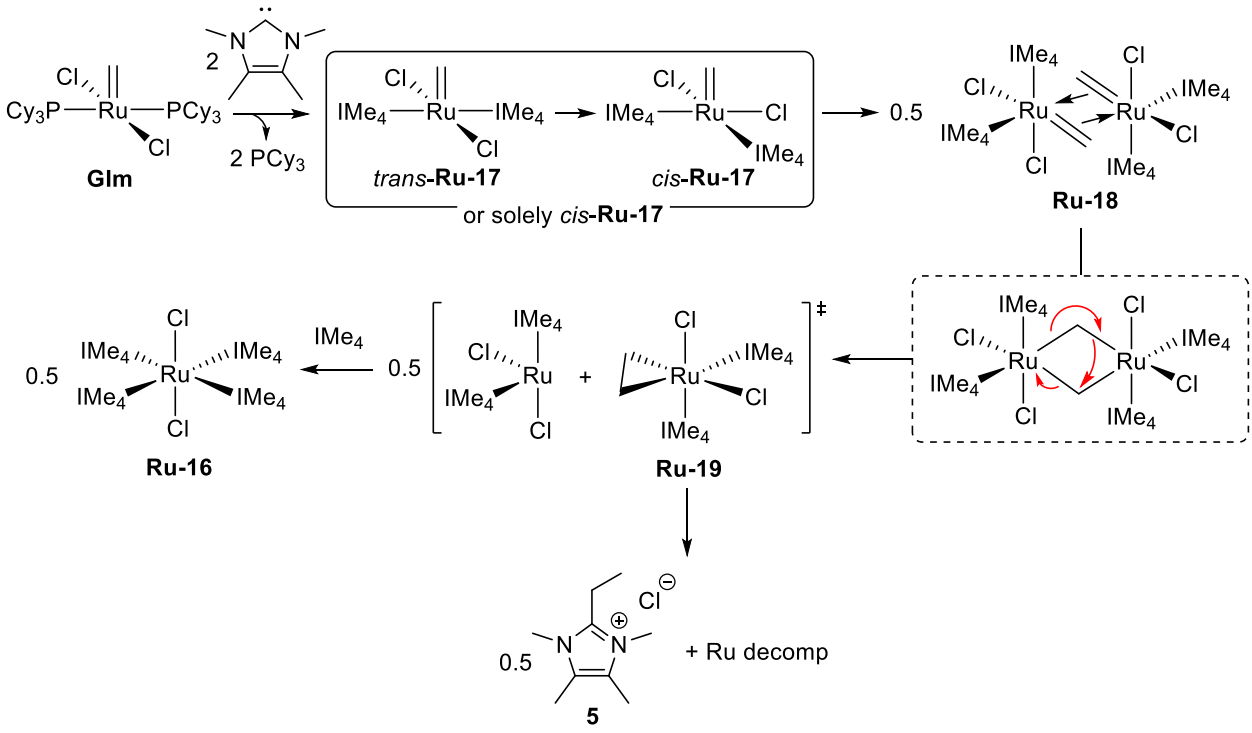

A potential pathway by which imidazolium salt **5** could form is shown in Scheme 4.7. Strong backbonding from the electron-rich Ru center in **Ru-19** may favour the metallacyclopropene structure shown. Abstraction of a proton from an *N*-CH_3 group could plausibly convert the bound olefin to an ethyl ligand, insertion of which into an IMe$_4$ ligand could liberate Et–IMe$_4$. Abstraction of a chloride ligand, as for [MePCy$_3$]Cl, is well precedented. Such migratory insertion of an alkyl group onto an adjacent NHC carbon has been reported for Pd[62-65]and Ni[66-68] systems. In these scenarios, reductive elimination of the alkyl imidazolium salt is facile provided effective overlap of the C_{alkyl} and C_{NHC} p_π orbitals.[69] Of particular note, the Cavell group reported decomposition of bis-IMe$_4$ complexes of Pd and Ni by migratory methyl insertion/reductive elimination, with liberation of the respective methyl imidazolium salt (a methyl analogue to ethyl imidazolium salt **5**).[67]

References begin on page 68

Scheme 4.7 Proposed reaction of intermediate Ru-19 to liberate imidazolium salt 5.

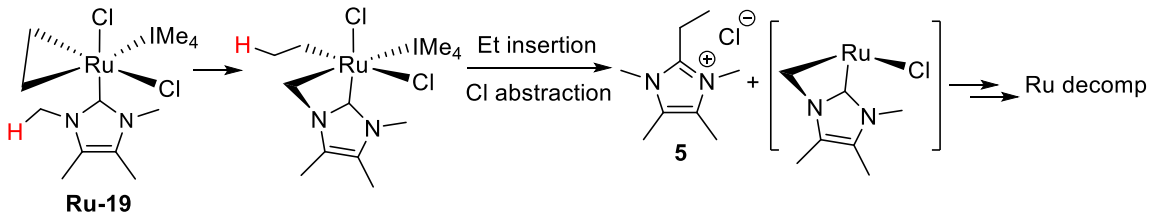

While full characterization of the Ru decomposition products has not yet been achieved, these preliminary results demonstrate that NHC truncation greatly increases the susceptibility of the methylidene species to decomposition via BMC. Notably, this susceptibility completely inhibits methylidene abstraction by free PCy_3, a primary vector for decomposition in the parent H_2IMes and IMes systems. The absence of any such coupling in the benzylidene system is consistent with the increased steric bulk of the benzylidene ligands relative to methylidene, which commonly retards this decomposition pathway for [M]=CHR derivatives.[1,61]

4.3 Conclusions and Future Work

The foregoing gives insight into the impact of NHC truncation on the behaviour of metathesis catalysts. While incorporation of a small NHC in such complexes has been suggested as a method to inhibit catalyst decomposition by C-H activation, this Chapter highlights several challenges arising from the steric accessibility of the Ru centres. First, the reaction of **GI** with IMe_4 was shown to effect displacement of both PCy_3 ligands. Facile dimerization precluded isolation of the putative intermediate *cis*-$RuCl_2(IMe_4)_2(=CHPh)$ **Ru-10**, instead affording the face-bridged ruthenium dimer $[Ru_2(\mu\text{-}Cl)_3(IMe_4)_4(=CHPh)_2]Cl$ **Ru-11a**. The small size of the IMe_4 ligand results in a rich dynamic behaviour for **Ru-11a** in solution, with rapid rotation of both the NHC and the benzylidene ligands on the NMR timescale. This complex exhibited poor metathesis activity, even in the simple RCM of DDM. This low productivity was attributed to the high

References begin on page 68

thermodynamic stability associated with face-bridged dimers, and was not resolved by abstraction of a bridging chloride to give edge-bridged $[RuCl(IMe_4)_2(=CHPh)]_2[BAr_4^F]_2$ **Ru-12**. Despite precedents for improved catalytic activity with edge-bridged dimers, this was precluded by reformation of face-bridged **Ru-11a** during metathesis. Metathesis activity requires access to complexes bearing just one NHC per Ru.

Another potential route to a mono-IMe_4 complex was therefore explored, in which the steric bulk of the anionic ligands of **GI** was increased from Cl to thioaryloxide. However, difficulties were again encountered with NHC over-addition, and incomplete consumption of the first-generation starting complex. These difficulties in accessing complexes bearing one IMe_4 ligand per Ru argue against the viability of such **GII** analogues in catalyst redesign. While useful, however, these findings with benzylidene IMe_4 complexes did not report on the original question: does a small NHC inhibit decomposition of the active catalyst, or does it instead result in *faster* methylidene abstraction, owing to a lack of protection at the Ru centre?

Installation of IMe_4 in the active methylidene complex showed that the truncated NHC is in fact deleterious, resulting in rapid loss of the methylidene ligand. Unexpectedly, however, decomposition did not involve methylidene abstraction by free PCy_3, the pathway described in Chapter 3 as a major vector for decomposition of Grubbs-class catalysts. Instead, bimolecular coupling resulted in elimination of ethylene. The absence of any $[MePCy_3]Cl$ coproduct indicates that such coupling out-competes nucleophilic attack on the methylidene ligand. NHC truncation is thus detrimental owing to the increased steric accessibility of the methylidene site. Catalyst redesign for longer lifetimes should therefore focus not on NHC truncation, but on steric protection of the methylidene ligand.

References begin on page 68

4.4 References

(1) Schrodi, Y., Mechanisms of Olefin Metathesis Catalyst Decomposition and Methods of Catalyst Reactivation. In *Handbook of Metathesis*, Grubbs, R. H.; Wenzel, A. G., Eds. Wiley-VCH: Weinheim, 2015; pp 323–342.
(2) Crabtree, R. H. *Chem. Rev.* **2015**, *115*, 127–150.
(3) Chadwick, J. C.; Duchateau, R.; Freixa, Z.; van Leeuwen, P. W. N. M., *Homogeneous Catalysts: Activity – Stability – Deactivation*. Wiley-VCH: Weinheim, 2011.
(4) Poater, A.; Ragone, F.; Correa, A.; Cavallo, L. *J. Am. Chem. Soc.* **2009**, *131*, 9000-9006.
(5) Hong, S. H.; Wenzel, A. G.; Salguero, T. T.; Day, M. W.; Grubbs, R. H. *J. Am. Chem. Soc.* **2007**, *129*, 7961–7968.
(6) Leitao, E. M.; Dubberley, S. R.; Piers, W. E.; Wu, Q.; McDonald, R. *Chem. – Eur. J.* **2008**, *14*, 11565–11572.
(7) Burling, S., et al. *J. Am. Chem. Soc.* **2007**, *129*, 1987–1995.
(8) Abdur-Rashid, K.; Fedorkiw, T.; Lough, A. J.; Morris, R. H. *Organometallics* **2004**, *23*, 86–94.
(9) Trnka, T. M., et al. *J. Am. Chem. Soc.* **2003**, *125*, 2546–2558.
(10) Hong, S. H.; Chlenov, A.; Day, M. W.; Grubbs, R. H. *Angew. Chem., Int. Ed.* **2007**, *46*, 5148–5151.
(11) Mathew, J.; Koga, N.; Suresh, C. H. *Organometallics* **2008**, *27*, 4666–4670.
(12) Vieille-Petit, L., et al. *Chem. Commun.* **2009**, 3783–3785.
(13) Vehlow, K.; Gessler, S.; Blechert, S. *Angew. Chem., Int. Ed.* **2007**, *46*, 8082–8085.
(14) Herbert, M. B., et al. *J. Am. Chem. Soc.* **2012**, *134*, 7861–7866.
(15) Jonas, L., et al. *J. Am. Chem. Soc.* **2010**, *132*, 18408–18416.
(16) Tang, C. Y.; Smith, W.; Vidovic, D.; Thompson, A. L.; Chaplin, A. B.; Aldridge, S. *Organometallics* **2009**, *28*, 3059–3066.
(17) Louie, J.; Grubbs, R. H. *Angew. Chem., Int. Ed.* **2001**, *40*, 247–249.
(18) Engl, P. S.; Fedorov, A.; Copéret, C.; Togni, A. *Organometallics* **2016**, *35*, 887—893.
(19) Reade, S. P.; Nama, D.; Mahon, M. F.; Pregosin, P. S.; Whittlesey, M. K. *Organometallics* **2007**, *26*, 3484–3491.
(20) Davies, C. J. E.; Lowe, J. P.; Mahon, M. F.; Poulten, R. C.; Whittlesey, M. K. *Organometallics* **2013**, *32*, 4927–4937.
(21) Cybulski, M. K.; Nicholls, J. E.; Lowe, J. P.; Mahon, M. F.; Whittlesey, M. K. *Organometallics* **2017**, *36*, 2308–2316.
(22) Burling, S., et al. *Chem. – Eur. J.* **2009**, *15*, 10912–10923.
(23) Wolf, S.; Plenio, H. *Green Chem.* **2011**, *13*, 2008–2012.
(24) Peeck, L. H.; Plenio, H. *Organometallics* **2010**, *29*, 2761–2766.
(25) Sashuk, V.; Peeck, L. H.; Plenio, H. *Chem. – Eur. J.* **2010**, *16*, 3983–3993.
(26) Weskamp, T.; Schattenmann, W. C.; Spiegler, M.; Herrmann, W. A. *Angew. Chem., Int. Ed.* **1998**, *37*, 2490–2493.
(27) Herrmann, W. A. *Angew. Chem., Int. Ed.* **1999**, *38*, 262–262.
(28) Amoroso, D.; Snelgrove, J. L.; Conrad, J. C.; Drouin, S. D.; Yap, G. P. A.; Fogg, D. E. *Adv. Synth. Catal.* **2002**, *344*, 757–763.
(29) Amoroso, D.; Yap, G. P. A.; Fogg, D. E. *Organometallics* **2002**, *21*, 3335–3343.
(30) Drouin, S. D.; Foucault, H. M.; Yap, G. P. A.; Fogg, D. E. *Organometallics* **2004**, *23*, 2583–2590.

References begin on page 68

(31) Lund, C. L.; Sgro, M. J.; Stephan, D. W. *Organometallics* **2012**, *31*, 580–587.
(32) Hansen, S. M.; Rominger, F.; Metz, M.; Hofmann, P. *Chem. – Eur. J.* **1999**, *5*, 557–566.
(33) Lummiss, J. A. M.; McClennan, W. L.; McDonald, R.; Fogg, D. E. *Organometallics* **2014**, *33*, 6738–6741.
(34) Lummiss, J. A. M.; Ireland, B. J.; Sommers, J. M.; Fogg, D. E. *ChemCatChem* **2014**, *6*, 459–463.
(35) Higman, C. S.; Rufh, S. A.; Fogg, D. E. *J. Organomet. Chem.* **2017**, in press.
(36) Salem, H., et al. *Organometallics* **2013**, *32*, 29−46.
(37) Barbasiewicz, M.; Szadkowska, A.; Bujok, R.; Grela, K. *Organometallics* **2006**, *25*, 3599–3604.
(38) Aharoni, A.; Vidavsky, Y.; Diesendruck, C. E.; Ben-Asuly, A.; Goldberg, I.; Lemcoff, N. G. *Organometallics* **2011**, *30*, 1607–1615.
(39) Pump, E.; Fischer, R. C.; Slugovc, C. *Organometallics* **2012**, *31*, 6972−6979, and references therein.
(40) Bantreil, X.; Schmid, T. E.; Randall, R. A. M.; Slawin, A. M. Z.; Cazin, C. S. J. *Chem. Commun.* **2010**, *46*, 7115–7117.
(41) Love, J. A.; Sanford, M. S.; Day, M. W.; Grubbs, R. H. *J. Am. Chem. Soc.* **2003**, *125*, 10103–10109.
(42) Lummiss, J. A. M.; Higman, C. S.; Fyson, D. L.; McDonald, R.; Fogg, D. E. *Chem. Sci.* **2015**, *6*, 6739–6746.
(43) Back, O.; Henry-Ellinger, M.; Martin, C. D.; Martin, D.; Bertrand, G. *Angew. Chem., Int. Ed.* **2013**, *52*, 2939 –2943.
(44) Verlinden, K.; Buhl, H.; Frank, W.; Ganter, C. *Eur. J. Inorg. Chem.* **2015**, *2015*, 2416–2425.
(45) Vummaleti, S. V. C., et al. *Chem. Sci.* **2015**, *8*, 1895–1904.
(46) Occhipinti, G.; Jensen, V. R. *Organometallics* **2011**, *30*, 3522–3529.
(47) Occhipinti, G.; Bjorsvik, H.-R.; Jensen, V. R. *J. Am. Chem. Soc.* **2006**, *128*, 6952–6964.
(48) Yang, H.-C.; Huang, Y.-C.; Lan, Y.-K.; Luh, T.-Y.; Zhao, Y.; Truhlar, D. G. *Organometallics* **2011**, *30*, 4196–4200.
(49) Straub, B. F. *Angew. Chem., Int. Ed.* **2005**, *44*, 5974–5978.
(50) Fürstner, A., et al. *Chem. – Eur. J.* **2001**, *7*, 3236–3253.
(51) Rouen, M., et al. *Chem. – Eur. J.* **2014**, *20*, 13716–13721.
(52) Hansen, S. M.; Volland, M. A. O.; Rominger, F.; Eisentrager, F.; Hofmann, P. *Angew. Chem., Int. Ed.* **1999**, *38*, 1273–1276.
(53) Wolf, R.; Plois, M.; Hepp, A. *Eur. J. Inorg. Chem.* **2010**, *2010*, 918–925.
(54) Jensen, V. R.; Occhipinti, G.; Hansen, F. R. Novel Olefin Metathesis Catalyts. WO 2012/032131 A1, 2012.
(55) Conrad, J. C.; Parnas, H. H.; Snelgrove, J. L.; Fogg, D. E. *J. Am. Chem. Soc.* **2005**, *127*, 11882–11883.
(56) Conrad, J. C.; Amoroso, D.; Czechura, P.; Yap, G. P. A.; Fogg, D. E. *Organometallics* **2003**, *22*, 3634–3636.
(57) Lopez, L. P. H.; Schrock, R. R. *J. Am. Chem. Soc.* **2004**, *126*, 9526–9527.
(58) Lopez, L. P. H.; Schrock, R. R.; Muller, P. *Organometallics* **2006**, *25*, 1978–1986.
(59) Roger, C.; Bodner, G. S.; Hatton, W. G.; Gladysz, J. A. *Organometallics* **1991**, *10*, 3266–3274.

References begin on page 68

(60) Merrifield, J. H.; Lin, G.-Y.; Kiel, W. A.; Gladysz, J. A. *J. Am. Chem. Soc.* **1983**, *105*, 5811–5819.
(61) Bailey, G. A.; Higman, C. S.; Day, C. S.; Fogg, D. E. *J. Am. Chem. Soc.* **2017**, submitted.
(62) McGuinness, D. S.; Saendig, N.; Yates, B. F.; Cavell, K. J. *J. Am. Chem. Soc.* **2001**, *123*, 4029–4040.
(63) Normand, A. T.; Stasch, A.; Ooi, L.-L.; Cavell, K. J. *Organometallics* **2008**, *27*, 6507–6520.
(64) McGuinness, D. S.; Green, M. J.; Cavell, K. J.; Skelton, B. W.; White, A. H. *J. Organomet. Chem.* **1998**, *565*, 165-178.
(65) Magill, A. M., et al. *J. Organomet. Chem.* **2001**, *617–618*, 546-560.
(66) Ren, X.; Gourlaouen, C.; Wesolek, M.; Braunstein, P. *Angew. Chem., Int. Ed.* **2017**, EarlyView article.
(67) McGuinness, D. S.; Cavell, K. J.; Skelton, B. W.; White, A. H. *Organometallics* **1999**, *18*, 1596–1605.
(68) Steinke, T.; Shaw, B. K.; Jong, H.; Patrick, B. O.; Fryzuk, M. D.; Green, J. C. *J. Am. Chem. Soc.* **2009**, *131*, 10461–10466.
(69) Cazin, C. S. J., *N-Heterocyclic Carbenes in Transition Metal Catalysis and Organocatalysis*. Springer: New York, 2011; Vol. 32.

References begin on page 68

Chapter 5. Conclusions and Future Work

Notwithstanding the important place of olefin metathesis in contemporary organic synthesis, catalyst decomposition remains an obstacle to full deployment of metathesis methodologies in sustainable chemical manufacturing. The need for improved understanding of the pathways responsible, and potential solutions, provide a context for the work outlined in this thesis. Initial studies examined a key weakness of phosphine-stabilized catalysts, the susceptibility of the off-cycle resting state $RuCl_2(H_2IMes)(PCy_3)(=CH_2)$ **GIIm** to "donor-accelerated decomposition." This pathway involves displacement of the phosphine ligand by sterically accessible Lewis donors, which promotes rapid nucleophilic attack by PCy_3 at the [Ru]=CH_2 carbon. A key finding was the ease with which even weak Lewis bases such as THF, MeOH, and H_2O promote this decomposition pathway. The impact of such donors on RCM yields, even for a readily-cyclized substrate, has important implications for metathesis in "green" solvents such as ethers and water. These results are also important in giving the first direct insight into the negative impact of water on productivity in Ru-catalyzed olefin metathesis. While the immediate focus of this work was on phosphine-mediated decomposition, broader questions center on the potential for such weak donors to promote abstraction of the methylidene ligand by other, non-phosphine, nucleophiles.

Attention was then turned to potential solutions, beginning with methods for limiting methylidene abstraction. First, the use of phosphine scavengers in metathesis was examined, to determine whether the performance of phosphine-stabilized catalysts in donor solvents could be improved. An iodide version of the Merrifield resin, which was previously unreported as a scavenger during metathesis reactions, was shown to increase RCM yields in both toluene and THF. Although CuI remained a more efficient scavenger in both solvents, the use of Merrifield-I (particularly in

metathesis of functionalized olefins) offers an attractive alternative, in view of the rich oxidation chemistry established for Cu(I) salts. Additionally, Merrifield-I is advantageous for this purpose due to its complete insolubility in organic solvents, which facilitates purification post-metathesis. Further studies of substrate scope with the Merrifield-I resin are recommended, to determine its compatibility with various functional groups, and its effectiveness relative to CuI.

An alternative means of inhibiting catalyst decomposition is curtailing the size of the NHC ligand to prevent C-H activation. In this work, two truncated versions of the benchmark NHC ligand H_2IMes were examined, in which one or both mesityl ligands are truncated to methyl. The "one-armed" NHC IMeMes was incorporated into a new Ru catalyst, $RuCl_2$(IMeMes)(PCy_3)(=CHPh) **Ru-6**, which displayed modest activity in the RCM of readily-cyclized DDM. This suggests that ligand truncation is ineffective as a strategy for improving catalyst activity. To probe the impact of small NHC size on catalyst decomposition, the more dramatically truncated IMe_4 ligand was examined.

Use of IMe_4 gave unequivocal evidence that small NHC ligands are detrimental to catalyst lifetimes. First, it was shown that the reaction of IMe_4 with the first-generation Grubbs catalyst $RuCl_2(PCy_3)_2$(=CHPh) **GI** results in uncontrolled loss of both PCy_3 ligands. Poor steric protection at the Ru centre enables dimerization, generating a highly stable face-bridged complex $[Ru_2Cl_3(IMe_4)_4(=CHPh)_2]Cl$ **Ru-11a**. The metathesis activity of this dimer is poor, as expected from the behaviour of related triply-bridged complexes. Abstraction of a bridging chloride to synthesize edge-bridged analogue $[RuCl(IMe_4)_2(=CHPh)]_2[BAr_4^F]_2$ **Ru-12** did not significantly improve activity. Efforts to access an *active* catalyst bearing one IMe_4 ligand per Ru were undertaken by use of bulky arylthiolate ligands in place of chlorides, but were unsuccessful.

Deeper insight came from studies probing the impact of small NHC size on decomposition of methylidene species. The widespread belief that a truncated NHC could curb decomposition by inhibiting C-H activation was shown to be invalid. Rather, this work showed that [Ru]=CH_2 decomposition is *faster* when IMe_4 is present. This was exemplified by the reaction of the first-generation methylidene complex $RuCl_2(PCy_3)_2(=CH_2)$ (**GIm**) with excess IMe_4. Both PCy_3 ligands were displaced by IMe_4, and immediate loss of all methylidene signals was observed by ^1H NMR. Surprisingly, however, this rapid decomposition is not due to abstraction of the sterically unprotected methylidene by PCy_3, as expected from the chemistry of Chapter 3. Instead, bimolecular coupling causes loss of the methylidene ligand, with the ethylene byproduct ultimately inserting into a Ru-IMe_4 bond. This highlights the striking susceptibility of sterically unprotected Ru centres to bimolecular decomposition, and shows that small NHC ligands, such as IMe_4, are profoundly detrimental. Future work should therefore focus on larger σ-donating ligands of the NHC or CAAC class (CAAC = cyclic alkyl amino carbene) to protect the [Ru]=CH_2 moiety against both bimolecular coupling and nucleophilic abstraction.

Appendix 1. Supplementary Data for Chapter 3

A1.1 NMR Spectra for Compounds Synthesized

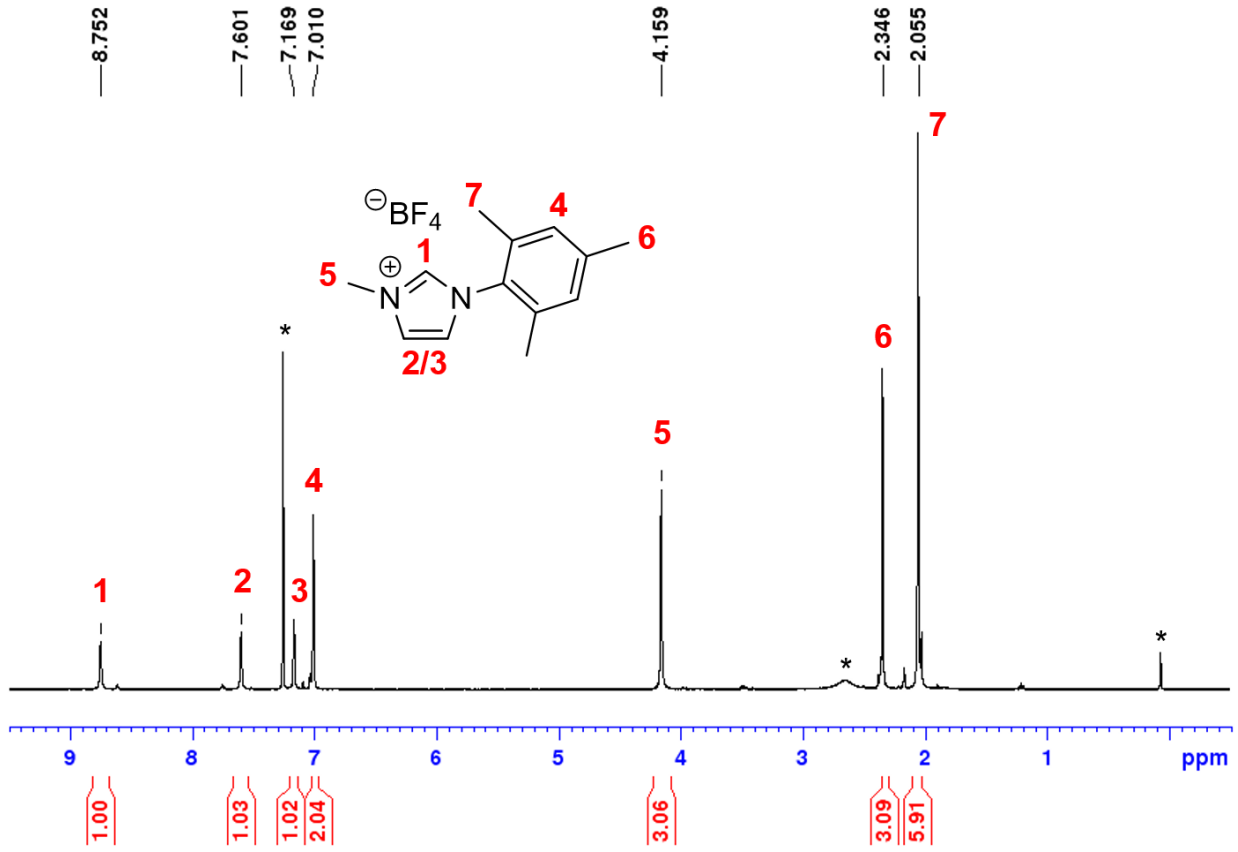

Figure A1. ^{1}H NMR spectrum (400 MHz, $CDCl_3$) of 1-methyl-3-(2,4,6-trimethylphenyl)imidazolium tetrafluoroborate (2b). Residual solvent impurities are denoted with *.

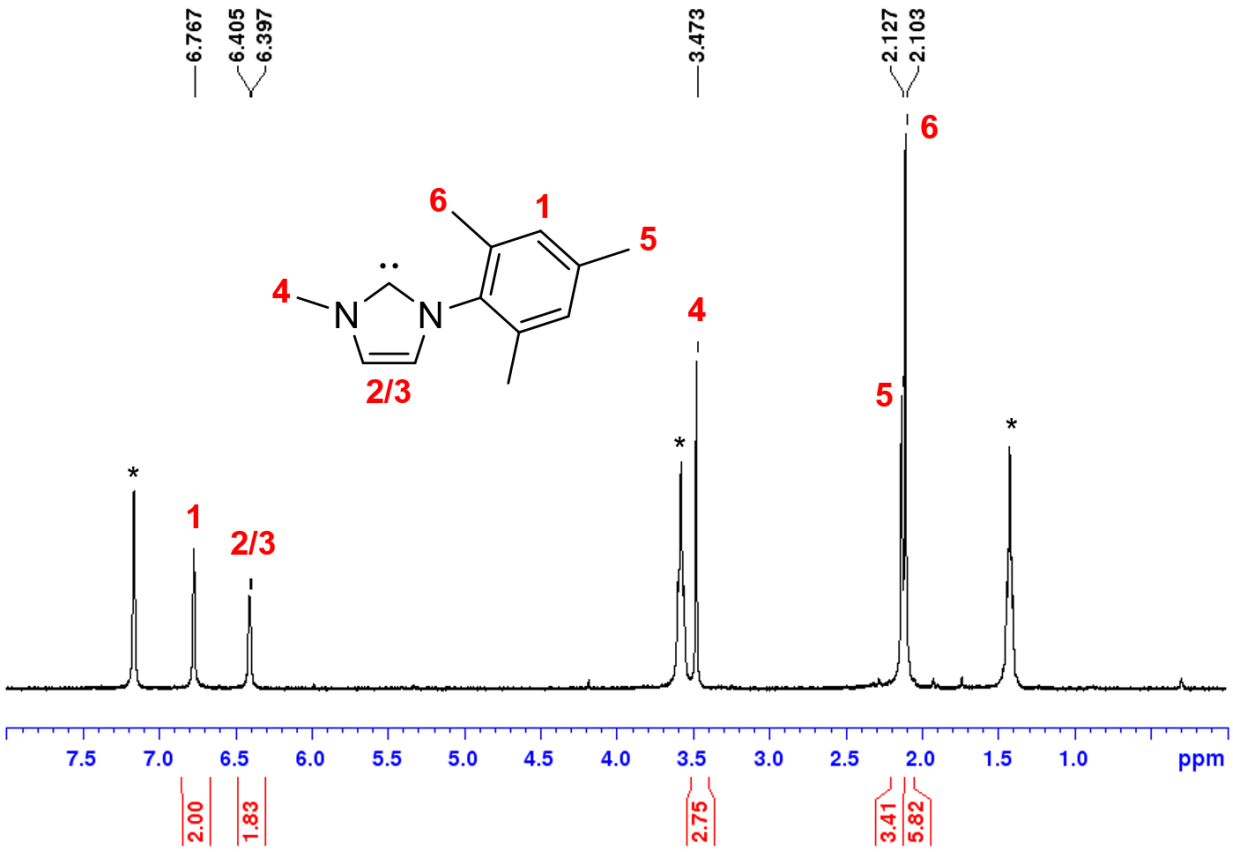

Figure A2. ^{1}H NMR spectrum (400 MHz, $CDCl_3$) of 1-methyl-3-(2,4,6-trimethylphenyl)imidazole-2-ylidene (IMeMes). Residual solvent impurities are denoted with *.

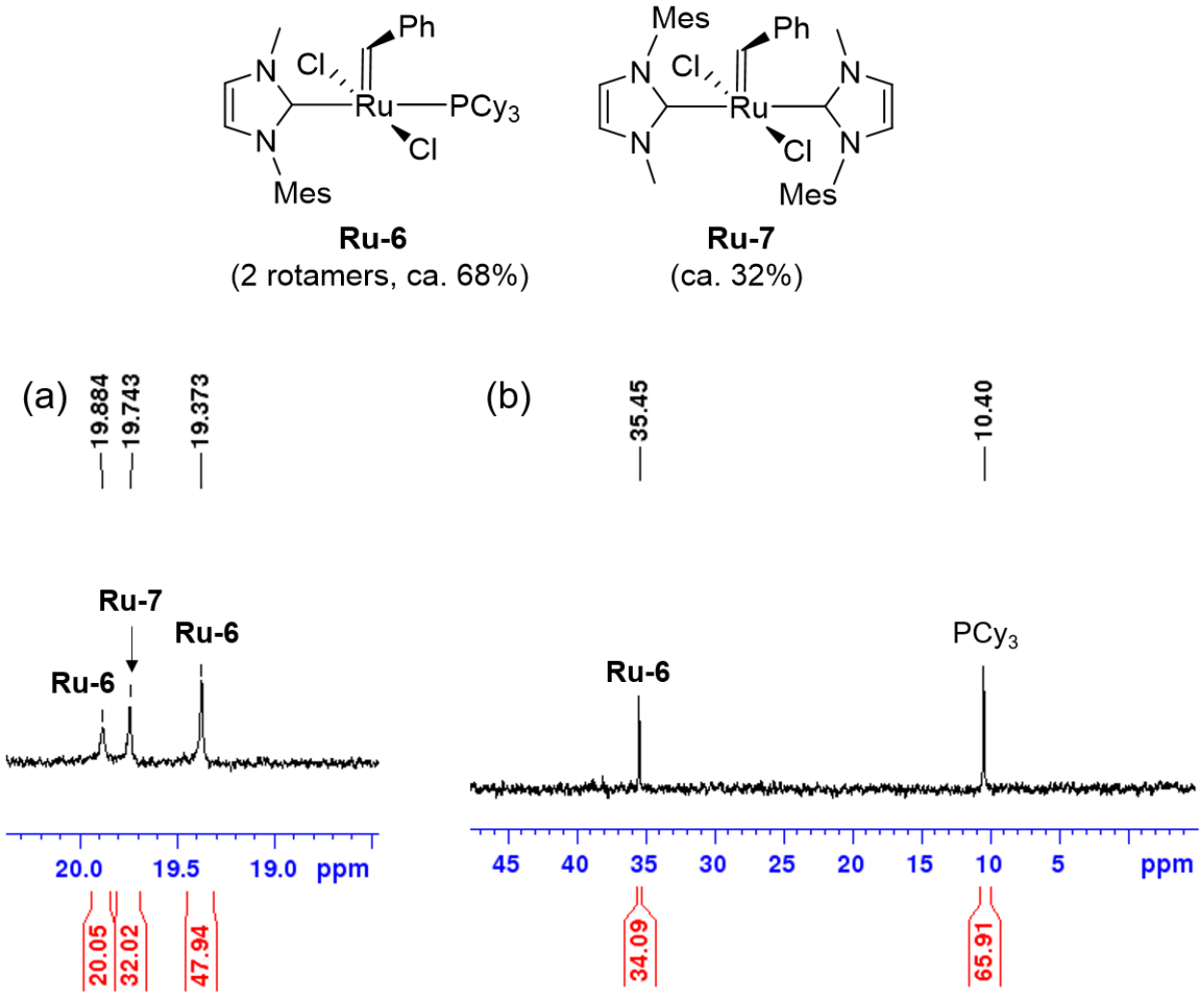

Figure A3. NMR spectra (C_6D_6) showing key chemical shifts for complexes $RuCl_2(IMeMes)(PCy_3)(=CHPh)$ Ru-6 and $RuCl_2(IMeMes)_2(=CHPh)$ Ru-7, and their relative proportions formed. (a) ^1H NMR spectrum (300 MHz), alkylidene region only. Proportions given are percentages of total alkylidene integration. (b) $^{31}P\{^1H\}$ NMR spectrum (121 MHz) before resin treatment to remove free PCy_3. Proportions given are percentages of total ^{31}P integration.

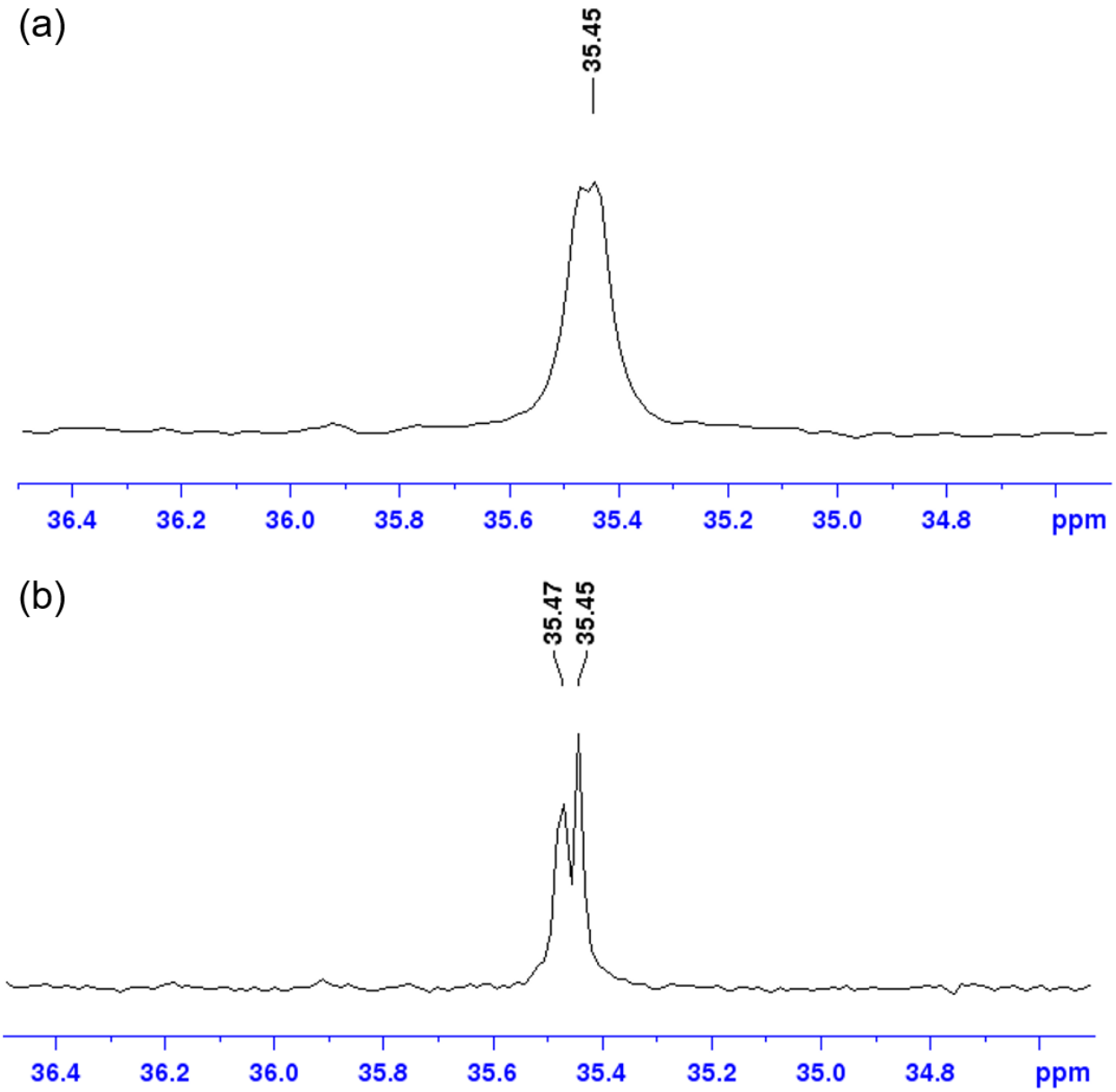

Figure A4. Variable temperature $^{31}P\{^{1}H\}$ NMR spectra (121 MHz, protio-THF) of $RuCl_2(IMeMes)(PCy_3)(=CHPh)$ Ru-6, showing separation of (a) phosphine singlet at RT into (b) two phosphine singlets at –60 °C.

A1.2 NMR Spectra for Monitored Reactions

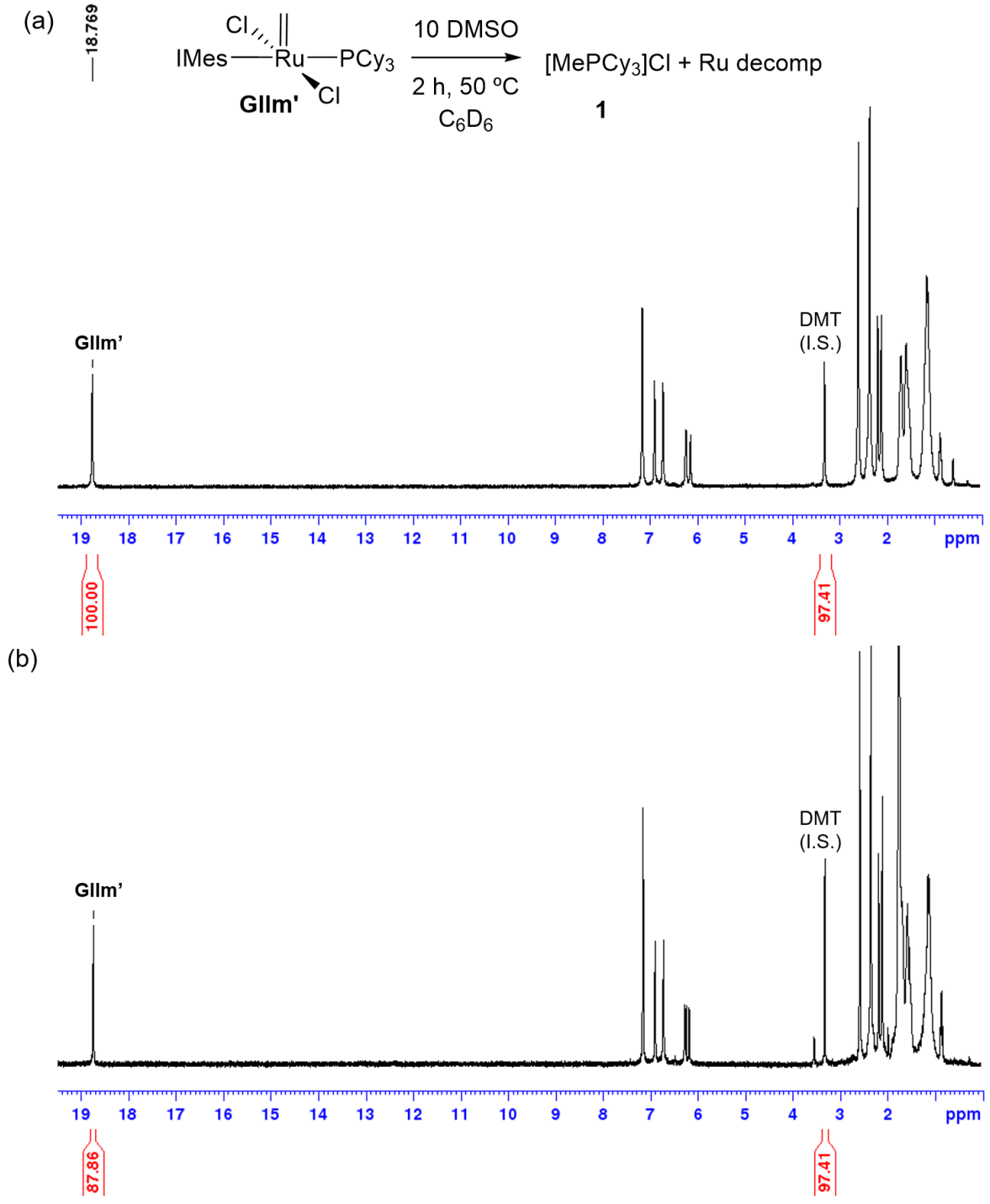

Figure A5. Decomposition of GIIm' in the presence of 10 DMSO (50 °C) measured by ^{1}H NMR (300 MHz, C_6D_6), vs DMT (internal standard). (a) Before addition of DMSO (t = 0), 100% GIIm'. (b) After addition of DMSO (t = 2 h), 88% GIIm'.

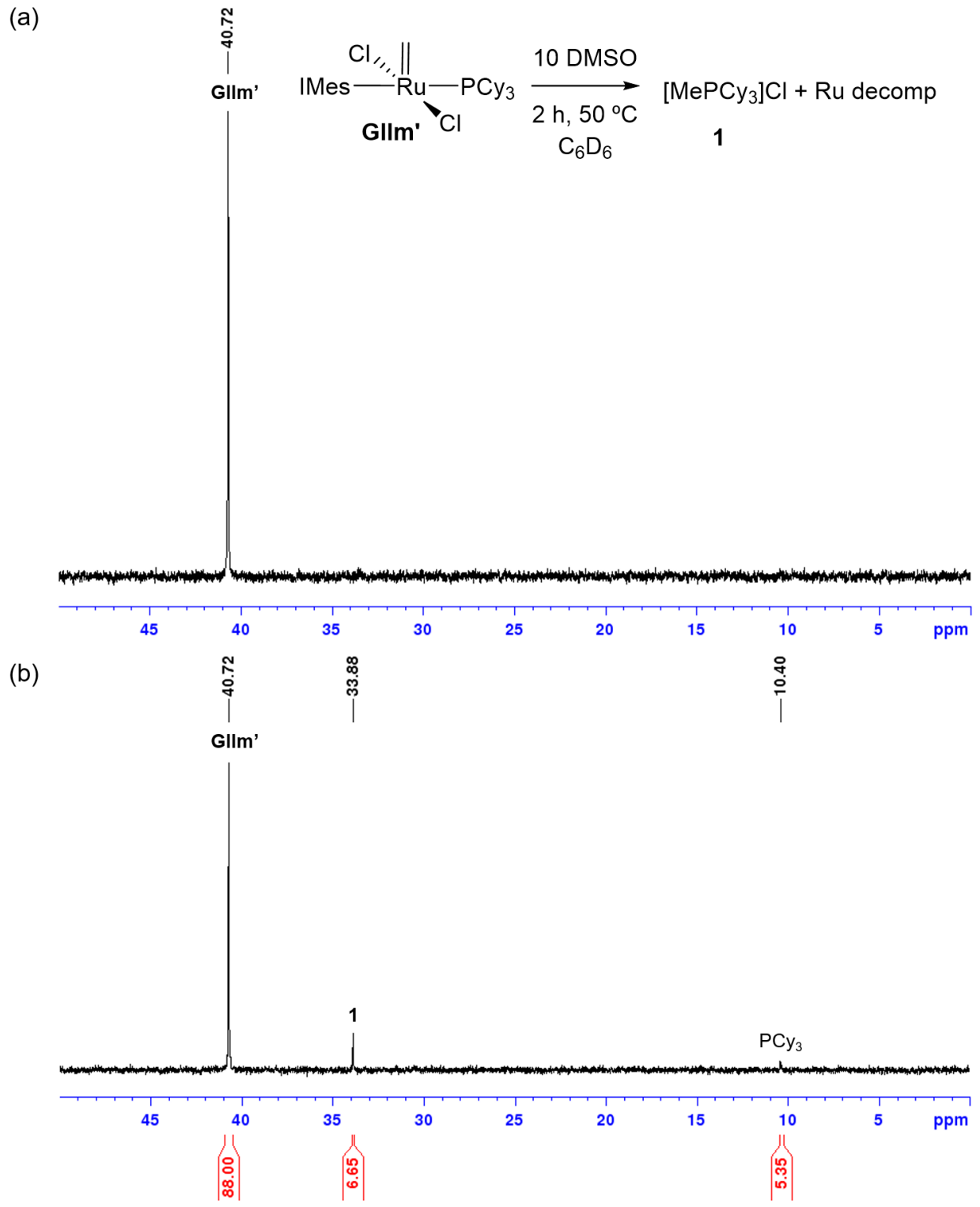

Figure A6. Decomposition of GIIm' in the presence of 10 DMSO (50 °C) measured by $^{31}P\{^{1}H\}$ NMR (121 MHz, C_6D_6). (a) Before addition of DMSO (t = 0), 100% GIIm'. (b) After addition of DMSO (t = 2 h), 88% GIIm', 7% [$MePCy_3$]Cl (1), 5% PCy_3.

A1.3 Representative GC Data

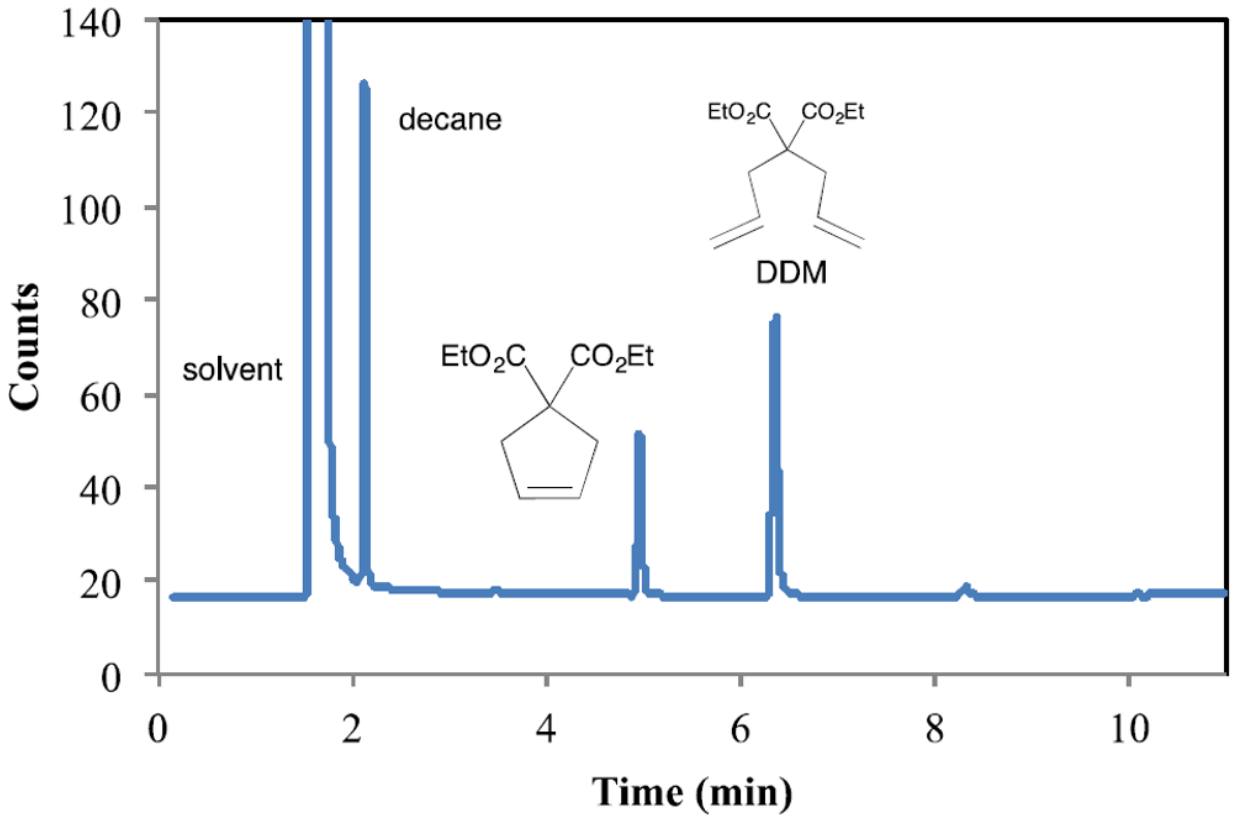

Figure A7. GC-FID trace for RCM of DDM by $RuCl_2(H_2IMes)(PCy_3)(=CHPh)$ GII in the presence of 90 µL water at 2 h.

Appendix 2. Supplementary Data for Chapter 4

A2.1 NMR Spectra for Compounds Synthesized

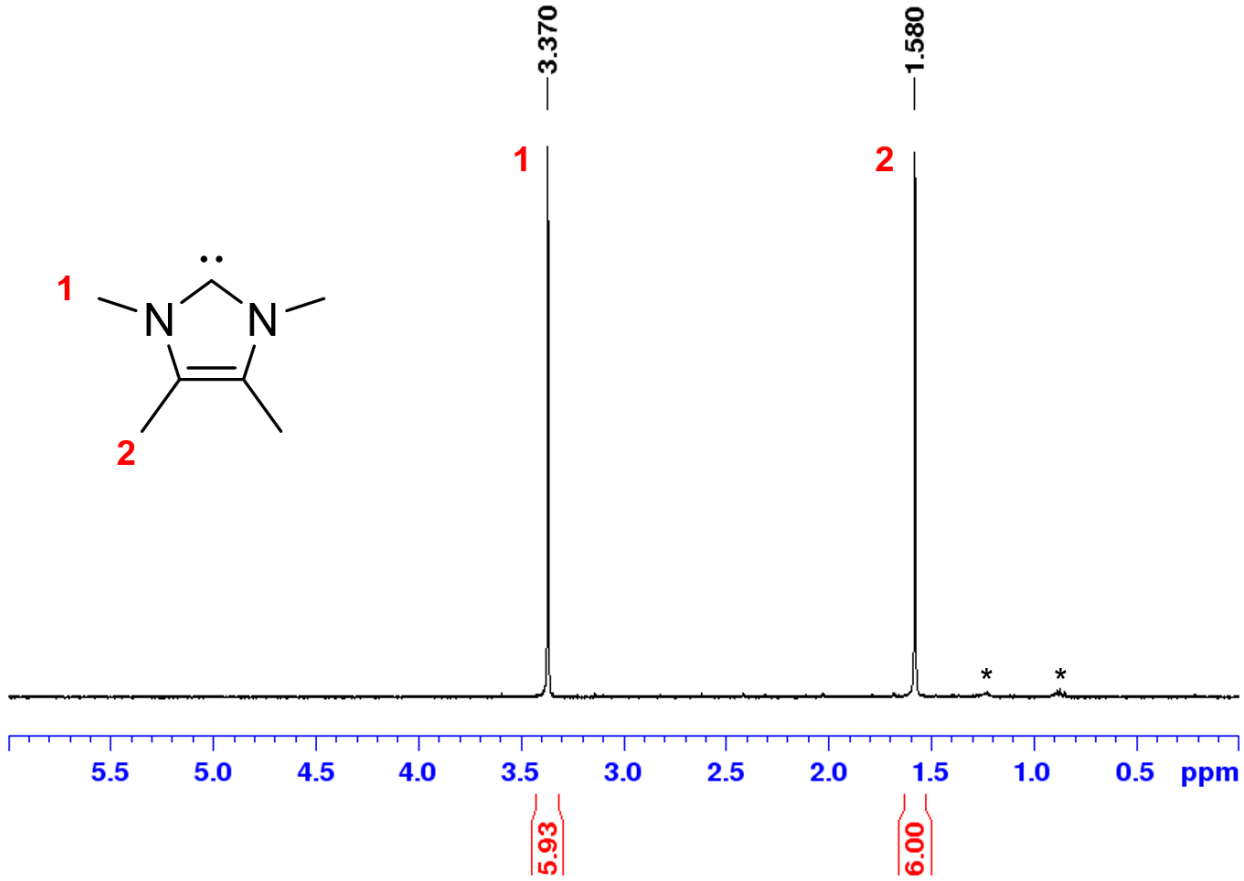

Figure A8. ^{1}H NMR spectrum (300 MHz, C_6D_6) of 1,3,4,5-tetramethylimidazol-2-ylidene (IMe_4). Residual solvent impurities are denoted with *.

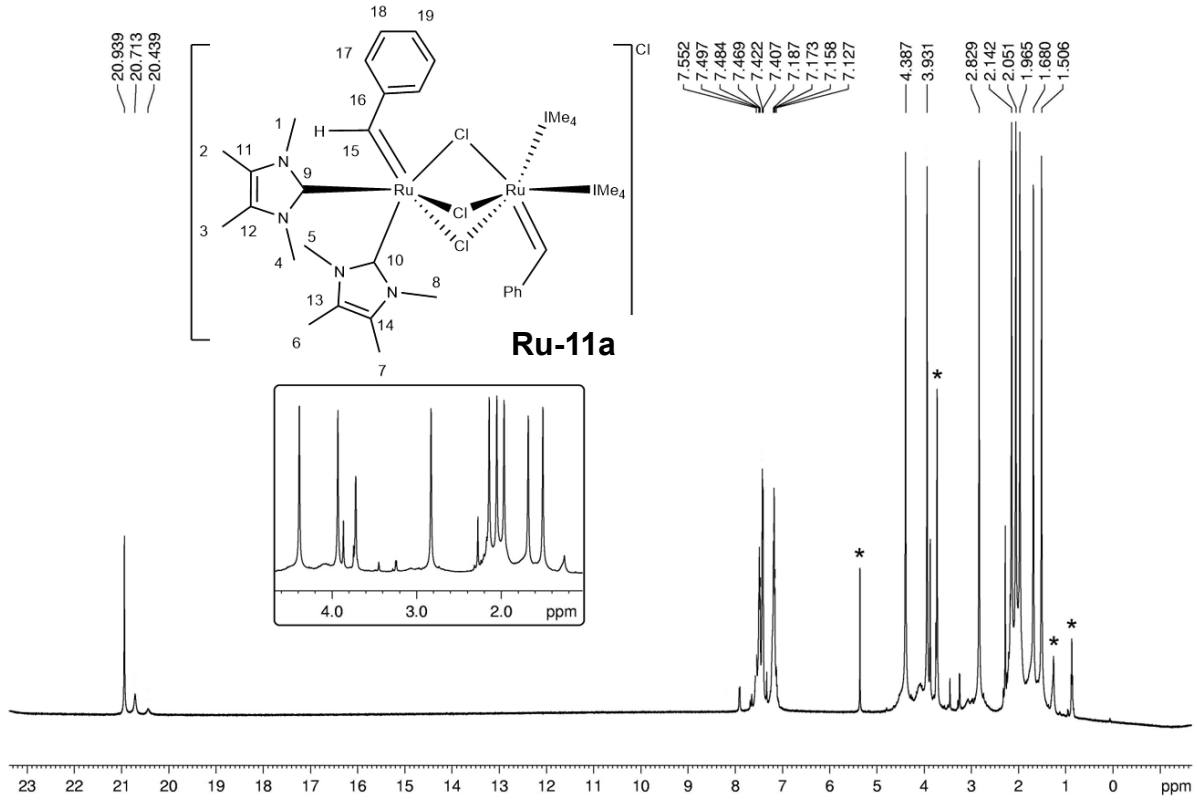

Figure A9. ^{1}H NMR spectrum of $[Ru_2Cl_3(IMe_4)_4(=CHPh)_2]Cl$ Ru-11a (DCE-d_4, 500 MHz, 298 K). Residual solvent impurities are denoted with *.

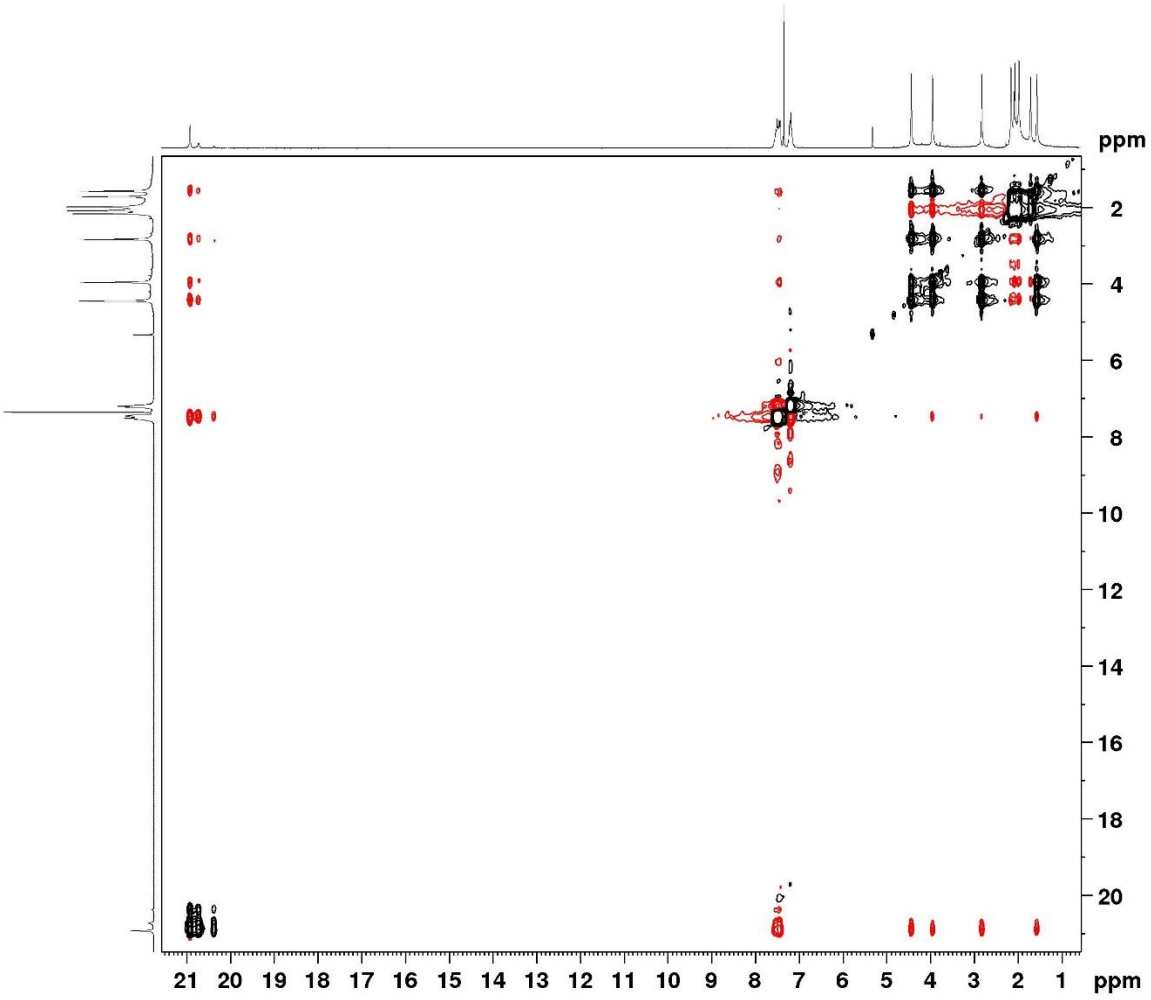

Figure A10. ^{1}H-^{1}H EXSY/NOESY spectrum (300 MHz, CD_2Cl_2) of $[Ru_2Cl_3(IMe_4)_4(=CHPh)_2]Cl$ Ru-11a. EXSY correlations are shown in black; NOESY correlations are shown in red.

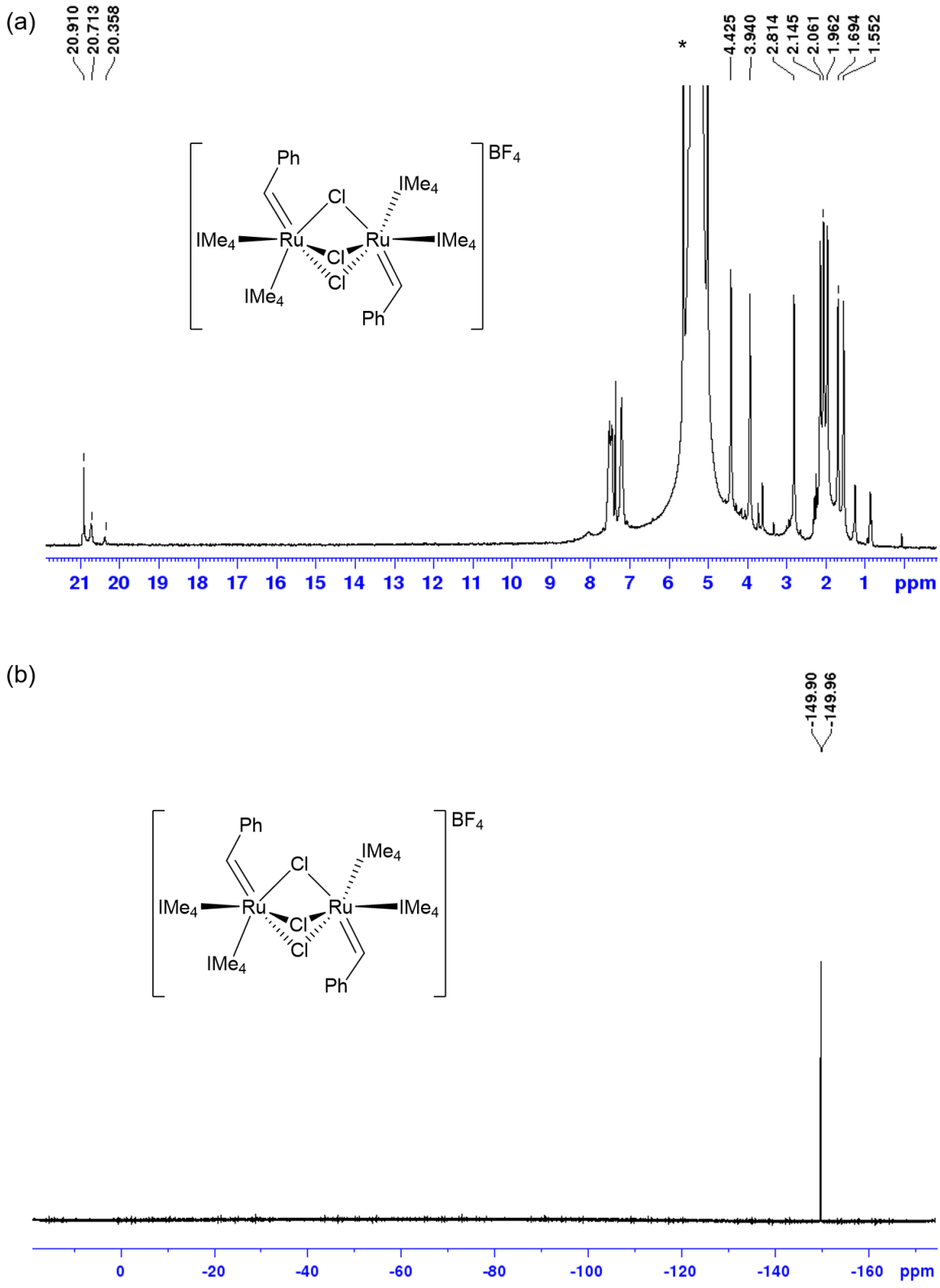

Figure A11. NMR spectra (CH_2Cl_2) of $[Ru_2Cl_3(IMe_4)_4(CHPh)_2]BF_4$ Ru-11b. (a) ^1H NMR spectrum (300 MHz). CH_2Cl_2 solvent peak denoted with *. (b) ^{19}F NMR spectrum (282 MHz).

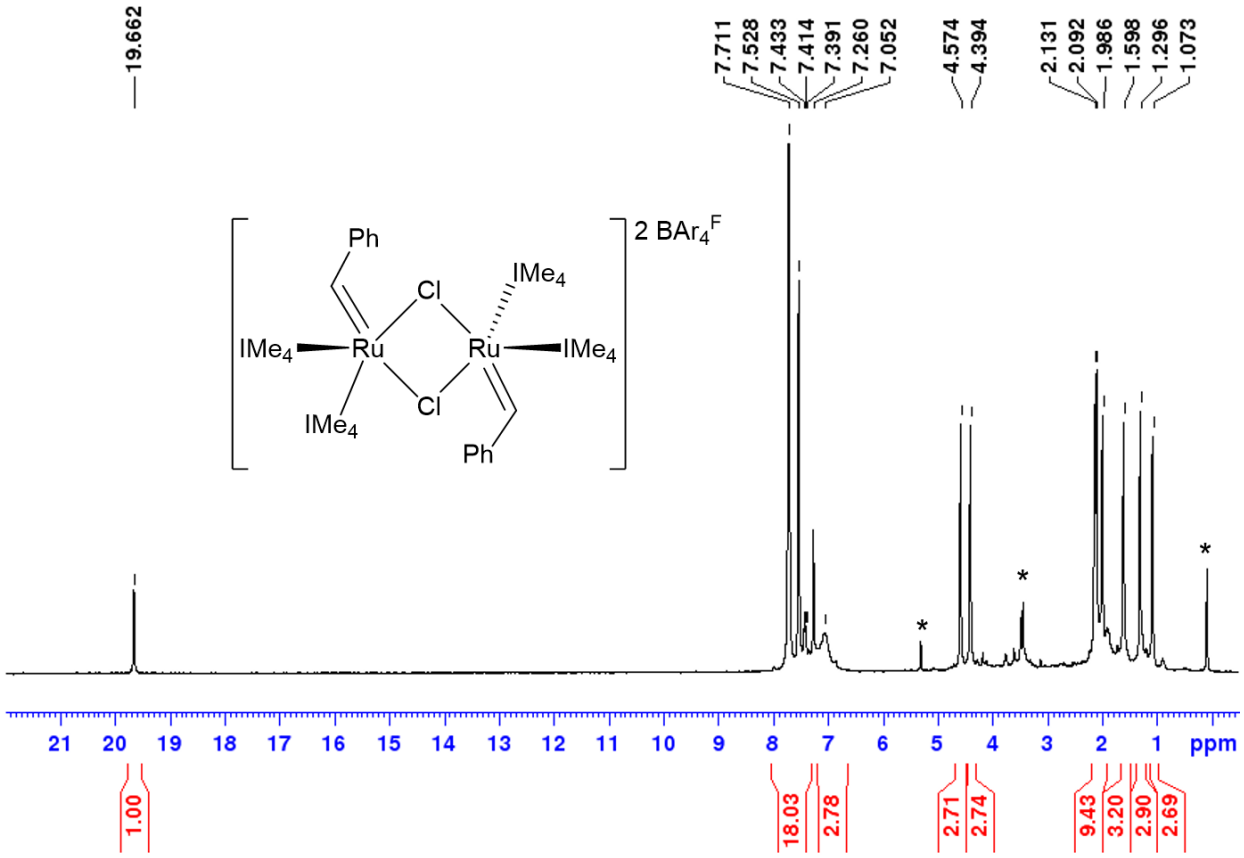

Figure A12. ^{1}H NMR spectrum (300 MHz, $CDCl_3$) of $[RuCl(IMe_4)_2(CHPh)]_2[BAR_4^F]_2$ Ru-12. Residual solvent impurities denoted with *.

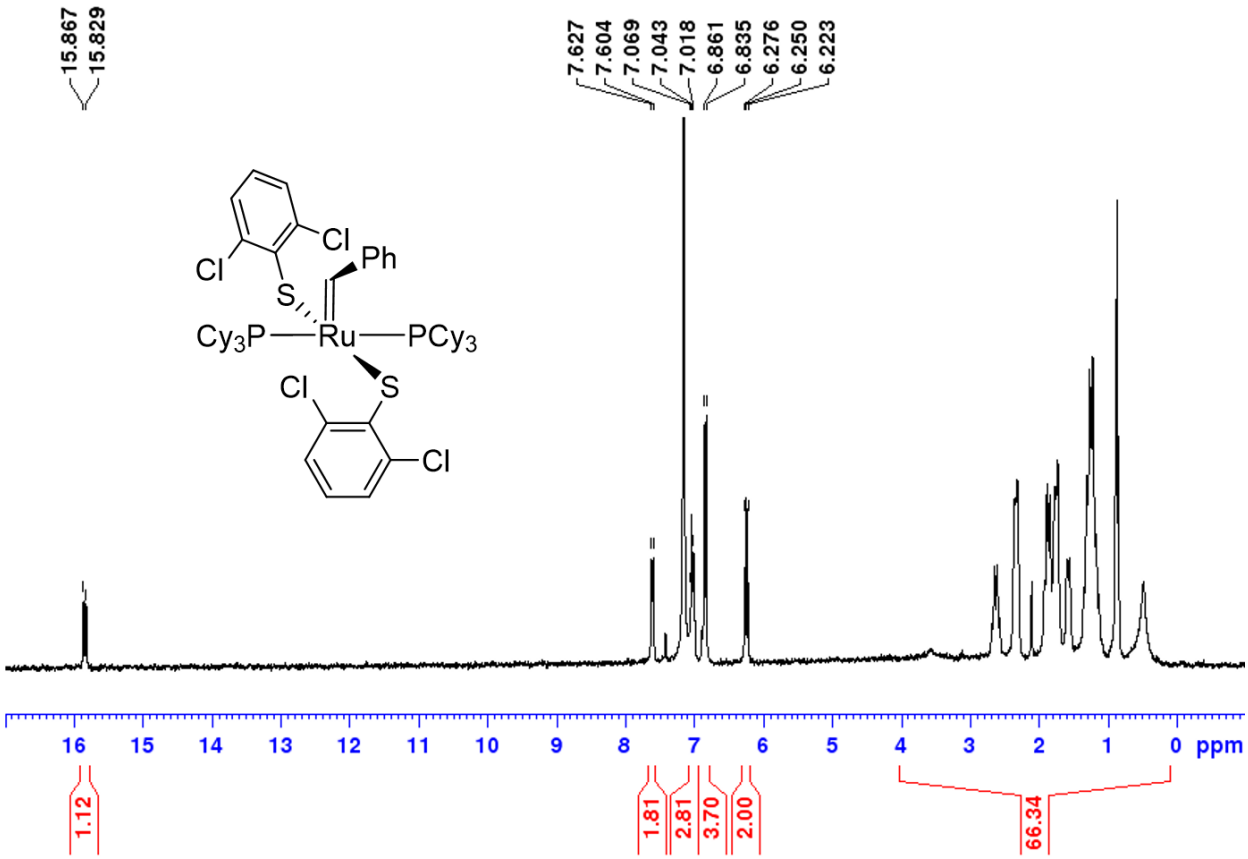

Figure A13. ^{1}H NMR spectrum (300 MHz, C_6D_6) of Ru(S(2,6-dichlorobenzene))$_2$(PCy_3)$_2$(=CHPh) Ru-13.

A2.2 NMR Spectra for Monitored Reactions

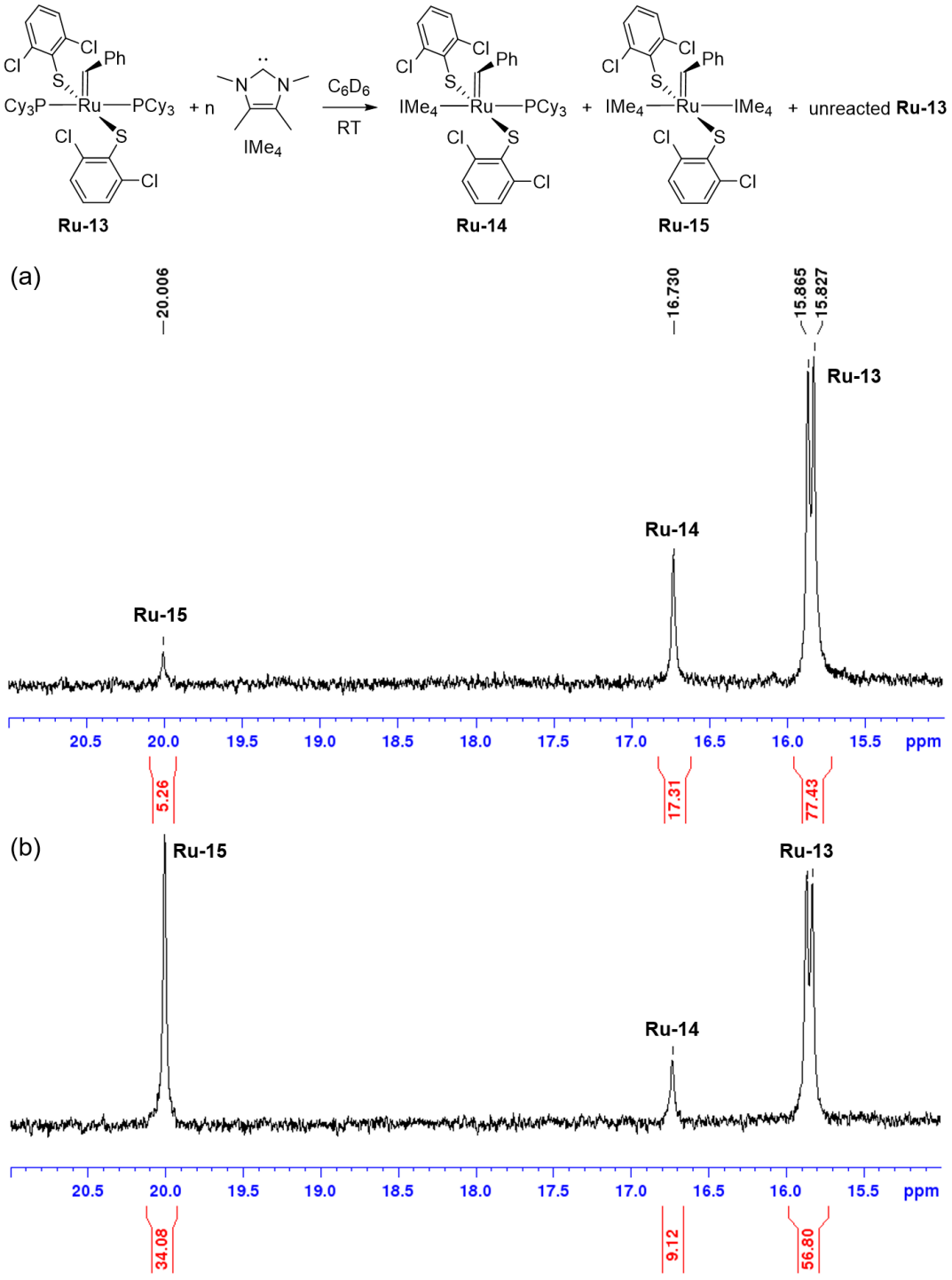

Figure A14. ^{1}H NMR spectra (300 MHz, C_6D_6) showing final alkylidene distribution from the reaction of Ru(S(2,6-dichlorobenzene))$_2$(PCy$_3$)$_2$(=CHPh) Ru-13 with (a) 1.0 equiv IMe$_4$, (b) 2.0 equiv IMe$_4$. Proportions given are percentage of total alkylidene integration.

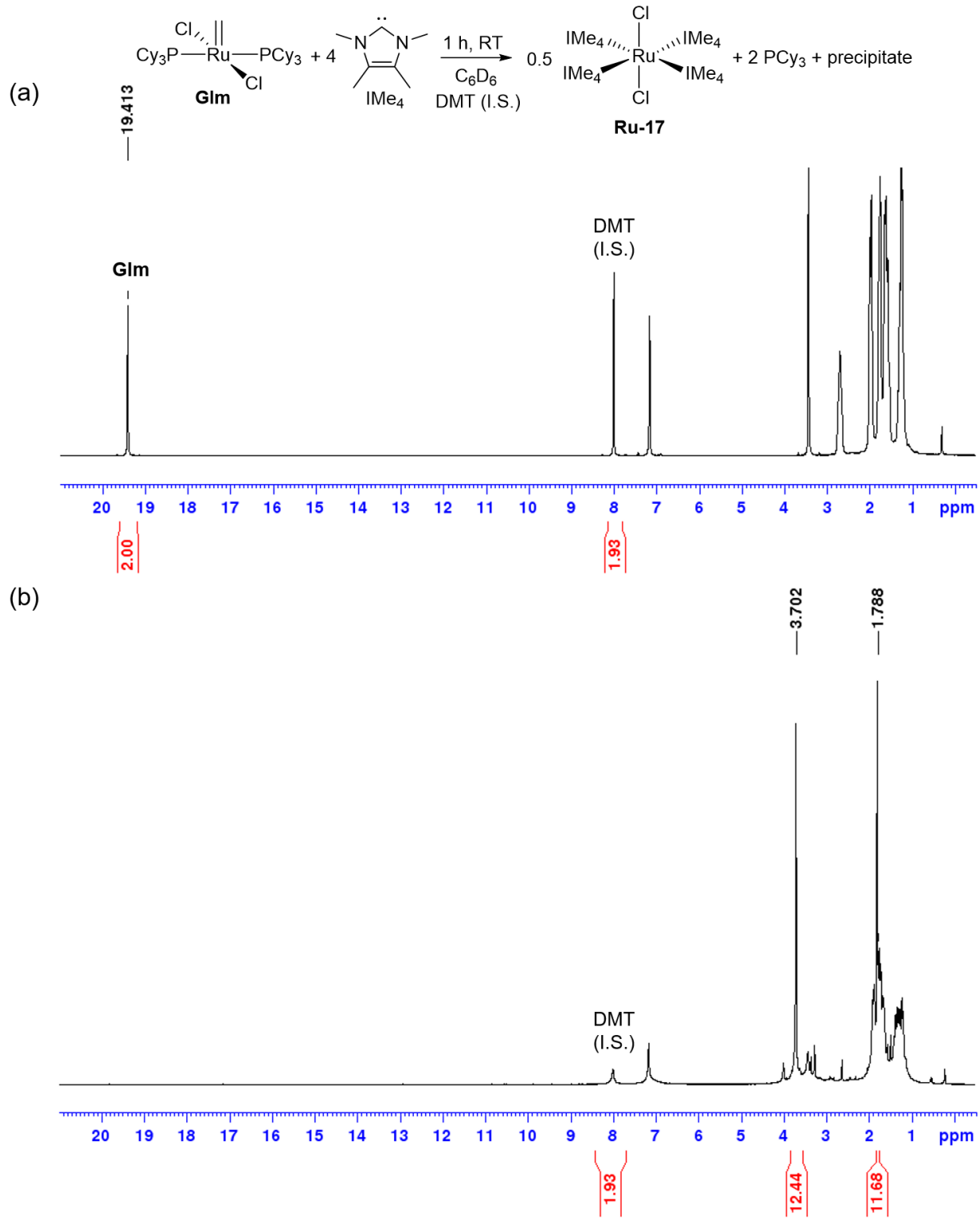

Figure A15. Decomposition of GIm in the presence of 4 IMe_4 (RT) measured by ^1H NMR (300 MHz, C_6D_6), vs DMT (internal standard). (a) Before addition of IMe_4 (t = 0), 100% GIm. (b) After addition of IMe_4 (t = 1 h), complete loss GIm, 50% Ru-16 formed.

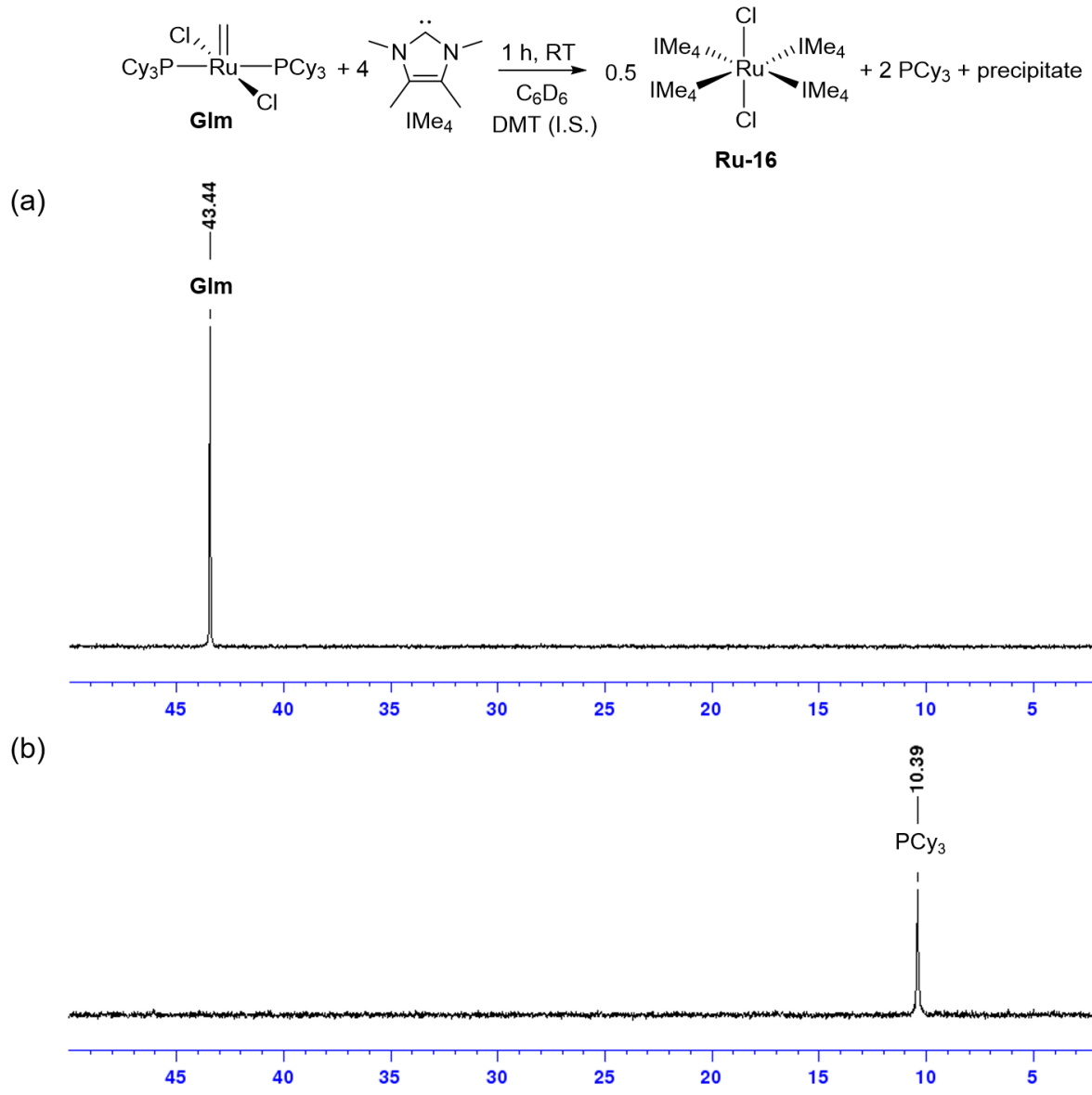

Figure A16. Decomposition of GIm in the presence of 4 IMe_4 (RT) measured by $^{31}P\{^1H\}$ NMR (121 MHz, C_6D_6). (a) Before addition of IMe_4 (t = 0), 100% GIm (by total ^{31}P integration). (b) After addition of IMe_4 (t = 1 h), complete loss GIm, PCy_3 is only P-containing product formed.

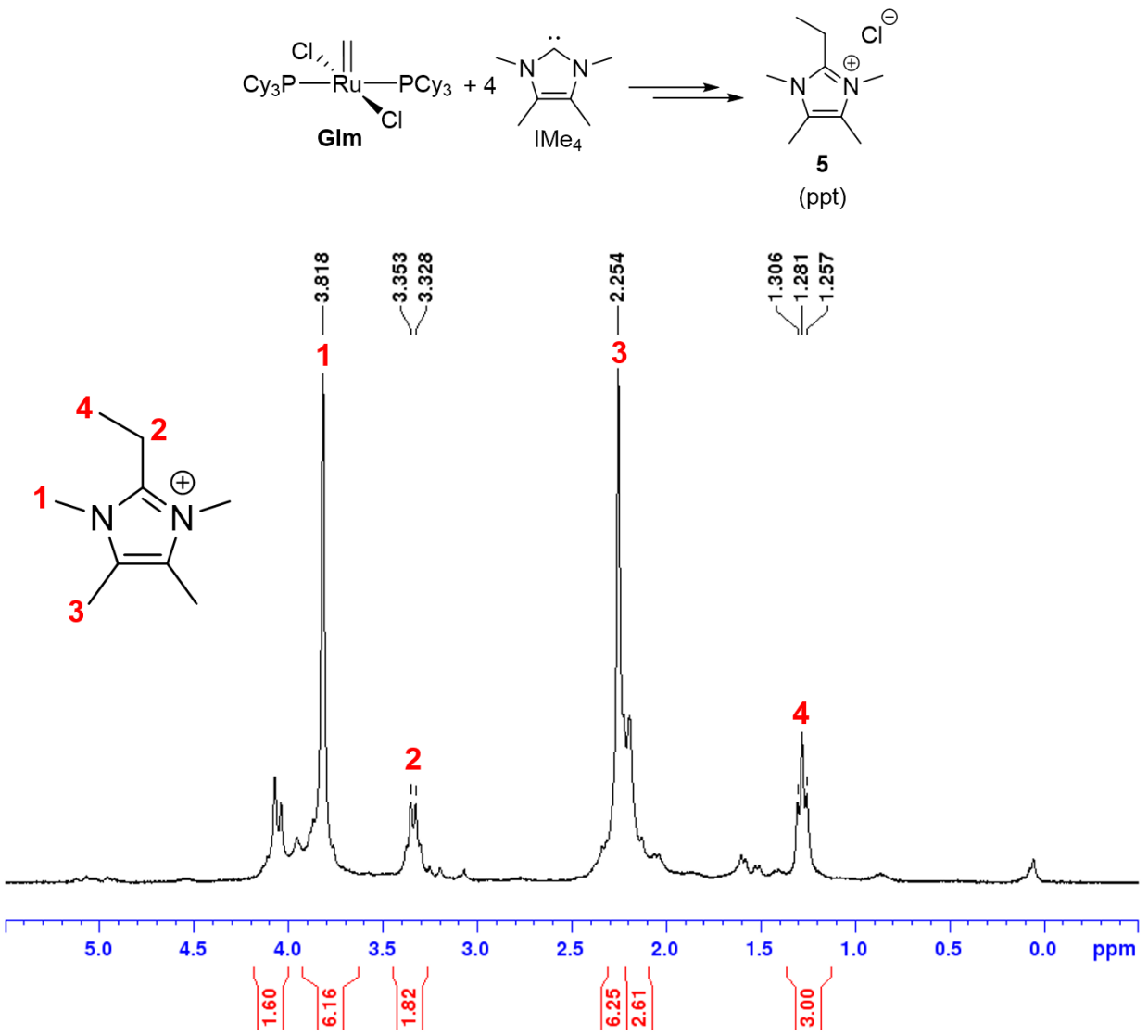

Figure A17. ^{1}H NMR spectrum (300 MHz, $CDCl_3$) of isolated precipitate from the decomposition of $RuCl_2(PCy_3)_2(=CH_2)$ GIm in the presence of 4 equiv IMe_4. Key identified peaks from imidazolium salt 5 are labelled.

A2.3 MALDI-TOF Mass Spectra

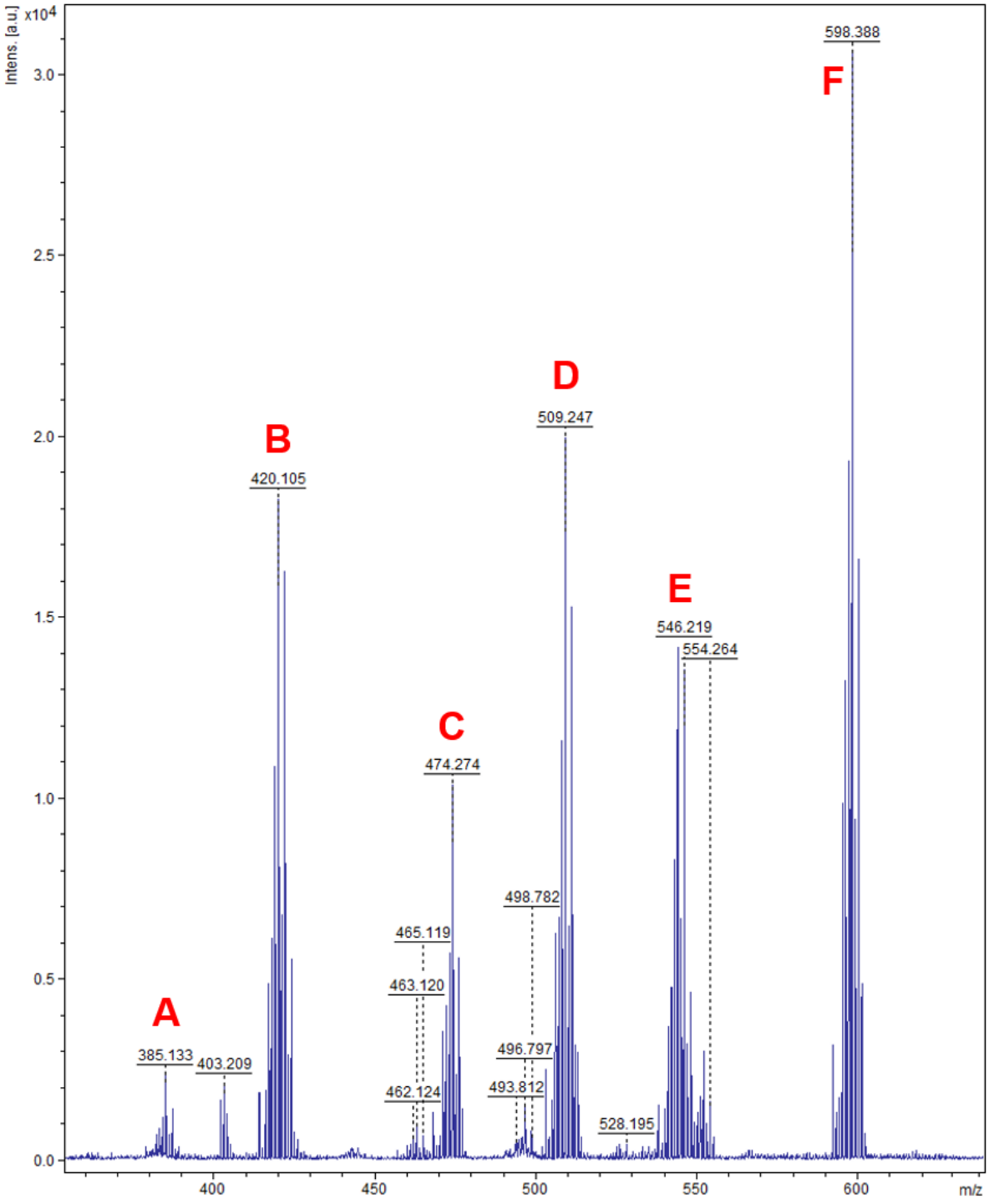

Figure A18. MALDI-TOF mass spectrum (matrix = pyrene) from the decomposition of $RuCl_2(PCy_3)_2(=CH_2)$ in the presence of 4 equiv IMe_4 (product from supernatant). For a summary of key peak assignments, see Table A1 below.

Table A1. Summary of key MALDI-TOF data from Figure A16.

Fragment	Assignment on spectrum	m/z observed	m/z calculated
$RuCl_2(IMe_4)_4$	not observed	-	668.24
M–[2 Cl]	F	598.388	598.30
M–[IMe_4]	E	546.219	544.14
M–[Cl]–[IMe_4]	D	509.247	509.17
M–[2 Cl]–[IMe_4]	C	474.274	474.20
M–[2 IMe_4]	B	420.105	420.04
M–[Cl]–[2 IMe_4]	A	385.133	385.07

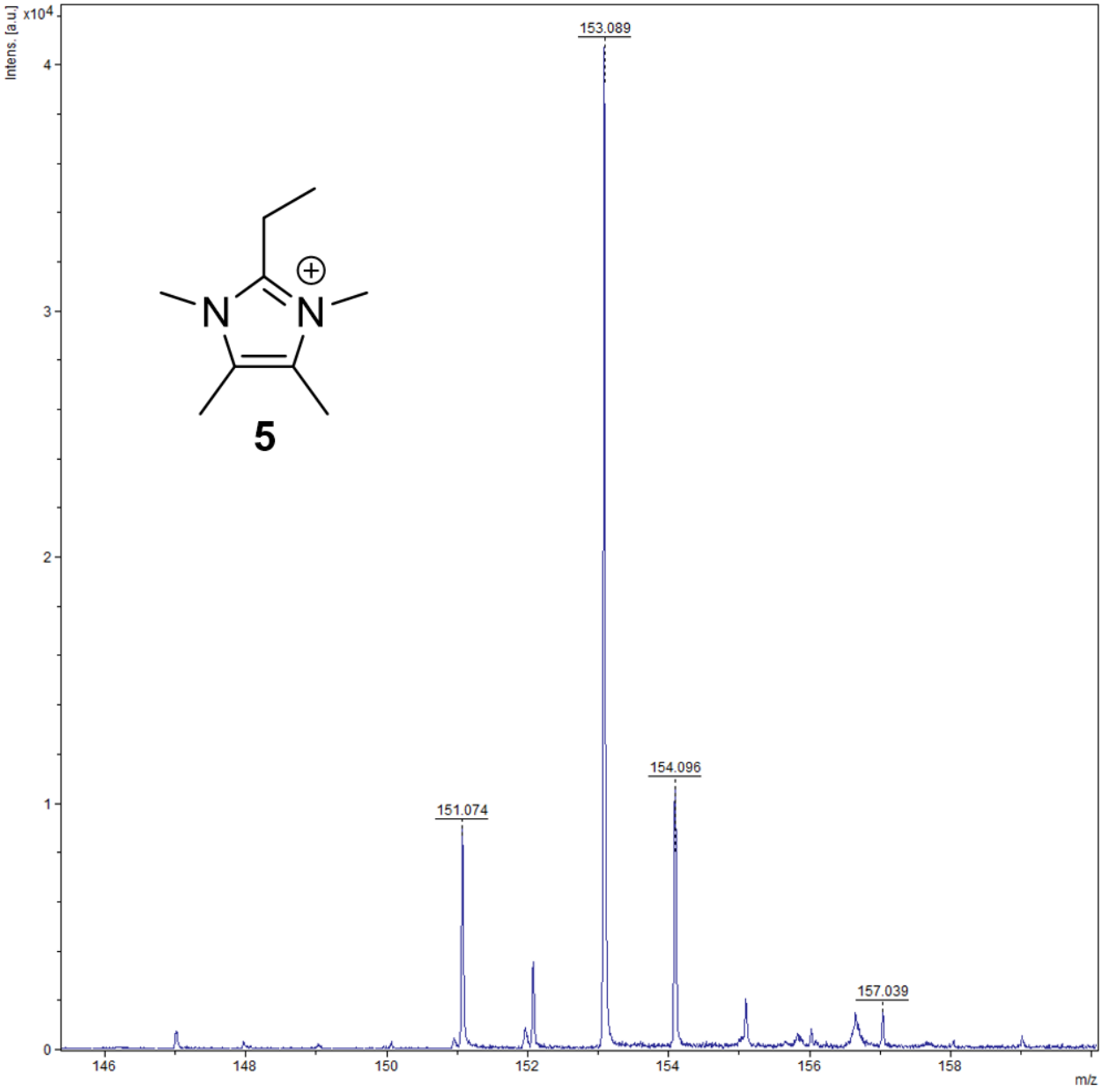

Figure A19. MALDI-TOF mass spectrum (matrix = anthracene) from the decomposition of $RuCl_2(PCy_3)_2(=CH_2)$ in the presence of 4 equiv IMe_4 (product from precipitate). Key identified isotope pattern for imidazolium salt 5 shown.